



Glassy and jammed states of harmonic spheres

Hugo Jacquin

► To cite this version:

Hugo Jacquin. Glassy and jammed states of harmonic spheres. Statistical Mechanics [cond-mat.stat-mech]. Université Paris-Diderot - Paris VII, 2012. English. NNT: . tel-00734605v1

HAL Id: tel-00734605

<https://theses.hal.science/tel-00734605v1>

Submitted on 24 Sep 2012 (v1), last revised 14 Apr 2014 (v2)

HAL is a multi-disciplinary open access archive for the deposit and dissemination of scientific research documents, whether they are published or not. The documents may come from teaching and research institutions in France or abroad, or from public or private research centers.

L'archive ouverte pluridisciplinaire **HAL**, est destinée au dépôt et à la diffusion de documents scientifiques de niveau recherche, publiés ou non, émanant des établissements d'enseignement et de recherche français ou étrangers, des laboratoires publics ou privés.

UNIVERSITÉ PARIS DIDEROT (PARIS 7) - U.F.R. DE PHYSIQUE

LABORATOIRE MATIÈRE ET SYSTÈMES COMPLEXES

THÈSE DE DOCTORAT DE L'UNIVERSITÉ PARIS VII

Spécialité: **Physique théorique**

École doctorale 107 **Physique de la région Parisienne**

présentée par

Hugo JACQUIN

sous la direction de Frédéric VAN WIJLAND

Sujet:

Etats vitreux et bloqués des sphères harmoniques

Jury composé de :

M. <i>Jean-Louis Barrat</i>	Examineur
M. <i>Ludovic Berthier</i>	Invité
M. <i>David Dean</i>	Rapporteur
M. <i>Silvio Franz</i>	Examineur
M. <i>Hisao Hayakawa</i>	Rapporteur
M. <i>Frédéric van Wijland</i>	Directeur de thèse

Thèse soutenue le 29 Juin 2012

Résumé

Cette thèse est consacrée à l'étude théorique de la transition vers l'état solide amorphe. Les solides amorphes peuvent être séparés en deux catégories : les verres structuraux dont la transition vers l'état amorphe, appelée transition vitreuse, s'effectue en présence de fluctuations thermiques, et les matériaux dont la transition vers l'état solide amorphe, alors dénommée transition de blocage, s'effectue en l'absence de fluctuations thermiques.

Nous étudions un système modèle de sphères sans friction interagissant par un potentiel faiblement répulsif et de portée finie : les sphères harmoniques. Ce système, étudié à température finie sert de modèle de verre et présente une transition vers un état amorphe. Étudié à température nulle, il permet aussi d'étudier la transition de blocage. Ces deux phénomènes, *a priori* distincts, sont parfois supposés reliés, la transition de blocage étant imaginée comme l'équivalent à température nulle de la transition vitreuse.

Deux approches théoriques coexistent dans l'étude de la transition vitreuse : la théorie de couplage de modes, qui tente de décrire le ralentissement de la dynamique des verres structuraux à l'approche de leur transition vitreuse, et la théorie de la transition de premier ordre aléatoire, qui se focalise sur la description aux temps longs de ces systèmes, en faisant des hypothèses sur la distribution de leurs états métastables. Pour certains modèles de systèmes désordonnés en champ moyen, ces deux approches peuvent être conciliées de façon exacte, mais la situation en dimension finie, sur laquelle cette thèse se concentre, laisse plusieurs questions en suspens.

Nous présentons en premier lieu une approche théorique de la dynamique des verres qui permet de clarifier certaines approximations impliquées dans la théorie de couplage de modes, et qui fournit un point de départ solide pour aller au-delà de cette théorie. En second lieu nous nous intéressons aux liens qui peuvent exister entre les deux approches décrites ci-dessus, et montrons qu'une partie au moins des résultats de la théorie de couplage de modes est contenue dans l'approche statique inhérente à la théorie de transition de premier ordre aléatoire, tout en fournissant un point de départ clair pour améliorer les résultats de cette dernière. Finalement, nous étudions le modèle des sphères harmoniques à très basse température et développons une théorie microscopique de sa transition de blocage qui capture une grande partie des observations expérimentales et numériques. Nous montrons que dans le cadre de nos approximations, la transition vitreuse et la transition de blocage sont deux phénomènes bien distincts.

Summary

This thesis is devoted to the theoretical study of the transition towards the amorphous solid state. Amorphous solids can be divided into two categories: those that undergo the so-called glass transition at finite temperature, and those that undergo the so-called jamming transition, without any thermal fluctuations.

We study a model system of spherical and frictionless particles interacting via a finite range, mildly repulsive pair potential: the harmonic spheres. Studied at finite temperature, it models structural glasses, and undergoes a glass transition. Studied at zero temperature, it also allows to investigate the jamming transition. These two phenomena, which are *a priori* distinct, are sometimes thought to be related, the jamming transition supposedly being the zero temperature manifestation of the glass transition.

Two theoretical approaches coexist in the study of the glass transition: mode-coupling theory, which describes the slowing down of the dynamics of glasses upon approaching their glass transition, and the random-first-order transition theory, which focuses on the long time behavior of the system by making hypotheses on the distribution of its metastable states. For a given class of mean-field disordered systems, these two approaches can be reconciled, but the situation in finite dimension, which this thesis is about, leaves a large number of questions unresolved.

We first present a theoretical approach of the dynamics of glasses which allows us to clarify the approximations implied in mode-coupling theory, and gives a solid starting point to go further. We then study the links that can exist between the two approaches described above, and show that at least a part of mode-coupling results is contained in the static approach of the random-first-order theory, while providing a starting point that would permit to improve the latter. Finally we study harmonic spheres at very low temperature and develop a microscopic theory of its jamming transition, that captures a large set of numerical and experimental observations. We show that, within our approximations, the glass transition and the jamming transition are two separate phenomena.

Acknowledgments

This thesis was founded by a Fondation CFM-JP Aguilar grant. I want here to thank Jean-Philippe Bouchaud for giving me the opportunity to benefit from this grant.

Remerciements

En premier lieu je remercie mon directeur de thèse Frédéric pour sa patience et son extrême disponibilité, et pour avoir supporté mes caprices tout au long de la thèse. Frédéric m’a toujours accueilli à bras ouvert dans son bureau, sans jamais se départir de sa bonne humeur. Il consitue une source inépuisable d’idées et de motivation, et son optimisme sans borne m’a plusieurs fois sauvé d’un certain découragement face à un sujet de thèse qui s’est avéré bien plus ardu qu’escompté.

En plus de la présence de Frédéric, j’ai pu bénéficier de nombreuses interactions avec Ludovic Berthier durant les deux premières années de ma thèse. Il est difficile de rivaliser avec sa parfaite compréhension des phénomènes physiques et sa très vaste connaissance de la littérature dans ses domaines d’intérêt, et j’espère avoir acquis ne serait-ce qu’un tout petit peu de ces talents durant ma thèse. Je garde un souvenir impérissable des pauses cigarette sur le campus de Montpellier.

Finalement tout au long de la thèse je n’ai cessé de rendre visite à Francesco Zamponi. Même si travailler avec lui peut donner la sensation d’avoir toujours un train de retard, sa terrible efficacité et son ouverture d’esprit sont des sources de motivations trop addictives pour imaginer pouvoir s’en passer. Mes nombreuses discussions avec lui sont à l’origine d’une grande partie des travaux présentés dans cette thèse, et je l’en remercie vivement.

Frédéric, Ludovic et Francesco sont trois personnalités assez différentes, scientifiquement comme humainement, et d’avoir eu l’opportunité de faire cette thèse sous leur triple influence est une formidable chance.

Je remercie les deux rapporteurs de cette thèse, David Dean et Hisao Hayakawa, pour avoir accepté cette lourde tâche et pour leurs commentaires, ainsi que Jean-Louis Barrat, Ludovic Berthier et Silvio Franz pour avoir accepté de faire partie du jury.

Je remercie les organisateurs et participants de Beg Rohu 2010, qui m’a permis de découvrir (ou redécouvrir) beaucoup de personnes, dont certaines sont restées à ce jour des amis. Je pense notamment, dans le désordre, à Giulio Biroli, Marco Tarzia, Olivier Dauchot, Florent Krzakala, Vivien Lecomte, Vincent Démery, Elisabeth Agoritsas, Khanh-Dang Nguyen Thu Lam, Fédérico Benitez, Elia Zarinelli, Joachim Rambeau, Céline Nadal, ... Je remercie Bertrand Delamotte pour une partie de baby-foot mémorable en plein milieu de la nuit, et pour les nombreuses discussions (scientifiques cette fois) qui ont suivies.

Un grand merci à tous les doctorants du laboratoire avec qui j’ai eu l’occasion de passer du temps, dans le désordre et entre autres: Jean Baptiste, Pierre, Félix, Jimmy, Loudjy, Anne-Florence, Rémi, Gérald, Jonathan, Clément, Nathalie, Pauline, Luc...

Je remercie tous les membres des laboratoire MSC, Charles Coulomb à Montpellier, LPT à l’ENS et plus récemment l’INFN à Rome, pour m’avoir accueilli ou fourni des soutiens logistiques à divers moments de la thèse.

Merci à mes parents et à ma grand mère, à mes amis de toujours, Diego et Louis, et à Jon, Fanny, Simon, Corentin, Fabien, Franz, Laura, pour toutes les bières, voyages et séances d’escalade. Grâce à eux entre autres, j’ai pu trouver un équilibre fragile entre mes différentes passions. Finalement merci à Christelle, pour son amour et sa patience, et grâce à qui cette dernière année de thèse a été particulièrement heureuse, et sans qui je n’aurais pas pu trouver cet équilibre.

Frou !

Contents

1	Introduction	13
1.1	Theory of amorphous solids	13
1.1.1	Thermal systems: the glass transition	14
1.1.2	A-thermal systems: the jamming transition	18
1.2	Current theoretical approaches	20
1.2.1	Dynamics: Mode-Coupling theory	20
1.2.2	Random-First-Order Transition theory	22
1.3	Questions discussed in this work	24
1.3.1	Approach developed in this thesis	24
1.3.2	What is the theoretical status of the Mode-Coupling transition ?	24
1.3.3	Does the relation between MCT and the RFOT scenario hold beyond mean-field ?	24
1.3.4	What is the relation between jamming and the glass transition ?	25
2	Formalism of many-body systems	27
2.1	Statistical field theories	27
2.1.1	Feynman diagrams	28
2.1.2	Reduction of diagrams: first Legendre transform	30
2.1.3	Reduction of diagrams: second Legendre transform	34
2.2	Theory of liquids	35
2.2.1	The case of the ideal gas	37
2.2.2	Mayer diagrams	38
2.2.3	Morita & Hiroike functional	39
2.2.4	Hyper-Netted-Chain approximation	40
3	Dynamics near the glass transition: a field theory approach	43
3.1	Field theory for supercooled liquids	43
3.1.1	Formulation in terms of the density and field-theoretic formulation	44
3.1.2	Diagrammatic structure of the theory	46
3.1.3	Structure of the perturbative expansion	47
3.1.4	Symmetries and approximations	48
3.1.5	Linearizing the time-reversal	49
3.2	A way around: effective quantum mechanical formulation	50
3.2.1	Master equation and Doi-Peliti formalism	50
3.2.2	Passage to a field theory	53
3.2.3	Cole-Hopf transformation	55

3.2.4	An alternative linearization of the time-reversal	55
3.3	A detour by the Fredrickson-Andersen model	57
3.3.1	The model: dynamics without the statics	58
3.3.2	Building self-consistent equations for correlation functions	60
3.3.3	Mode-Coupling like equation	61
3.4	Application to the dynamics of harmonic spheres	64
3.4.1	Diagrammatic structure and time-reversal	64
3.4.2	Mori-Zwanzig equation	65
3.4.3	Calculation to lowest order in the potential	66
3.4.4	A new symmetry	69
3.4.5	Discussion	69
4	The replica method for structural glasses	71
4.1	Focusing on the long time limit: the replica method	71
4.1.1	Ergodicity breaking and complexity	72
4.1.2	Order parameter for the glass transition	73
4.1.3	Computing the complexity with replicas	75
4.2	Replicated liquid theory	76
4.2.1	Replicated Hyper-Netted-Chain approximation	78
4.2.2	Expansion in the non-ergodicity parameter	80
4.3	Expansion at third order	81
4.3.1	Computing the liquid three-body correlations	84
4.3.2	Conclusion	85
5	Jamming transition of harmonic spheres	87
5.1	Jammed states as the densest glassy states	87
5.1.1	Thermodynamics of the glass phase	89
5.1.2	Effective potential approximation	90
5.1.3	Low temperature liquid theory approximation	92
5.2	Thermodynamics of the glass	93
5.2.1	Complexity and phase diagram	93
5.2.2	Relaxation time and glass fragility	94
5.2.3	Free-energy of the glass	95
5.3	Jamming point of harmonic spheres	96
5.3.1	Zero temperature, below close packing	97
5.3.2	Zero temperature, above close packing	97
5.3.3	Scaling around jamming	98
5.4	The pair correlation function	99
5.4.1	General expression of the correlation function of the glass	99
5.4.2	Scaling of the peak of the pair correlation at finite temperature	100
5.4.3	Zero temperature below jamming: hard spheres	101
5.4.4	Zero temperature above jamming	102
5.5	Scaling around jamming: comparison with numerical data	103
5.5.1	Details of the numerical procedure	103
5.5.2	Difficulties in the comparison with the theory	103
5.5.3	Energy, pressure, average coordination	104

5.5.4	Correlation function	105
5.5.5	Discussion	106
5.6	Conclusions	109
5.6.1	Summary of results	109
5.6.2	Technical aspects	109
5.6.3	Some general directions for future work	110
6	Conclusion and perspectives	111
6.1	Dynamics near the glass transition	111
6.2	Bridging the gap between statics and dynamics	112
6.3	Towards a full theory of the jamming transition	113
	Publications	115
	Bibliography	116

Chapter 1

Introduction

1.1 Theory of amorphous solids

This thesis is devoted to the theoretical analysis of the properties of amorphous solids. Amorphous solids are ubiquitous in daily life: window glass, optical fibers, metallic glasses, plastics, ... all of those are amorphous solids, i.e. materials that have a disordered microscopic structure similar to that of dense liquids, while being solid on macroscopic scales. Despite many years of research efforts by theoreticians and experimentalists, the understanding of this kind of materials is still largely empirical, and no comprehensive physical theory has been devised yet. Many theoretical scenarios exist [14], but for the moment a coherent and quantitative theory of amorphous solids that would start from the microscopic scale, aiming at deriving the existence and properties of an amorphous solid phase, is still lacking.

This state of affairs poorly compares with the situation in liquid theory [74] or solid-state theory [7], where accurate quantitative theories allow for first-principles predictions for virtually any model. In liquid state theory, the validity of the ergodic hypothesis, i.e. the assumption that the system is able to visit all its possible configurations in a “short” time (when compared to the typical time of an experiment) allows for the use of equilibrium statistical mechanics, greatly reducing the theoretical difficulty. In the case of the solid state, the existence of a fixed lattice on which particles are attached allow for the treatment of quantum fluctuations thanks to invariance properties of the lattice, and to the localized classical trajectories of the particles.

In the case of amorphous solids, the disordered, liquid-like, positions of the particles require a description with the level of complexity of the liquid state theory, at least for what concerns static properties, but the ergodic hypothesis is not verified: amorphous materials are generically out of equilibrium, either because their relaxation time is comparable to the duration of an experiment or because microscopic configurations are forbidden due to mechanical constraints. Additionally, no underlying lattice symmetry is present to simplify the problem. As a consequence, the theoretical treatment of amorphous solids is mostly based on tools borrowed from liquid state theory, and a short introduction to its formalism is presented in the second part of chapter 2 of this thesis.

Many of the theoretical developments in the field of the glass transition have been concentrated on the study of idealized models [116], that aim at suppressing the complexity of the problem while keeping the essential ingredients needed to observe a phenomenology akin to that of amorphous solids. In this thesis we will systematically start from realistic finite-dimensional models, trying to derive from first-principles, and in a controlled way, the existence and properties of an amorphous phase, and to

understand the relations between different existing theoretical scenarios. Because of the difficulty of dealing with finite-dimensional, non-idealized systems, the range of questions addressed by such an approach is limited when compared to what can be learnt from numerical experiments or by heuristic arguments, but we believe that the quantitative implementation of the vast amount of theoretical ideas that emerged in the last decades in realistic models will give a firm basis for future developments of the field, and is complementary to other approaches.

Glassy and jammed systems

Amorphous materials can be separated into two classes: the ones that are composed of molecules or atoms of size of the order of the Angström, and are formed at finite temperature, that are called structural glasses [22], and the ones composed of a large number of particles of sizes ranging from the micrometer to the centimeter, insensitive to thermal fluctuations [136].

Structural glasses can be formed starting from virtually any stable liquid, by many procedures [6], the most common one being the quench: the liquid has to be sufficiently rapidly cooled down below its melting temperature, avoiding the formation of crystalline states [35]. This is always possible thanks to the nature of the transition from liquid to solid: the formation of the crystalline structure requires the nucleation of a droplet of crystal inside the liquid, which is locally unfavorable when compared to the liquid structure, even though it is thermodynamically more stable. Thus cooling down at a sufficiently large rate will not open up the possibility of such nucleation, at least on experimental time scales. When the liquid has been placed below its melting temperature, it is said to be supercooled. The physical properties of supercooled liquids are at first indistinguishable from their liquid counterparts and can be deduced from the standard theory of liquids. However, when the system is further cooled down, its dynamics start to slow down very rapidly, and its viscosity increases by many orders of magnitude. The system then falls out of equilibrium and becomes an amorphous solid.

Athermal amorphous solids are formed by starting from a dilute assembly of particles in a box, and either pouring more and more objects in the box [12], inflating them [100] at constant rate while allowing the particles to move, or performing a sequence of inflations and minimization of the energy of the system [127], all procedures having the effect of increasing the density of objects, until mechanical rigidity is attained. These procedures are in essence non-equilibrium, free of thermal fluctuations that govern the behavior of glasses. As a consequence, the final states attained by these procedures, sometimes called jammed states, strongly depend on the followed protocol. The question of the maximal density that can be realized by such amorphous solids and the properties of the corresponding packings are largely open questions, and have deep connections in mathematics and computational sciences [44].

1.1.1 Thermal systems: the glass transition

The very large increase of the viscosity upon cooling liquids below their melting point is called the glass transition, suggesting the idea that a proper thermodynamic phase transition exists from the liquid to the amorphous solid. However, experimentally no sharp transition can be detected: for example following the evolution of the viscosity, no proper divergence can be extracted from experiments, and the glass transition temperature T_g is often arbitrarily set to the temperature at which the viscosity η has reached 10^{13} Poise. One can alternatively follow the evolution of the relaxation time of the system, that also increases drastically upon lowering the temperature. An early important remark is that structural glasses separate into two important classes: fragile and strong. This separation is

obvious when we represent the evolution of the viscosity on an Angell plot [5, 72], i.e. representing the logarithm of the viscosity against the temperature in units of T_g . An example of such plot, taken from [5], is given in Figure 1.1. By definition of T_g , all curves must meet at $T/T_g = 1$ for which the logarithm of the viscosity (in base 10) must be equal to 13. We see that two tendencies arise: strong liquids for which the growth of the viscosity is essentially exponential, and fragile ones for which the growth is super-exponential upon approaching the transition. This dramatic increase of viscosity is

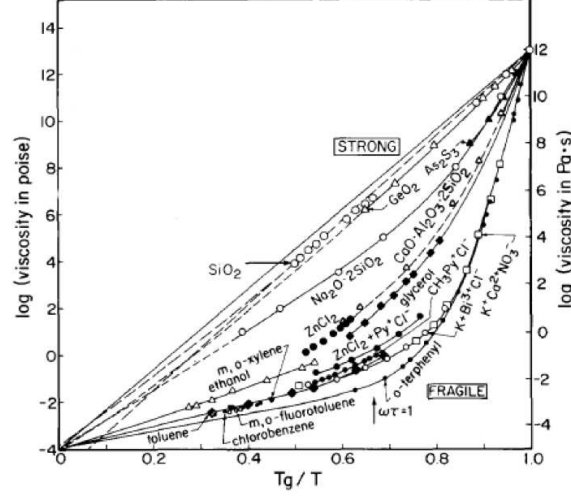


Figure 1.1: Viscosity against reduced temperature for various glass formers. A clear cut separation between two classes of glasses is observed, and corresponds to different behaviors of the activation energy required for relaxation. (from [5])

directly linked to the relaxation time τ_α of the system through a Maxwell model that gives $\eta = G_\infty \tau_\alpha$, where G_∞ is the instantaneous shear modulus. Relaxation processes in the system can schematically be imagined to be an accumulation of well-defined single events, such as the sudden escape of one particle from its local environment, that have an energy cost E (the “activation” energy). In that case the relaxation time will be described by an Arrhenius law:

$$\tau_\alpha = \tau_0 \exp\left(\frac{E}{k_B T}\right), \quad (1.1)$$

and the behavior of the viscosity in Fig. 1.1 allows us to identify the activation energy as the slope of the curves. For strong materials, such as Silica, the Arrhenius law is satisfied, but for fragile materials such as o-Terphenyl, the activation energy itself depends on temperature. This is consistent with the commonly observed Vogel-Fulcher-Tamman law which states that the relaxation time should diverge with inverse temperature as:

$$\tau_\alpha = \tau_0 \exp\left(\frac{DT_0}{T - T_0}\right), \quad (1.2)$$

and seems to be consistent with several sets of experimental data. This picture suggests that, for fragile liquids, the relaxation events in a supercooled liquid upon approaching its glass transition become more and more energetically costly, i.e. more and more cooperative, possibly associated with a divergence at finite temperature T_0 , which should thus be identified with T_g , the glass transition. However the range of available data is not sufficient to provide an unambiguous fit, and other functional forms can be chosen, that support a transition at zero temperature. The idea of a local “cage” formed

by the neighbors of each particle is however appealing, and is thought to be the basic mechanism behind the physics of amorphous solids.

In dense liquids, a way to quantify the local environment of a single particle is to consider the radial distribution function $g(r)$, which is the probability of finding a particle at distance r of a given particle [74]. To compute it, we first define the microscopic density $\hat{\rho}$ as:

$$\hat{\rho}(x, t) = \sum_{i=1}^N \delta(x - x_i(t)), \quad (1.3)$$

where $x_i(t)$ is the position of particle i at time t . Obviously the average of this over many different experiments will give the average number of particles in the system ρ :

$$\rho(x, t) = \langle \hat{\rho}(x, t) \rangle. \quad (1.4)$$

Not much can be learnt from this quantity since it is expected to be constant in time and space if translational and time-translational invariance are respected, i.e. for homogeneous liquids at equilibrium. The radial distribution function is thus by definition related to the (normalized) equal time value of the second moment of this quantity:

$$g(x - y) = \frac{\left\langle \sum_{i \neq j} \delta(x - x_i(0)) \delta(y - x_j(0)) \right\rangle}{\rho^2} = 1 + \frac{\langle (\hat{\rho}(x, 0) - \rho)(\hat{\rho}(y, 0) - \rho) \rangle}{\rho^2} - \frac{1}{\rho} \delta(x - y), \quad (1.5)$$

where we made it obvious that for homogeneous systems, g only depends on one variable. The static structure factor $S(k)$ is related to the Fourier transform of g by:

$$S(k) = 1 + \rho \int_x e^{ik \cdot x} [g(x) - 1] = \frac{1}{\rho} \int_x e^{ik \cdot (x-y)} \langle (\hat{\rho}(x, 0) - \rho)(\hat{\rho}(y, 0) - \rho) \rangle. \quad (1.6)$$

The function g has a characteristic shape in dense liquids, shown in the left frame of Fig. 1.2: it is

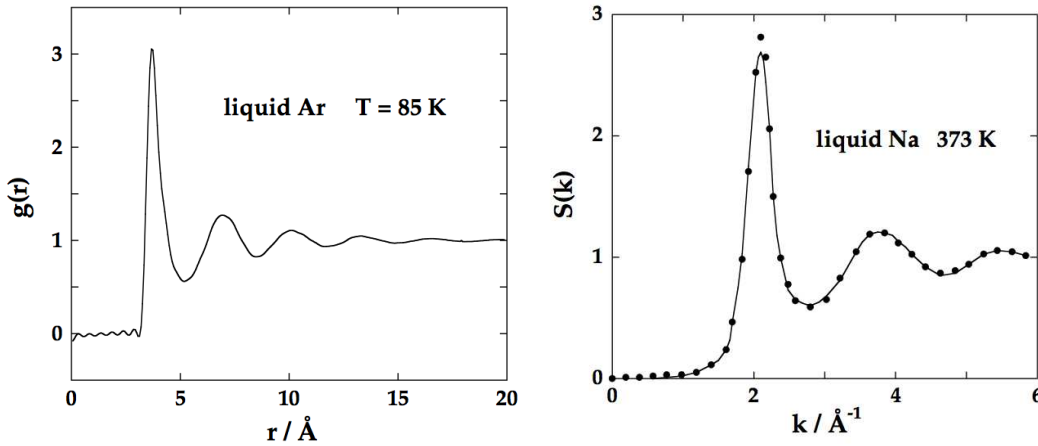


Figure 1.2: Left: Schematic form of the radial distribution function of a simple liquid. $g(r)$ is equal to 0 for small distances, has marked peaks at $\sigma, 2\sigma, \dots$, and decays to 1 at large distances. Right: Corresponding schematic form of the structure factor of a simple liquid. From [74]

equal to zero for distances smaller than the particle diameters σ , reflecting the hard-core repulsion between particles, has a very strong peak at $r = \sigma$ reflecting the fact that a particle is surrounded by

a spherical shell of neighbors, then has subsequent peaks at $r = 2\sigma, 3\sigma, \dots$ of decreasing intensity, and finally decreases to 1 at long distances, reflecting the fact that no long range order exists in a liquid. The Fourier transform of $g(r) - 1$, shown in the right frame, is called the structure factor $S(k)$, and is directly accessible in neutron diffusion experiments, or light diffusion experiments in the case of colloids [13].

For liquid states, the knowledge of the pair distribution function, i.e. a static two-point function is enough to quantitatively deduce the thermodynamics and dynamics of the system. However such observable is essentially blind to the presence of the glass transition, since it is observed in the experiments that the glass is essentially an arrested liquid configuration. A better observable has to be found in order to discriminate between the supercooled liquid and the amorphous solid.

Order parameters for the glass transition

This idea of a caging effect is better described by a dynamic correlation function: consider the time evolution of the position of one particle of the fluid. If a caging effect is present, the particle will spend most of its time vibrating around its initial position, until it will eventually be able to escape its cage. Instead of computing the density-density correlation function at equal times as in Eq.(1.6), we can compute the dynamic structure factor $S(k, t)$ with:

$$S(k, t) = \frac{1}{\rho} \int_x e^{ik \cdot (x-y)} \langle (\hat{\rho}(x, t) - \rho)(\hat{\rho}(y, 0) - \rho) \rangle. \quad (1.7)$$

By definition this function reduces to the static structure factor at $t = 0$. The behavior of $S(k, t)$ for

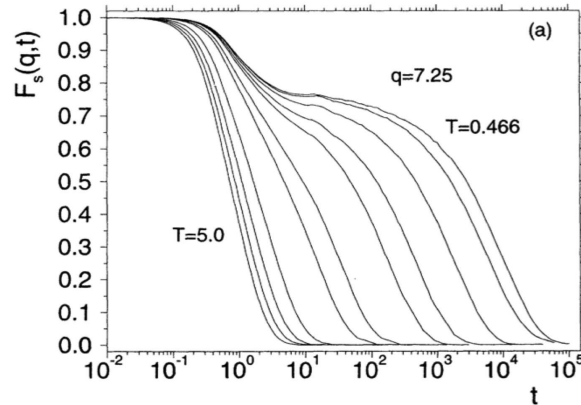


Figure 1.3: Time evolution of the self part (i.e. restricting to $i = j$ in Eq. (1.5)) of the dynamical structure factor of a model of glass-former, for wave vector $2\pi/\sigma$, for several temperatures above the glass transition. (from [94])

a typical glass former is shown in Fig. 1.3 for one given wave vector $k \approx 2\pi/\sigma$, which corresponds to a probe of the dynamics at the scale of one particle. At high enough temperatures, the relaxation is exponential just like in a liquid, particles are able to move freely in the fluid. However when the temperature is decreased, the function presents a two step relaxation: this is the signature of the cage effect discussed above. First a typical particle vibrates inside its cage, which corresponds to the initial relaxation, a process called β relaxation, then the relaxation saturates for a long time, while the particle is confined into its cage, finally the particle is able to escape its cage, and starts to explore more of its phase space, which leads eventually to its final de-correlation, the so-called α

relaxation (which explains the α subscript of the relaxation time of the system in Eq.(1.1)). Below the glass transition temperature, when the system falls out of equilibrium, the plateau developed by $S(k, t)$ eventually extends to infinite times, which reflects the fact that $\tau_\alpha \rightarrow \infty$, which implies broken ergodicity. Thus this dynamical function appears as a good order parameter for the glass transition: defining the non-ergodicity factor $f(k)$ as:

$$f(k) \equiv \lim_{t \rightarrow \infty} \frac{S(k, t)}{S(k)}, \quad (1.8)$$

f jumps from 0 in a supercooled liquid, ergodic, phase, to non-zero values below the glass transition.

The correct order parameter for the glass transition is thus a two-point quantity, and the first task of a microscopic theory of glasses is to be able to derive from first-principles the existence of correlation functions that do not decay to zero at long times. This is a very different situation from that of the liquid-gas or the liquid-solid transitions: in both transitions the one-point density is enough to discriminate between different phases. In the liquid-gas transition the system will separate from a gas phase with uniform density to a coexistence between liquid and gas, where the density takes two different values. In the liquid-solid transition, the density switches from a uniform value in the system to a non-uniform value which presents modulations that reflect the lattice symmetry of the ordered phase. Thus accurate theories, such as the density functional theory [144] described below, can be built by looking at the free-energy of the system as a function of density, and comparing uniform density profiles to non-uniform profiles. For example the Ramakrishnan-Yussouf theory of freezing [134], which is the starting point of many theories of freezing, even in the context of glasses [145, 48, 88, 38], aims at finding non-uniform density profiles minima for a suitable free-energy. In this way amorphous glassy profiles can be obtained, as well as periodic density profiles that correspond to a crystal phase.

1.1.2 A-thermal systems: the jamming transition

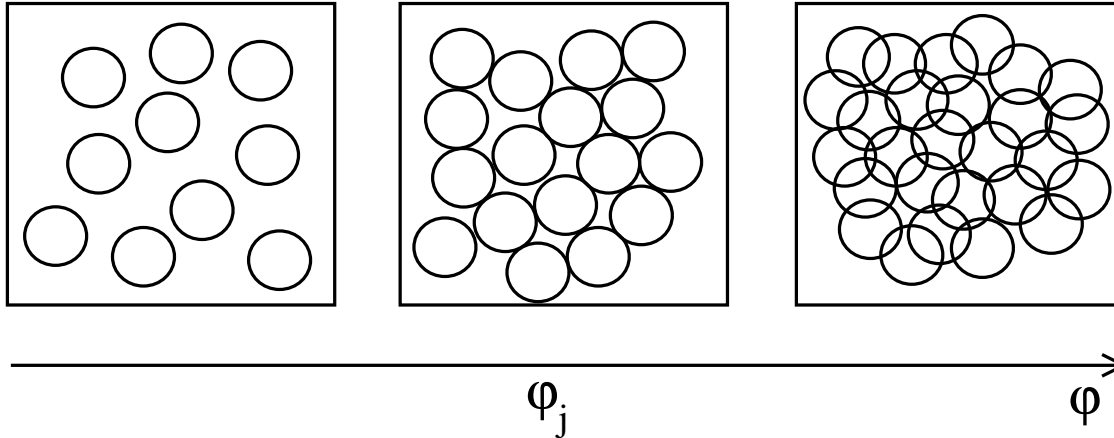


Figure 1.4: Schematic picture of the jamming transition. Upon increasing $\varphi = \pi\rho\sigma^3/6$, the fraction of the volume of space occupied by the spheres, a transition from zero contacts states to states with finite number of contacts is observed.

In the case of a-thermal systems such as heaps of grains, powders or foams, it has been observed experimentally and numerically that many physical quantities display critical scaling around the density at which the system acquires rigidity. A very large amount of numerical effort has been put since

several years for the study of frictionless, spherical and deformable particles, that have a finite range interaction, and here we restrict the discussion to such systems for simplicity.

In commonly used algorithms [148, 127, 100], an assembly of such particles, initially randomly distributed, is gradually inflated, while minimizing its energy, or running microscopic dynamics, between each inflation step. Physical observables are then computed as averages over many realizations of one of the packing protocols described above. As long as the density is low, the lowest energy (amorphous) configuration is a state where there are no contacts between spheres. Of course this situation can not persist forever and a density exists above which no amorphous configuration without contacts can be found, and spheres begin to be deformed with finite energetic cost.

This situation is pictorially described in Figure 1.4. The density φ_J at which contacts begin to appear is called the Jamming point. At jamming, roughly situated around 0.64 for 3 dimensional frictionless spheres, the average number of contacts per particle z jumps from 0 to a finite value z_c , equal to $2d$ for spherical frictionless particles [126], where d is the spatial dimension (2 or 3 for the systems of experimental interest). This value is precisely the minimal number of contacts required for a packing of spheres to be mechanically rigid: the packings are called isostatic [106]. When compressing the spheres further, z displays critical scaling with $\varphi - \varphi_J$, the distance to the jamming density, and so do thermodynamic quantities such as pressure and energy.

The radial distribution function defined above develops a diverging peak at $r = \sigma$ upon approaching jamming, reflecting the fact that particles are found at contact with probability 1. Indeed the integral of this diverging peak counts the number of neighbors, and thus is equal to $2d$ at jamming. Many more interesting scaling relations and critical behaviors, also concerning the rheology of these packings have been discovered, but the first-principles approach adopted in our work will be limited to the aforementioned properties, and the reader is advised to refer to specific reviews ([155], [81]).

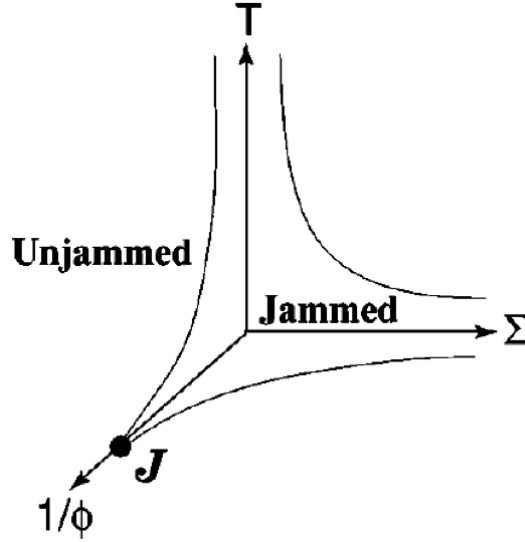


Figure 1.5: Jamming phase diagram, as proposed by Liu and Nagel. The inverse volume fraction, temperature and Stress imposed on the material are the three main control parameters involved in amorphous solids. The temperature–density plane contains the structural and colloidal glasses, while the plane stress–density concerns granular matter. The Jamming point is a point on the zero temperature and zero applied stress axis, and is postulated to influence its vicinity at $T \neq 0$. (from [127])

The jamming transition can be seen as the extreme case of the cage effect: at jamming the particles do not have any space available to vibrate. It is thus tempting to associate the two phenomena by imagining that the jamming transition could be the real mechanism behind the glass transition. This hypothesis would support the idea of a true divergence of the relaxation time at zero temperature.

Following this line of thought, Liu and Nagel [97] proposed to gather all amorphous solids on a single phase diagram, shown in Fig. 1.5. In a diagram with inverse density, applied stress and temperatures as the axes, they identify a jammed phase for high density, low temperature and low applied stress. Indeed, an amorphous solid will always yield under a high enough stress, or start to flow at high enough temperature, or low enough density. The proper jamming point lies at a high density in the zero temperature, zero applied stress axis, and is postulated to control its vicinity. In particular the glass transition would be controlled by this zero-temperature fixed point. Although physically appealing, such relation between jamming and glass transition is mostly hypothetical, since the studies of the jamming transition almost exclusively focus on the zero temperature part of this phase diagram.

1.2 Current theoretical approaches

There are currently two analytical approaches that are able to predict the divergence of the viscosity for realistic models of glass formers by starting from a microscopic description and performing well-defined approximations (even if they are not *a priori* justified !): Mode-Coupling Theory (MCT) [146, 70], which is a theory that describes the dynamics of dense liquids in terms of the dynamical structure factor $S(k, t)$, and the Random First Order Transition theory (RFOT) [90, 91] which is a theory that focuses on the long time limit of the dynamical processes, working in a static framework only.

In the context of the jamming transition, no microscopic theory is able to predict the existence of jammed states and deduce the critical scalings of the different physical observables that are observed numerically or in the experiments. However, an adaptation of the RFOT to high-density states of hard spheres [130] has been able to identify glassy states of hard spheres with diverging pressure at a value close to the usual random close packing density 0.64 in three dimensions, and contact number very close to the isostatic value.

1.2.1 Dynamics: Mode-Coupling theory

Starting from Hamiltonian dynamics and focusing on slowly varying collective variables such as the density, one is able to formally derive, using the so-called Mori-Zwanzig projection operator formalism [167, 120], a closed equation for the dynamical structure factor $S(k, t)$ defined in Eq.(1.7) that reads:

$$\frac{m}{k_B T} \frac{\partial^2 S(k, t)}{\partial t^2} + \frac{k^2}{S(k)} S(k, t) + \frac{\rho}{2} \int_0^t dt' K(k, t - t') \frac{\partial S(k, t')}{\partial t'} = 0. \quad (1.9)$$

All the complexity of the dynamics is now hidden in the calculation of the memory kernel K , which involves correlations between the density and all the other hydrodynamic variables in the system. The closure approximations made within Mode-Coupling Theory (MCT) lead to the following form for the memory kernel [11]:

$$K(k, t) = \int_q \left[\frac{k \cdot q}{k} c(q) + \frac{k \cdot (k - q)}{k} c(k - q) + \rho c^{(3)}(k, -q) \right]^2 S(q, t) S(k - q, t) \quad (1.10)$$

The third-order direct correlation function that appears in the kernel is usually neglected by resorting to the factorization approximation whose effect is to simply eliminate it. Furthermore, it has been shown to be negligible when compared to the term involving the second-order direct correlation function [9]. Eq.(1.9) combined with Eq.(1.10) constitutes a closed equation bearing on $S(k, t)$ that can be solved given the equilibrium correlations of the liquid.

Letting the time go to infinity in these equations gives a self-consistent equation for the non-ergodicity parameter $f(k)$ defined in Eq.(1.8):

$$\frac{f(k)}{1 - f(k)} = \frac{\rho S(k)}{2} \int_q \left[\frac{k \cdot q}{k^2} c(q) + \frac{k \cdot (k - q)}{k^2} c(k - q) + \rho c^{(3)}(q, k - q) \right]^2 S(q) S(k - q) f(q) f(k - q) \quad (1.11)$$

Numerically solving this self-consistent equation predicts the appearance, at constant density and below a critical temperature T_{MCT} , of a non-zero solution for $f(k)$, signaling ergodicity breaking and the appearance of a glass phase. Within MCT, the relaxation time is predicted to diverge at T_{MCT} with a power-law:

$$\tau_\alpha \sim \left(\frac{T - T_{\text{MCT}}}{T_{\text{MCT}}} \right)^{-\gamma}, \quad (1.12)$$

For T very close to the critical temperature, $S(k, t)$ presents a two-step behavior such as the one showed in Fig. 1.3. The approach of $S(k, t)$ to its plateau value (the β -relaxation) is given by:

$$\frac{S(k, t)}{S(k)} - f(k) \sim t^{-a}, \quad (1.13)$$

and the beginning of the α -relaxation, i.e. the final de-correlation at long times in the ergodic phase is given by:

$$\frac{S(k, t)}{S(k)} - f(k) \sim -t^b \quad (1.14)$$

The three exponents a, b and γ are not independent, but verify scaling relations [11, 68]:

$$\lambda = \frac{\Gamma(1 - a)^2}{\Gamma(1 - 2a)} = \frac{\Gamma(1 - b)^2}{\Gamma(1 - 2b)}, \quad (1.15)$$

$$\gamma = \frac{1}{2a} + \frac{1}{2b}, \quad (1.16)$$

so that all exponents can be deduced from the knowledge of λ , which itself solely depends on the structure of the equation for the non-ergodicity factor Eq.(1.11) [68]. The predictions of MCT for the power-law scalings Eq.(1.13,1.14) are well verified experimentally [69], but the prediction for the critical temperature T_{MCT} is too high, predicted by MCT to be higher than T_g , the experimental glass transition, which is at worst an upper bound for the true transition, if it exists at all. Thus when comparing experiments with theoretical predictions, adjustments of γ and T_{MCT} are usually made to obtain the values of a and b for example. Given the difficulty to obtain accurate measurements for very long times, the ambiguities inherent to such adjustments can not be ignored.

Recently, several experiments [28, 62] have confirmed that the scalings predicted by MCT are only valid when the system is not too close to the transition, while closer to the transition the system enters another regime, where the power-law divergence of the relaxation time is strictly ruled out. The failure of MCT is commonly explained by the fact that MCT neglects activated events, i.e. temperature-induced escapes of local metastable states. MCT is thus seen as a “mean-field” theory, even though it has been shown recently to break down in high dimensions [36]. The approximations involved when expressing the kernel K in Eq.(1.9) are thus probably ill-behaved and call for improvement [26].

Careful inspection of equivalent dynamical theories have shown [4] under mild assumptions that the scaling predictions Eqs.(1.13–1.16) are in fact universal predictions for any dynamical theory that predicts the existence of a critical temperature at which $S(k, t)$ does not decay to zero at long times. Thus the quantitative failure of MCT must not hide the fact that it could provide an excellent starting point in order find an accurate theory, able to predict the avoided singularity that seems to be observed numerically and experimentally. Recent extensions of MCT [47, 71] have claimed to predict this avoided singularity by including coupling to currents in the theory. However, the approximations performed to obtain this theory were later shown to violate a number of physical requirements [34], and have to be rejected for now. Moreover, such currents do not exist in colloidal systems, and another scenario must be built to deal with that case.

1.2.2 Random-First-Order Transition theory

Kauzmann noted very early that if one separates the total entropy of a glass former into a vibrational part, that accounts for the solid-like motions of the particles inside their cages, and a configurational part, that accounts for the liquid-like rearrangements that occur when cooperative movements allow the cages to reorganize, the latter is seen to decrease upon approaching the glass transition [84], as is shown in Fig. 1.6. The system then falls out of equilibrium and the configurational entropy saturates

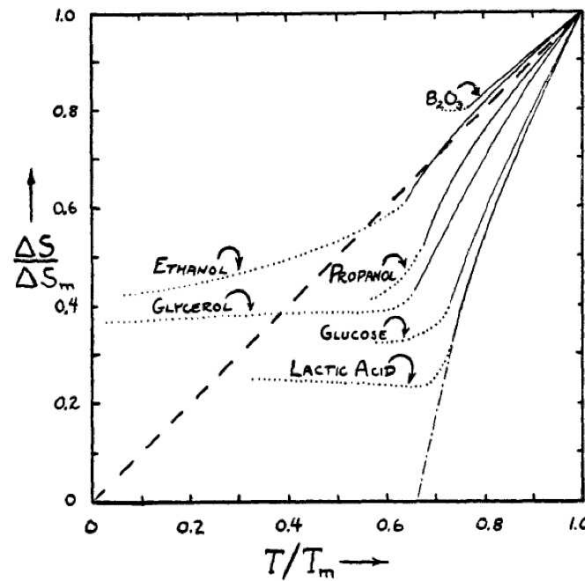


Figure 1.6

at a finite value. But Kauzmann noted that one could extrapolate the decrease of the configurational entropy all the way to zero, and that this canceling would then occur at a non-zero temperature T_K . Since an entropy cannot become negative, the system has to undergo a phase transition at this point. This hypothetic transition is commonly called the Kauzmann ideal glass transition.

Adam, Gibbs and Di Marzio [66, 1] have interpreted this in terms of cooperatively rearranging regions, the sizes of which increase upon lowering the temperature. As more and more particles need to be cooperatively moved in order to perform a structural relaxation of the system, the relaxation

time increases accordingly. The relaxation time would then obey:

$$\tau_\alpha = A \exp \left(\frac{C}{TS_c(T)} \right), \quad (1.17)$$

where S_c is the configurational entropy. An entropy crisis where $S_c \rightarrow 0$ thus leads to a diverging relaxation time. In particular if the configurational entropy was found to vanish linearly, we would obtain the VFT law of Eq.(1.2).

This scenario has found a concrete application in the case of mean-field models of spin-glasses [116, 33], where it has been shown to hold exactly. The p-spin glass model [56, 73] is the paradigmatic model that has the phenomenology closest to that of structural glasses. In this model it is found that below a certain temperature T_d , a dynamical transition takes place because of the appearance of an extensive number of metastable states. One is led to define the complexity Σ as the extensive part of the number \mathcal{N} of metastable states:

$$\Sigma = \lim_{N \rightarrow \infty} \frac{1}{N} \ln \mathcal{N}, \quad (1.18)$$

where N is the number of particles in the system, and a finite Σ is found to appear for $T < T_d$.

Because these are mean-field models, the free-energy barriers between these states are infinite, and the system dynamically gets stuck for infinite times in one state, causing ergodicity breaking. However, thermodynamically, all these states are equivalent and no proper transition occurs at T_d . Upon decreasing the temperature, the number of relevant metastable states diminishes, until becoming sub-extensive. At that point, a thermodynamic phase transition occurs and there is only one state that dominates the partition function: the ideal glass. This critical temperature is thus naturally associated to the Kauzmann temperature T_K .

Beyond mean-field, activated events can allow for jumps between different metastable states, and one thus expects that the relaxation time will not diverge at T_d but only at T_K [90, 27]. Making the identification $S_c \leftrightarrow \Sigma$, the relaxation time should thus diverge at T_K as:

$$\tau_\alpha \sim \exp \left(\frac{C}{T\Sigma(T)} \right), \quad (1.19)$$

making contact with the Vogel-Fulcher-Tamman law and the conjecture of Kauzmann.

Furthermore, the divergence of the relaxation time was shown [90] to be described by equations similar to the Mode-Coupling ones at T_d . The hypothetical extension of this set of predictions made on mean-field disordered spin glasses to finite dimensional structural glasses has been named the Random-First-Order Transition theory. It is an elegant construction, but until recently, it was solely based on exact results found in models that can be argued to be quite far from the reality of structural glasses.

However, a series of works of Monasson [118], Mézard and Parisi [113, 114], and Cardenas, Franz and Parisi [31] have shown that this theoretical approach could be applied to models of structural glass formers, with qualitative success only.

1.3 Questions discussed in this work

1.3.1 Approach developed in this thesis

In this thesis, we have studied a model of harmonic spheres. This is a system of spherical and frictionless particles that interact via a pair potential

$$v(r) = \begin{cases} \varepsilon \left(1 - \frac{r}{\sigma}\right)^2 & \text{if } r < \sigma \\ 0 & \text{otherwise} \end{cases}, \quad (1.20)$$

where ε is an energy scale, r is the distance between two centers of spheres, and σ is the diameter of the spheres. This model has been introduced by Durian in the context of foam mechanics [60], and is now one of the paradigmatic models for studying the jamming transition [127].

Apart from being useful in the context of jamming, this pair potential can be seen as modelling the interaction between soft colloids in a dense regime [140, 63]. These colloids usually are polymer particles of poly (methylmethacrylate) (PMMA) [158, 62] or poly(N-isopropylacrylamide) (p-NIPAM) [142, 43] immersed in a solvent. Each polymer particle undergoes Brownian motion due to the presence of the solvent at finite temperature, and in the case where they are able to interpenetrate slightly, their mutual repulsion can be modeled by a simple harmonic repulsion like Eq.(1.20). Their Brownian nature introduces thermal fluctuations, which allows for a statistical treatment of the dynamics, contrary to Hamiltonian dynamics. They have been studied at finite temperature [20, 21, 165] and shown to reproduce the behavior of structural glass formers.

From the point of view of liquid theory, this potential has a well defined positive Fourier transform, which simplifies the computations. Furthermore, when the temperature decreases to zero, the finite repulsion between two particles cannot be overcome anymore, and the particles become exactly hard-spheres. Indeed, when the temperature goes to zero, the energy scale ε becomes infinite when compared to the thermal fluctuations (i.e. $\varepsilon/k_B T \rightarrow \infty$) and the potential becomes equivalent to an infinite repulsion for $r \leq \sigma$, while still having zero repulsion for $r > \sigma$. This choice of model allows one to investigate both the athermal and the thermal amorphous solids, in a simplified way.

In this thesis, we attempt, without resorting to mean-field toy models and solely by focusing on the harmonic sphere model, to address several questions, which we summarize in the following.

1.3.2 What is the theoretical status of the Mode-Coupling transition ?

Can we find a theoretical framework where Mode-Coupling (or a corrected version of it) is well defined and easily generalizable, without resorting to unphysical approximations ? This question is the object of Chapter 3, where we propose a new framework that makes contact with the field of particle physics, and that solves several difficulties inherent to the treatment of the dynamics of glasses.

In view of the recent results and the RFOT scenario, the ideal result would be to obtain a theory where the dynamical transition is avoided, and a cross-over to a thermodynamic transition is observed.

1.3.3 Does the relation between MCT and the RFOT scenario hold beyond mean-field ?

For the moment, in non mean-field models, Mode-Coupling theory and the RFOT inspired calculations are intrinsically different and can not be compared. Can we make bridges between the two approaches ? This is the subject of Chapter 4, where we compute, from replica theory, a self-consistent equation for the non-ergodicity factor similar to Eq.(1.11).

1.3.4 What is the relation between jamming and the glass transition ?

Finally, is the jamming transition at $T = 0$ related to the glass transition at finite temperature ? Krzakala and Kurchan [86] then Mari, Krzakala and Kurchan [103] have studied mean field models where it has been possible to prove, using replica theory or numerical simulations, that the dynamical arrest of the glass transition and the jamming transition are distinct mechanisms. Whether this situation persists in finite dimensional models is addressed in Chapter 5, where we show that replica theory allows us to properly disentangle the two phenomena, and show that they are indeed different.

Chapter 2

Formalism of many-body systems

We have seen that the proper order parameter for the glass transition is a dynamic two-point quantity. In chapter 4, we will see that, in the context of the random-first-order transition theory, the glass transition can also be characterized by a static two point quantity, via the introduction of replicas. In order to obtain theories that are able to capture a phase transition in terms of two-point quantities, it is convenient to resort to the so-called two-particle irreducible effective action, be it in the dynamic context or in a static context. In the dynamic case, this formalism is well documented in the context of quantum field theory, but less so in the context of classical statistical mechanics. Quantum field theory textbooks give only partial accounts, or do not mention it. In this chapter, we present an overview of the two-particle irreducible effective action, for a generic field theory, and in the special case of liquid theory.

2.1 Statistical field theories

We will generically denote by φ a microstate of the system, i.e. a set of variables or fields that completely determines its microscopic properties. In the case of equilibrium liquid theory, φ can be chosen to be the microscopic density of particles of the system. In the case of a dynamic theory, it can be for example the set of all time trajectories of density profiles. We will in the following denote the space and/or time variables, as well as internal indices (such as spin state for quantum mechanics, or replica indices in the last chapters of this manuscript), by a single number in subscript. Implicit summation over repeated indices is always assumed.

The macroscopic state of the system is supposed to be fully determined by a functional of φ , that we will denote by S . In a statistical field theory, S stands for the action, in the case of equilibrium theory, S would be replaced with the Hamiltonian of the system. The statistical weight of a particular configuration of the field, $\mathcal{P}[\varphi]$, is supposed to be of the form

$$\mathcal{P}[\varphi] = e^{-S[\varphi]}. \quad (2.1)$$

We will be interested in computing the statistical average of an observable \mathcal{O} that depends on the field. This average, denoted by $\langle \cdot \rangle$ in the following, is obtained by summing over all possible realizations of the field, properly weighted by their statistical weights:

$$\langle \mathcal{O}[\varphi] \rangle = \frac{1}{Z} \text{Tr} \mathcal{O}[\varphi] e^{-S[\varphi]}, \quad (2.2)$$

where $\text{Tr} \equiv \int \mathcal{D}\varphi$ and the normalization factor is Z the partition function:

$$Z = \text{Tr} e^{-S[\varphi]}. \quad (2.3)$$

Usually, one wants to compute averages of the field φ or powers of the field. A useful way to generate all averages of φ is to artificially introduce an external field J that is linearly coupled to φ in the action, and consider Z as a functional of the field J . Averages of φ will then be generated by successively differentiating Z with respect to J , and setting J to zero after the calculation to come back to the original theory:

$$\phi_1 \equiv \langle \varphi_1 \rangle = \frac{1}{Z} \frac{\delta Z}{\delta J_1} \Big|_{J=0}, \quad (2.4)$$

$$\langle \varphi_1 \cdots \varphi_n \rangle = \frac{1}{Z} \frac{\delta^n Z}{\delta J_1 \cdots \delta J_n} \Big|_{J=0}, \quad (2.5)$$

where we defined the average field ϕ in equation (2.4). Taking the logarithm of the partition function leads to a new functional W

$$W = \ln Z, \quad (2.6)$$

that generates the set of all cumulants of φ :

$$\phi_1 = \frac{\delta W}{\delta J_1} = \frac{1}{Z} \frac{\delta Z}{\delta J_1} \Big|_{J=0}, \quad (2.7)$$

$$G_{12} \equiv \langle \varphi_1 \varphi_2 \rangle - \langle \varphi_1 \rangle \langle \varphi_2 \rangle = \frac{\delta^2 W}{\delta J_1 \delta J_2} \Big|_{J=0}, \quad (2.8)$$

$$W_{1,\dots,n}^{(n)} \equiv \frac{\delta^n W}{\delta J_1 \cdots \delta J_n} \Big|_{J=0}, \quad (2.9)$$

where we defined the propagator G in Eq.(2.8) because of its specific relevance with respect to higher-order members of the hierarchy. At each order, the n -th cumulant of φ is related to all averages of φ of order lesser or equal to n . To first order the average coincides with the cumulant. The relation at second order is shown in Eq.(2.8). We show here for future use the relation for three-body functions:

$$\begin{aligned} W_{123}^{(3)} &= \langle \varphi_1 \varphi_2 \varphi_3 \rangle - \langle \varphi_1 \rangle \langle \varphi_2 \varphi_3 \rangle + 2 \langle \varphi_1 \rangle \langle \varphi_2 \rangle \langle \varphi_3 \rangle \\ &\quad - \langle \varphi_2 \rangle \langle \varphi_1 \varphi_3 \rangle \\ &\quad - \langle \varphi_3 \rangle \langle \varphi_1 \varphi_2 \rangle, \end{aligned} \quad (2.10)$$

which can be rewritten as:

$$W_{123}^{(3)} = \langle \varphi_1 \varphi_2 \varphi_3 \rangle - \phi_1 G_{23} - \phi_2 G_{13} - \phi_3 G_{12} - \phi_1 \phi_2 \phi_3. \quad (2.11)$$

2.1.1 Feynman diagrams

The action S is, in many-body problems such as the ones we will be interested in, usually too complex to be treated exactly, and one usually resorts to an expansion around a given approximation of the action, that is exactly solvable. In the case of quantum mechanics, the saddle point of the action corresponds to the classical trajectories, so that we can build semi-classical approximations by expanding the action around the saddle-point in inverse powers of Planck's constant. This starting point for expansions is not always justified, depending on the statistical theory that we are considering.

Following the example of quantum mechanics, we evaluate the partition function at its saddle point:

$$\left\{ \begin{array}{l} Z \approx Z^{(0)} \equiv e^{-S[\varphi^*]}, \\ \left. \frac{\delta S[\varphi]}{\delta \varphi_1} \right|_{\varphi^*} = 0, \end{array} \right. \quad (2.12)$$

Now we make a change of variables $\varphi \rightarrow \varphi - \varphi^*$ in the trace defining the partition function:

$$Z = \text{Tr} e^{-S[\varphi + \varphi^*]} \quad (2.13)$$

$$= Z^{(0)} \text{Tr} \exp \left(-\frac{1}{2} \varphi_1 \left. \frac{\delta^2 S[\varphi]}{\delta \varphi_1 \delta \varphi_2} \right|_{\varphi^*} \varphi_2 - \sum_{N=3}^{\infty} \left. \frac{\delta^N S[\varphi]}{\delta \varphi_1 \cdots \delta \varphi_N} \right|_{\varphi^*} \varphi_1 \cdots \varphi_N \right), \quad (2.14)$$

where we performed an expansion of the action around φ^* in powers of φ , and integration over indices is assumed. The expansion around the saddle point has the effect to cancel the constant and linear terms in the action. We gather all the cubic and higher order terms in a functional $S_{\text{ng}}[\varphi]$ and define V_{12} as the quadratic coefficient. We now artificially once again add an external source J coupled to φ to get the following expression of the partition function:

$$Z = Z^{(0)} \text{Tr} e^{-\frac{1}{2} \varphi_1 V_{12} \varphi_2 - S_{\text{ng}}[\varphi] + J_1 \varphi_1} \quad (2.15)$$

In an Ising model, the φ field could be the local magnetization, and the source J would in that case be an external magnetic field. In the case of liquid theory, the field φ is usually the local microscopic density in the liquid, and J is the chemical potential and a possible inhomogeneous external field. Now calculating the partition function can be done perturbatively around the quadratic part:

$$\begin{aligned} Z &= Z^{(0)} \text{Tr} e^{-\frac{1}{2} \varphi_1 V_{12} \varphi_2 + J_1 \varphi_1} e^{-S_{\text{ng}}[\varphi]} \\ &= Z^{(0)} \sum_{N=0}^{\infty} \frac{(-1)^N}{N!} \text{Tr} S_{\text{ng}}[\varphi]^N e^{-\frac{1}{2} \varphi_1 V_{12} \varphi_2 + J_1 \varphi_1}. \end{aligned} \quad (2.16)$$

Expanding S_{ng} in powers of the field, the calculation of Z is reduced to an infinite sum of averages of φ with respect to a quadratic statistical weight. For example if S_{ng} was composed of a cubic term plus a quartic one:

$$S_{\text{ng}}[\varphi] = \frac{g_3}{3!} \varphi_1 \varphi_1 \varphi_1 + \frac{g_4}{4!} \varphi_1 \varphi_1 \varphi_1 \varphi_1 \quad (2.17)$$

the expansion of Z would then become:

$$Z = Z^{(0)} Z_{\text{quad}} \left(1 + \sum_{N=1}^{\infty} \frac{(-1)^N}{N!} \frac{1}{Z_{\text{quad}}} \text{Tr} \left[\frac{g_3}{3!} \varphi_1 \varphi_1 \varphi_1 + \frac{g_4}{4!} \varphi_1 \varphi_1 \varphi_1 \varphi_1 \right]^N e^{-\frac{1}{2} \varphi_1 V_{12} \varphi_2 + J_1 \varphi_1} \right), \quad (2.18)$$

$$(2.19)$$

where Z_{quad} is the partition function of the quadratic theory. This is indeed an infinite sum of averages of φ , under a quadratic weight. The quadratic weight is a generalization of a Gaussian distribution and thus integrals needed to compute averages of φ under such distribution are tractable, at least on a formal level. The average of a product of fields under quadratic weight is given by Wick's theorem [161], and simply expresses the fact that, for a quadratic weight, high-order averages of the field φ only depend on its two first cumulants, that we will call $\phi^{(0)}$ and $G^{(0)}$. The calculation of these quantities is straightforward when looking at Z_{quad} :

$$Z_{\text{quad}}[J] = \text{Tr} e^{-\frac{1}{2} \varphi_1 V_{12} \varphi_2 + J_1 \varphi_1} = \text{Cte} e^{-\frac{1}{2} \int_{12} \ln V_{12} e^{\frac{1}{2} J_1 V_{12}^{-1} J_2}}, \quad (2.20)$$

$$(2.21)$$

hence

$$\phi_1^{(0)} = \frac{1}{Z} \frac{\delta Z}{\delta J_1} \Big|_{J=0} = 0, \quad (2.22)$$

$$G_{12}^{(0)} = \frac{\delta^2 W[J]}{\delta J_1 \delta J_2} \Big|_{J=0} = V_{12}^{-1}, \quad (2.23)$$

where we have set $J = 0$ at the end of the calculations to come back to the original theory. Thus, the full expression of Z will be a sum of integrals that will contain only $G^{(0)}$ functions (often called the “bare” propagator in field theory). This can pictorially be written, to second order in g_3 and g_4 , as (combinatorial factors have been omitted and can be dealt with by a proper definition of the diagrams):

$$Z = Z^{(0)} Z_{\text{quad}} \left(1 - g_4 \text{diagram} + g_3^2 \text{diagram} + g_3^2 \text{diagram} + g_4^2 \text{diagram} + g_4^2 \text{diagram} + g_4^2 \text{diagram} + \dots \right) \quad (2.24)$$

The diagrams above are defined as follows: a black point is an integration point bearing an index, a line joining two black points of indices, say 1 and 2, is a bare propagator V_{12}^{-1} . Integration over repeated indices is understood, and numerical factors have been omitted for simplicity. Also, two diagrams standing side by side mean that the product of the two diagrams is carried out.

Eqs.(2.12–2.24) is only a textbook example of a starting point for expansion and its associated diagrammatic expansion Eq.(2.23). Of course the type of integrals, and thus diagrams that represent them, will depend on the particular theory considered, as well as the approximate starting point for the expansion. The diagrams of liquid theory (the Mayer diagrams [138, 67, 74]) do not have the same characteristics as usual diagrams in dynamical field theories used for glasses. However, we will not need in this chapter to know the particular form of the diagrammatic expansion nor the starting point of calculation, and wish to stay on a more generic level.

2.1.2 Reduction of diagrams: first Legendre transform

Taking the logarithm of the partition function as we did in Eq.(2.6) has a dramatic effect on a diagrammatic expansion of the partition function: it systematically eliminates all diagrams that can be expressed as a product of other diagrams (they are usually called “connected” diagrams), and in a sense reduces the number of diagrams in the complete expression. As we saw in Eq.(2.8), the logarithm of the partition function is the generating functional of the cumulants of the field, that have the property of clustering: they are functions that decay to zero when two coordinates are infinitely far from each other. This property of clustering leads to the disappearance of the disconnected diagrams in the expansion of W . This is the “linked cluster theorem”, a physical demonstration of which can be found in [166], while a very elegant one in terms of replicas can be found in [124].

As an illustration, we show what Eq.(2.24) becomes upon taking its logarithm:

$$W = \ln Z = W^{(0)} + W_{\text{quad}} - g_4 \text{diagram} + g_3^2 \text{diagram} + g_3^2 \text{diagram} + g_4^2 \text{diagram} + g_4^2 \text{diagram} + g_4^2 \text{diagram} + \dots \quad (2.25)$$

The diagrams that were the product of two simpler diagrams have disappeared of the expression.

This procedure of diagrammatic reduction can be continued by performing a Legendre transformation of W with respect to the source field J . Define Γ_1 , a functional of ϕ , as:

$$\left\{ \begin{array}{l} \Gamma_1[\phi] = J_1^*[\phi]\phi_1 - W[J^*[\phi]], \\ \text{with } J^*[\phi] \text{ such that } \left. \frac{\delta W[J]}{\delta J_1} \right|_{J^*} = \phi_1. \end{array} \right. \quad (2.26)$$

We replaced one variable with its conjugate, here J with ϕ . Again this operation will have an effect on the diagrammatic expansion of W : each time a factor J will appear, it will have to be replaced with J^* , which has itself a whole expression as a function of ϕ . By definition of the Legendre transform, we have:

$$e^{-\Gamma_1[\phi]} = \int \mathcal{D}\varphi e^{-S[\varphi] + J^*[\varphi](\varphi - \phi)}. \quad (2.27)$$

Under this form, we see why the Γ_1 functional is often called the effective action: upon integrating the fluctuations (performing the path integral), the microscopic action S becomes a new “effective” action Γ_1 . Expanding Γ_1 and S in Taylor series, the coupling constants in S (g_3 and g_4 in our example) will be renormalized to give the corresponding effective couplings in Γ_1 . Expanding the action around ϕ , we get:

$$e^{-\Gamma_1[\phi]} = e^{-S[\phi]} \int \mathcal{D}\varphi \exp \left(-\frac{1}{2} \left. \frac{\delta^2 S[\varphi]}{\delta \varphi_1 \delta \varphi_2} \right|_{\phi} \varphi_1 \varphi_2 - S_{\text{ng}}[\varphi, \phi] + \left[J_1^*[\phi] - \left. \frac{\delta S[\varphi]}{\delta \varphi_1} \right|_{\phi} \right] \varphi \right), \quad (2.28)$$

where S_{ng} gathers all derivatives of the action of order higher than three, evaluated at ϕ :

$$S_{\text{ng}}[\varphi, \phi] \equiv \sum_{n=3}^{\infty} \frac{1}{n!} \int_{1,\dots,n} \left. \frac{\delta^n S[\varphi]}{\delta \varphi_1 \cdots \delta \varphi_n} \right|_{\phi} \varphi_1 \cdots \varphi_n \quad (2.29)$$

We get by taking the logarithm of Eq.(2.28):

$$\Gamma_1[\phi] = S[\phi] + \ln \left[\int \mathcal{D}\varphi \exp \left(-\frac{1}{2} \left. \frac{\delta^2 S[\varphi]}{\delta \varphi_1 \delta \varphi_2} \right|_{\phi} \varphi_1 \varphi_2 - S_{\text{ng}}[\varphi, \phi] + \left[J_1^*[\phi] - \left. \frac{\delta S[\varphi]}{\delta \varphi_1} \right|_{\phi} \right] \varphi \right) \right]. \quad (2.30)$$

As before, the evaluation of the path integral in Eq.(2.28) can be done by expanding around the quadratic part of the action. The linear term here exactly enforces that the average of φ is 0, a demonstration of which can be found in [79, 29]. Thus we forget about it in practice, but calculate all diagrams at zero average field. The calculation at lowest order, i.e. neglecting S_{ng} , is formally the same than in the expansion of Z and we thus get:

$$\ln \left[\int \mathcal{D}\varphi \exp \left(-\frac{1}{2} \left. \frac{\delta^2 S[\varphi]}{\delta \varphi_1 \delta \varphi_2} \right|_{\phi} \varphi_1 \varphi_2 \right) \right] = Cte - \frac{1}{2} \int_{1,2} \ln G_{12}^{(0)-1}. \quad (2.31)$$

Due to the Legendre transformation, the bare propagator $G^{(0)}$ is now defined as the inverse of

$$\left. \frac{\delta^2 S[\varphi]}{\delta \varphi_1 \delta \varphi_2} \right|_{\phi}, \quad (2.32)$$

whereas this second derivate was evaluated at φ^* before the Legendre transformation. We thus obtain:

$$\Gamma_1[\phi] = S[\phi] + \frac{1}{2} \int_{1,2} \ln \left(G_{12}^{(0)-1} \right) + \{1\text{PI diagrams}\}. \quad (2.33)$$

The 1PI diagrams in the above equation are called one-particle irreducible (1PI) diagrams: they are connected diagrams (because of the logarithm) that cannot be separated in two by removing one line. They must be calculated at zero mean value of the field ϕ because of the particular form of the source term as stated before. The property of one particle irreducibility of the diagrams is not obvious at all, but a transparent proof can be found in [166].

For example, upon performing the Legendre transformation, Eq.(2.25) now becomes:

$$\Gamma_1[\phi] = S[\phi] + \int_{12} \ln \left(G_{12}^{(0)-1} \right) + g_4 \text{ (diagram)} - g_3^2 \text{ (diagram)} - g_4^2 \text{ (diagram)} - g_4^2 \text{ (diagram)} + \dots \quad (2.34)$$

Only a few diagrams are left here to this order in this expansion. The lines in the diagrams, which were V_{12}^{-1} , are now $\left. \frac{\delta^2 S[\phi]}{\delta \phi_1 \delta \phi_2} \right|_{\phi}$, due to the Legendre transformation.

Finally, apart from simplifying computations in terms of diagrams, the Legendre transformation provides us with a variational principle to calculate both the average of the field and the free-energy. Starting from a trivial consequence of the Legendre transformation:

$$\begin{aligned} \Gamma_1^{(1)}[\phi] &\equiv \frac{\delta \Gamma_1[\phi]}{\delta \phi_1} = J_1^*[\phi] + \frac{\delta J_2^*[\phi]}{\delta \phi_1} \phi_2 - \frac{\delta W[J^*[\phi]]}{\delta \phi_1} \\ &= J_1^*[\phi] + \frac{\delta J_2^*[\phi]}{\delta \phi_1} \left(\phi_2 - \left. \frac{\delta W[J]}{\delta J_2} \right|_{J^*} \right) \\ &= J_1^*[\phi], \end{aligned} \quad (2.35)$$

where a use of the chain rule and of Eq.(2.4) has been made. Now starting from this equation, we can change again our viewpoint: instead of considering ϕ as a variable, and J^* defined as the value of J that fixes this particular value of $\langle \varphi \rangle$, we can choose for ϕ the physical average that corresponds to the initial value of J (which can be zero if it had been introduced by hand), let us call it ϕ^* . At this particular value of ϕ , we obtain the physical value of W as:

$$W[J] = J_1 \phi_1^*[J] - \Gamma_1[\phi^*[J]]. \quad (2.36)$$

Mathematically, we have performed the inverse Legendre transform.

Eq.(2.35) is important in regards of the physical symmetries of the problem: it is used to obtain the consequences of the symmetries of the action on the effective action (sometimes called Ward-Takahashi identities), in order to obtain, when performing approximations, a theory that respects all physical requirements.

The program to perform approximations on the partition function is then the following:

- Choose an approximate starting point for the expansion of $\ln Z$
- Write down the corresponding diagrammatic expansion
- Perform the Legendre transform to reduce diagrams
- Truncate the expansion by selecting a class of diagrams and obtain an approximate $\Gamma_1[\phi]$
- Use the variational principle Eq.(2.35) to obtain the approximate ϕ
- Evaluate the approximate functional Γ_1 at this particular value of ϕ to get $\ln Z$

This procedure is in fact much more than a reduction: one can show that keeping only one diagram in the expansion of Γ is equivalent to keeping an infinity of diagrams in $\ln Z$, thus providing better approximations.

Finally, this functional serves as the basis to define a new hierarchy of correlation functions, that we define as the successive functional derivatives of Γ_1 with respect to ϕ . Performing a functional derivative of Eq.(2.35) with respect to ϕ_2 we get:

$$\Gamma_{12}^{(2)}[\phi] \equiv \frac{\delta^2 \Gamma_1[\phi]}{\delta \phi_1 \delta \phi_2} = \frac{\delta J_1^*[\phi]}{\delta \phi_2}. \quad (2.37)$$

We can notice that the *r.h.s.* of the previous equation is nothing but the functional inverse of the propagator. Indeed making use of the chain rule again we can write that:

$$\left. \frac{\delta^2 W[J]}{\delta J_1 \delta J_3} \right|_{J^*} \frac{\delta J_3^*[\phi]}{\delta \phi_2} = \left. \frac{\delta \phi_1}{\delta J_3} \right|_{J^*} \frac{\delta J_3^*[\phi]}{\delta \phi_2} = \frac{\delta \phi_1}{\delta \phi_2} = \delta_{12}, \quad (2.38)$$

which proves, recalling Eq.(2.8), that the second derivative of Γ_1 is the functional inverse of the propagator:

$$\Gamma_{12}^{(2)}[\phi] = G_{12}[J^*[\phi]]^{-1}, \quad (2.39)$$

equivalently rewritten as:

$$\delta_{12} = \frac{\delta^2 \Gamma_1[\phi]}{\delta \phi_1 \delta \phi_4} \frac{\delta^2 W[J]}{\delta J_4 \delta J_2} \Big|_{J^*}. \quad (2.40)$$

Computing a third derivative of this expression with respect to ϕ_3 , we get formally:

$$0 = \frac{\delta^3 \Gamma_1[\phi]}{\delta \phi_1 \delta \phi_3 \delta \phi_4} \frac{\delta^2 W[J]}{\delta J_2 \delta J_4} \Big|_{J^*} + \frac{\delta^2 \Gamma_1[\phi]}{\delta \phi_1 \delta \phi_4} \frac{\delta^2 \Gamma_1[\phi]}{\delta \phi_4 \delta \phi_5} \frac{\delta^3 W[J]}{\delta J_2 \delta J_4 \delta J_5} \Big|_{J^*}, \quad (2.41)$$

And multiplying through by a second derivative of Γ and using Eq.(2.40), we get:

$$\Gamma_{123}^{(3)}[\phi] = -\Gamma_{11'}^{(2)}[\phi] \Gamma_{22'}^{(2)}[\phi] \Gamma_{33'}^{(2)}[\phi] W_{1'2'3'}^{(3)}[J^*[\phi]], \quad (2.42)$$

This is a standard equation that can be found in any textbook on field theory, for example in [166], that expresses the relation between the so-called vertex functions and the cumulants of the field. It is the starting point of a hierarchy of correlation functions $\Gamma_{1\dots n}^{(n)}$ related to the cumulants $W^{(n)}$. At each order, the n -th order functional $\Gamma^{(n)}$ involves all functionals $W^{(m)}$ of order lesser or equal to n . We will use such relations in Chapters 3 and 4. In the context of liquid theory, these functionals are related to the direct correlation functions. In the context of the dynamics of supercooled liquids, the second order functional $\Gamma^{(2)}$ can be identified with the memory kernel of the Mori-Zwanzig formalism.

In the presence of phase transitions, the propagators of the theory often develop singularities or divergences at large wave-lengths, making the diagrams in the expansion of W singular. The vertex functionals $\Gamma^{(2)}$ being the inverse (in Fourier space) of the propagator, they are often free of these divergences. For example, the direct correlation function of simple liquids develops no singularity near the liquid/gas transition [74]. If the order parameter of the transition is a one-point quantity (typically ϕ itself), then due to the regularity of these functions, the phase transition can be detected with approximations of Γ_1 , whereas performing approximations on W would lead to divergent integrals, making the analysis of the transition much harder.

Of course, when the order-parameter of the transition is a two-point quantity, which is the case in the glass transition, as explained in the introduction, it is necessary to go one step further in order to obtain approximations that are able to detect the transition. This is achieved by further Legendre transforming with respect to a two-point quantity, as explained in the following.

2.1.3 Reduction of diagrams: second Legendre transform

As we saw in the introduction, the natural order parameter for the glass transition is a two-point correlation function. Thus, in order to be able to detect a possible transition in terms of this order parameter, it is important to be able to perform accurate approximations on two-point functions. This can be achieved by introducing another Legendre transformation [102, 51, 52, 45], with respect to a two-point quantity.

We consider now Γ_1 as a functional of G_0 in addition of ϕ . By performing a functional derivative of W with respect to $G^{(0)-1}$, we easily see that $G^{(0)-1}$ is conjugated to the two-point average:

$$\begin{aligned} \frac{\delta W[J, K]}{\delta G_{12}^{(0)-1}} &= \frac{1}{2} \langle \varphi_1 \varphi_2 \rangle \\ &= \frac{1}{2} (G_{12}[J, V] + \phi_1 \phi_2), \end{aligned} \quad (2.43)$$

and the same thing holds for the derivative of Γ_1 by properties of the Legendre transform. A Legendre transformation of Γ_1 with respect to $G^{(0)-1}$ will thus have the effect of replacing the bare propagator by G since it will force $\langle \varphi_1 \varphi_2 \rangle = G_{12}$. We will thus obtain [51, 52]:

$$\Gamma_2[\phi, G] = S[\phi] + \frac{1}{2} \int_{12} \ln G_{12}^{-1} + \{2\text{PI diagrams}\}, \quad (2.44)$$

where the 2PI diagrams are now diagrams with G lines, due to the Legendre transformation that replaces $G^{(0)}$ by G , that can not be separated in two parts by cutting two lines. A very complete proof can be found in [45], and partially in modern textbooks such as [40, 29], although the demonstrations found in textbooks are most of the time only partial.

Equivalently to Eq.(2.35) we have as a consequence of the Legendre transformation:

$$\frac{\delta \Gamma_2[\phi, G]}{\delta G_{12}} = \frac{1}{2} \left(G_{12}^{(0)-1} \right)^* [\phi, G] \quad (2.45)$$

This equation can be seen as a variational principle that we can use to obtain approximations on the two-point function G . Performing the inverse Legendre transformation is done by setting $\left(G^{(0)-1} \right)^*$ to its physical value $G^{(0)-1}$.

Now the variational principle in Eq.(2.45) becomes:

$$\left(G_{12}^{(0)-1} \right)^* [\phi, G] - G_{12}^{-1} = 2 \frac{\delta}{\delta G_{12}} \{2\text{PI diagrams}\}. \quad (2.46)$$

Evaluating this equation at the physical correlator, we obtain:

$$\Sigma_{12} \equiv G_{12}^{(0)-1} - G_{12}^{-1} = 2 \frac{\delta}{\delta G_{12}} \{2\text{PI diagrams}\} \Big|_{G^*}. \quad (2.47)$$

$$(2.48)$$

where we have defined the two-point vertex functional Σ as the difference between the bare and renormalized inverse propagator.

To continue with our example, after this Legendre transformation, Eq.(2.49) becomes:

$$\Gamma_2[\phi, G] = \Gamma_{2,0}[\phi, G] + g_4 \text{ (diagram)} + g_3^2 \text{ (diagram)} - g_4^2 \text{ (diagram)} + \dots, \quad (2.49)$$

where $\Gamma_{2,0}$ is the functional written in Eq.(2.44). The lines of these diagrams are now the full propagators G .

In order to perform approximations on the correlation function, the program is then:

- Choose an approximate starting point for the expansion of $\ln Z$.
- Write down the corresponding diagrammatic expansion.
- Perform the double Legendre transform to reduce diagrams.
- Truncate the expansion by selecting a class of diagrams and obtain an approximation of $\Gamma_2[\phi, G]$.
- Use the variational principles Eq.(2.45) to obtain a self consistent equation on G .
- Evaluate the approximate functional Γ_2 at these particular values of ϕ and G to get $\ln Z$.

A crucial property of these truncation schemes is that if the Gaussian part and the non-Gaussian part of the action are separately invariant under a linear symmetry, then the deduced self-consistent equations for the propagator will also possess this symmetry [3]. If the non-Gaussian action is invariant, and if the diagrams are evaluated at the physical propagator, which respects this invariance, then automatically all the 2PI diagrams will also be invariant, and so will be Σ , whatever the chosen truncation of the diagrammatic series. This is true only for a linear symmetry, for which the consequences on the propagators are simply relations between them, that can be enforced when evaluating the diagrams, whereas for a non-linear symmetry, the propagators must satisfy relations that involve higher-order correlation functions, and building a consistent expansion would then require to keep a possibly infinite number of terms in the expansion.

We will exploit this property of the 2PI expansions in Chapter 3 in order to build self-consistent equations for the non-ergodicity parameter that preserves the time-reversal.

2.2 Theory of liquids

We review here the equivalent of the discussion above for the case of equilibrium liquid theory. In that case, the starting point for systematic expansions is chosen to be the ideal gas, and thus the diagrammatic formulation is different from that presented above. However, the idea is still to perform a double Legendre transform to obtain a functional of both mean-field and propagator. This leads to the standard hyper-netted chain approximation, which we will use in the following chapters of this manuscript, and provides the basis for the replica formulation of Chapter 4.

We consider spherical particles of diameter σ , the center of which is located at position x_i in a 3-dimensional space. The particles interact via a pair potential v , have a chemical potential μ and are placed in an external field Ψ . Finally the system is in contact with a thermal bath at temperature T , and can exchange particles with a particle reservoir, so that the probability P_N of observing N particles located at x_1, \dots, x_N is given by the following Boltzmann weight:

$$P_N[x_1, \dots, x_N] = e^{-\beta \sum_{i < j} v(x_i - x_j) + \sum_{j=1}^N (\beta\mu - \beta\Psi(x_i))}, \quad (2.50)$$

where β is the inverse temperature $1/k_B T$, k_B is the Boltzmann constant. We will be interested in computing the microscopic density defined in Eq.(1.4) and its cumulants. For simplicity in the following, three-dimensional space coordinates will be replaced by numerical subscripts, we gather the chemical potential and external field in a single field ν , and we define a dimensionless potential w :

$$\nu_1 = \beta\mu - \beta\Psi_1, \quad (2.51)$$

$$w_1 = -\beta v_1. \quad (2.52)$$

Note that we will most of the time stick to the notation w in the rest of the manuscript.

The probability P_N can be rewritten in terms of these quantities as:

$$P_N[\hat{\rho}, \nu] = e^{\frac{1}{2}w_{12}(\hat{\rho}_1\hat{\rho}_2 - \hat{\rho}_1\delta_{12}) + \nu_1\hat{\rho}_1}, \quad (2.53)$$

so that the equivalent of the action S in the previous section is the potential term $\frac{1}{2}w_{12}(\hat{\rho}_1\hat{\rho}_2 - \hat{\rho}_1\delta_{12})$, the field φ is replaced by $\hat{\rho}$ and the field J is replaced by ν .

Finally the partition function is obtained by summing over all possible configurations, i.e. summing over the number of particles N and integrating over all variables x_i :

$$Z[\nu, w] = \text{Tr} e^{\frac{1}{2}w_{12}(\hat{\rho}_1\hat{\rho}_2 - \hat{\rho}_1\delta_{12}) + \nu_1\hat{\rho}_1}, \quad (2.54)$$

where Tr must now be understood as $\sum_{N=0}^{\infty} \frac{1}{N!} \int dx_1 \cdots dx_N$.

Although it may seem redundant, it will prove useful in the following to consider that the Boltzmann weight is a functional of two fields, $\hat{\rho}$ and $\hat{\rho}^{(2)}$, with $\hat{\rho}^{(2)}$ defined as:

$$\hat{\rho}^{(2)} = \hat{\rho}_1\hat{\rho}_2 - \hat{\rho}_1\delta_{12}. \quad (2.55)$$

This gives:

$$Z[\nu, w] = \text{Tr} e^{\frac{1}{2}w_{12}\hat{\rho}_1^{(2)} + \nu_1\hat{\rho}_1}. \quad (2.56)$$

Since ν is the field conjugated to $\hat{\rho}$, $W[\nu]$ is the generating functional of the cumulants of the density, defined in the same way as in Eqs.(2.7–2.11):

$$\rho_1 \equiv \frac{\delta W[\nu]}{\delta \nu_1}, \quad (2.57)$$

and the propagator and third order cumulant are defined as in the previous section. More interestingly, w is coupled to the function $\hat{\rho}^{(2)}$:

$$\frac{\delta W[\nu, w]}{\delta w_{12}} = \frac{1}{2}\hat{\rho}_{12}^{(2)} \equiv \frac{1}{2}\langle \hat{\rho}_{12}^{(2)} \rangle. \quad (2.58)$$

The correlation function $\rho^{(2)}$ is called the two-point density. From this correlation function we recover the radial distribution function g and the pair correlation function h which is defined by $g - 1$:

$$g_{12} = \frac{\rho_{12}^{(2)}}{\rho_1\rho_2}, \quad (2.59)$$

$$h_{12} = g_{12} - 1. \quad (2.60)$$

The advantage of the pair correlation function h over g is that it is a clustering function: it decays to zero at large separation between 1 and 2. Since $\hat{\rho}^{(2)} = \hat{\rho}_1\hat{\rho}_2 - \hat{\rho}_1\delta_{12}$, the three functions are related to the propagator G of the theory:

$$G_{12} = \langle \hat{\rho}_1\hat{\rho}_2 \rangle - \rho_1\rho_2, \quad (2.61)$$

$$\rho_{12}^{(2)} = G_{12} + \rho_1\rho_2 - \rho_1\delta_{12}, \quad (2.62)$$

$$g_{12} = \frac{G_{12}}{\rho_1\rho_2} - \frac{1}{\rho_1}\delta_{12} + 1, \quad (2.63)$$

$$h_{12} = \frac{G_{12}}{\rho_1\rho_2} - \frac{1}{\rho_1}\delta_{12}. \quad (2.64)$$

Finally, for homogeneous liquids, the structure factor of Eq.(1.6) is related to the Fourier transform of h by:

$$S_k = 1 + \rho h_k = \frac{1}{\rho} G_k. \quad (2.65)$$

Note that the structure factor is sometimes defined as $1 + \rho g_k$, the difference between the two definitions being a delta function at $k = 0$. This term represents the unscattered light in a light diffusion experiment, and is most of the times eliminated by looking at the transmitted light under a small angle.

2.2.1 The case of the ideal gas

In the case $v = 0$, the partition function simplifies into:

$$\begin{aligned} Z[\nu, w = 0] &= \sum_{N=0}^{\infty} \frac{1}{N!} \int_{1, \dots, N} e^{\sum_{i=1}^N \nu_i} = \sum_{N=0}^{\infty} \frac{1}{N!} \left(\int_1 e^{\nu_1} \right)^N \\ &= \exp \left(\int_1 e^{\nu_1} \right). \end{aligned} \quad (2.66)$$

Which leads to:

$$W[\nu] = \int_1 e^{\nu_1}. \quad (2.67)$$

We can thus calculate the density at fixed chemical potential and external field:

$$\rho_1[\nu] = e^{\nu_1}, \quad (2.68)$$

and inverting this relation we find that the value of ν that fixes ρ_1 as density is:

$$\nu_1^*[\rho] = \ln \rho_1. \quad (2.69)$$

This allows to perform the Legendre transform of $W[\nu, w = 0]$ with respect to ν to get:

$$\begin{aligned} \Gamma_1[\rho, w = 0] &= \rho_1 \nu_1^*[\rho] - W[\nu^*[\rho]] = \rho_1 \ln \rho_1 - e^{\ln \rho_1} \\ &= \rho_1 [\ln \rho_1 - 1], \end{aligned} \quad (2.70)$$

which is the expected ideal gas term in the free-energy. We can also calculate the different two-point functions defined above:

$$G_{12}[\nu, w = 0] = e^{\nu_1} \delta_{12}, \quad (2.71)$$

$$\rho_{12}^{(2)}[\nu, w = 0] = e^{\nu_1} e^{\nu_2}, \quad (2.72)$$

$$g_{12}[\nu, w = 0] = 1, \quad (2.73)$$

$$h_{12}[\nu, w = 0] = 0, \quad (2.74)$$

and the derivatives of the functional Γ to get:

$$\Gamma_1^{(1)}[\rho, w = 0] = \ln \rho_1, \quad (2.75)$$

$$\Gamma_{1 \dots n}^{(n)}[\rho, w = 0] = \frac{(-1)^n}{(n-1)\rho_1^{n-1}} \prod_{i=2}^n \delta_{1i}. \quad (2.76)$$

We also see that the correlation functions defined by successive functional differentiation with respect to ρ are non-zero at every order, which leads to define the non-ideal gas part of these correlation functions, that are called the direct correlation functions in liquid theory:

$$c_{1 \dots n}^{(n)}[\rho] \equiv - \frac{\delta [\Gamma[\rho, w] - \Gamma[\rho, w = 0]]}{\delta \rho_1 \dots \delta \rho_n} = \frac{(-1)^n}{(n-1)\rho_1^{n-1}} \prod_{i=2}^n \delta_{1i} - \Gamma_{1 \dots n}^{(n)}[\rho, w] \quad (2.77)$$

where we have used the result of the previous subsection for the Legendre transform of $\ln Z[\nu, w = 0]$. This is the so-called virial expansion of liquid theory. At this stage, if we wanted to obtain approximations for two-point functions, we would have to perform another Legendre transform, this time with respect to w .

2.2.3 Morita & Hiroike functional

Since we have formulated our diagrammatic expansion with f lines instead of w lines, we need the correspondence between those two functions. We already know with Eq.(2.58) that w is coupled to the two-point density $\rho^{(2)}$, so if we perform a differentiation of W with respect to f we will obtain:

$$\begin{aligned} \frac{\delta W[\nu, f]}{\delta f_{12}} &= \frac{\delta w_{34}}{\delta f_{12}} \frac{\delta W[\nu, w]}{\delta w_{34}} = \frac{\delta \ln(1 + f_{34})}{\delta f_{12}} \frac{\delta W[\nu, w]}{\delta w_{34}} \\ \Leftrightarrow (1 + f_{12}) \frac{\delta W[\nu, f]}{\delta f_{12}} &= \frac{1}{2} \rho_{12}^{(2)}. \end{aligned} \quad (2.82)$$

The same relation applies to the functional $\Gamma_1[\rho, f]$ by properties of the Legendre transform:

$$(1 + f_{12}) \frac{\delta \Gamma_1[\rho, f]}{\delta f_{12}} = -\frac{1}{2} \rho_{12}^{(2)}. \quad (2.83)$$

Differentiating a diagram of Eq.(2.81) with respect to f_{12} amounts to erasing a line and labeling 1 and 2 the two points that were joined by this line. In every diagram, the two densities attached to the nodes 1 and 2 will factor out and give an overall factor $\rho_1 \rho_2$. In the following an open point will be a point without a density weight whose coordinates are not integrated over. The definition of the two point density in Eq.(2.83) gives then [107]:

$$g_{12} = \frac{\rho_{12}^{(2)}}{\rho_1 \rho_2} = e^{w_{12}} \left(1 + \begin{array}{c} \bullet \\ \diagup \quad \diagdown \\ \circ_1 \quad \circ_2 \end{array} + \begin{array}{c} \bullet \quad \bullet \\ | \quad | \\ \circ_1 \quad \circ_2 \end{array} + \begin{array}{c} \bullet \quad \bullet \\ \diagdown \quad \diagup \\ \circ_1 \quad \circ_2 \end{array} + \begin{array}{c} \bullet \quad \bullet \\ \diagup \quad \diagdown \\ \circ_1 \quad \circ_2 \end{array} + \begin{array}{c} \bullet \quad \bullet \\ \diagdown \quad \diagup \\ \circ_1 \quad \circ_2 \end{array} + \begin{array}{c} \bullet \quad \bullet \\ \diagup \quad \diagdown \\ \circ_1 \quad \circ_2 \end{array} + \dots \right), \quad (2.84)$$

which means that the function h behaves like $e^w - 1 = f$ to lowest order in density. This is also an *a-posteriori* justification for the choice of f as links in the diagrammatic expansion: Legendre transforming with respect to w will have the effect of replacing f links by h functions [110], which have the good behavior for us: it cancels in the ideal gas limit and decays to zero at large separations in all cases, giving rise to well-behaved integrals.

Morita & Hiroike [123] have performed the second Legendre transform, giving the following result:

$$\Gamma_2[\rho, h] = \rho_1 [\ln \rho_1 - 1] + \frac{1}{2} \rho_1 \rho_2 [(1 + h_{12}) \ln(1 + h_{12}) - h_{12}]$$

$$- \begin{array}{c} \bullet \\ \diagup \quad \diagdown \\ \bullet \quad \bullet \end{array} + \begin{array}{c} \bullet \quad \bullet \\ | \quad | \\ \bullet \quad \bullet \end{array} - \begin{array}{c} \bullet \\ \diagdown \quad \diagup \\ \bullet \quad \bullet \end{array} + \dots \quad (2.85)$$

$$+ \{2\text{PI diagrams}\} \quad (2.86)$$

Although this result was present in Morita's work, a clearer presentation in terms of Legendre transforms is found in [49, 10]. The diagrams above have ρ on the nodes and h links, due to the double Legendre transformation. The 2PI diagrams that we don't represent here are diagrams that do not separate in several parts if one or two h links are removed.

The sum of ring diagrams defined above can be related to the direct correlation function defined in Eq.(2.77). Indeed, we know that the propagator and the two-point vertex function $\Gamma^{(2)}$ are inverse

of each other by properties of the Legendre transform. Eq.(2.40) reads, in the notations of liquid state theory:

$$\begin{aligned} G_{13}\Gamma_{32}^{(2)} &= \delta_{12}, \\ \Leftrightarrow c_{12} &= h_{12} - h_{13}\rho_3 c_{32}. \end{aligned} \quad (2.87)$$

This equation can be solved iteratively in powers of h to get:

$$c_{12} = h_{12} - \sum_{n=2}^{\infty} (-1)^n h_{13}\rho_3 h_{34}\rho_4 \cdots h_{(n-2)2}, \quad (2.88)$$

which is exactly the derivative of the sum of ring diagrams in Eq.(2.86) with respect to h_{12} . Eq.(2.87) is called the Ornstein-Zernike equation [129, 137] and was introduced independently of its interpretation in terms of Legendre transformations. Thus to get the variational principle that will give a self-consistent equation on h , we perform the functional differentiation with respect to h_{12} and use Eq.(2.45) to get:

$$w_{12} = \ln(1 + h_{12}) - h_{12} + c_{12} + \frac{\delta}{\delta h_{12}} \{2\text{PI diagrams}\}. \quad (2.89)$$

Since the 2PI diagrams are functionals of ρ and h , to perform approximations, one way is to select a class of 2PI diagrams and discard the others, then perform the differentiation, to finally obtain a self-consistent equation bearing on h alone. Taking the exponential of this equation, we obtain:

$$h_{12} = e^{w_{12}} e^{h_{12} - c_{12} - \frac{\delta}{\delta h_{12}} \{2\text{PI diagrams}\}} - 1, \quad (2.90)$$

which is an exact equation derived originally by the Percus method [132]. The functional derivative of the 2PI diagrams appears under the terminology of “bridge function”. Cast in this form, we see that this equation is applicable to the hard-sphere case, where $e^{w_{12}}$ is a mere step function, and enforces the physical condition that g is equal to zero when $r < \sigma$, i.e. spheres can not overlap.

The Percus method uses the following property of the partition function of the liquid: consider a fluid of N particles subject to the influence of a $(N + 1)$ th particle at a fixed position. The effect of this additional particle can be treated in perturbation. But a crucial property for homogeneous systems is that when one computes the one-particle distribution function of the perturbed liquid, it is in fact equal to the two-particle distribution function of the unperturbed liquid. Thus performing a perturbation expansion in powers of the density will give integral equations in terms of the pair correlation function of the unperturbed liquid. By this mean, one can show that the bridge function, usually noted b , is equal to the sum of all third and higher order direct correlation functions:

$$b_{12} = -\frac{\delta}{\delta h_{12}} \{2\text{PI diagrams}\} = \sum_{n=2}^{\infty} \frac{1}{n!} c_{11'\dots n'}^{(n+1)} \rho_{1'} h_{1'2} \cdots \rho_{n'} h_{n'2}. \quad (2.91)$$

2.2.4 Hyper-Netted-Chain approximation

The Hyper-Netted-Chain (HNC) approximation, which was derived independently by Morita & Hiroike [122] and Van Leeuwen, Groeneveld and De Boer [157], simply consists in discarding all the 2PI diagrams in Eq.(2.86). By looking at Eq.(2.91), we see that it is equivalent to setting all the $c^{(n)}$'s with $n \geq 3$ to zero. Since a large use of this approximation will be made in the rest of the manuscript, a brief overview of the results within HNC approximation is presented here.

Discarding the 2PI diagrams in Eq.(2.89), we obtain a self consistent equation on h , which involves the direct correlation function c , which is related to h by Eq.(2.87). In the homogeneous case, two-point functions depend only on $r = |1 - 2|$, the modulus of the difference between the two points, and the HNC approximation thus reads in terms of the 1-dimensional functions h and c :

$$\begin{cases} c(r) &= e^{w(r)} e^{h(r)-c(r)} - 1 - [h(r) - c(r)] \\ h(k) &= \frac{\rho c(k)}{1 - \rho c(k)} \end{cases} \quad (2.92)$$

These equations are more easily solved in terms of the function $kc(k)$ since, for isotropic functions, the three-dimensional Fourier transform reads:

$$kc(k) = 4\pi \int_0^\infty dr \, rc(r) \sin(kr), \quad (2.93)$$

$$rc(r) = \frac{1}{2\pi^2} \int_0^\infty dk \, kc(k) \sin(kr). \quad (2.94)$$

We will need to solve these equations in the next three chapters: either in the dynamical context to solve the equations obtained for the non-ergodicity factor, which needs as an input the liquid structure, or in the context of replica theory where a replicated version of HNC is used, or when computing the thermodynamics of the jammed states of harmonic spheres. The scheme that we used for solving the HNC equations is an adaptation of a Picard iterative scheme:

- Start from a good guess for $kc(k)$
- Deduce the corresponding $kh(k)$ and thus $k[h(k) - c(k)]$
- Inverse Fourier transform to obtain $r[h(r) - c(r)]$
- Plug into the HNC equation to obtain a new estimate of $rc(r)$
- Fourier transform and mix the new solution with the old one to get the new estimate for $kc(k)$
- Iterate the procedure until the absolute value of the maximum of the difference between old and new solution is smaller than some prescribed accuracy

This kind of iterative scheme can be very sensitive to variations of $c(k)$. Indeed if an abrupt change in $c(k)$ occurs, the denominator in the Ornstein-Zernike equation Eq.(2.87) can reach zero, and make the calculation diverge. This is why at each step, the new solution is incorporated gradually within the old one, to avoid unphysical values of the functions. Also, the starting guess in the calculation is important, since the calculation can become unstable if we stand far away from the physical solution. Thus, we systematically started our calculations at high temperatures and/or low density, where the virial expansion is valid, and where the function g is equal approximately to e^w . Then when convergence is achieved at this high temperature/low density, we gradually increased the density or lowered the temperature to attain the ρ, T point of interest.

We show in the left frame of Figure 2.1 the result for the pair correlation function of harmonic spheres at high density $\rho = 1.2$ and very low a-dimensional temperature $k_B T / \epsilon = 3.58 \times 10^{-4}$. This pair correlation function satisfies all the physical requirements: it decays to 1 at large r , is almost equal to zero for $r < \sigma$, since at very low temperature, harmonic spheres behave like hard spheres, and thus no overlaps are authorized for $r < 1$, except on a very narrow regime close to 1. It presents a very pronounced first peak at $r = \sigma$, and secondary peaks at $r = 2\sigma, 3\sigma, \dots$, reflecting the shells of neighbors that develop in very dense liquids.

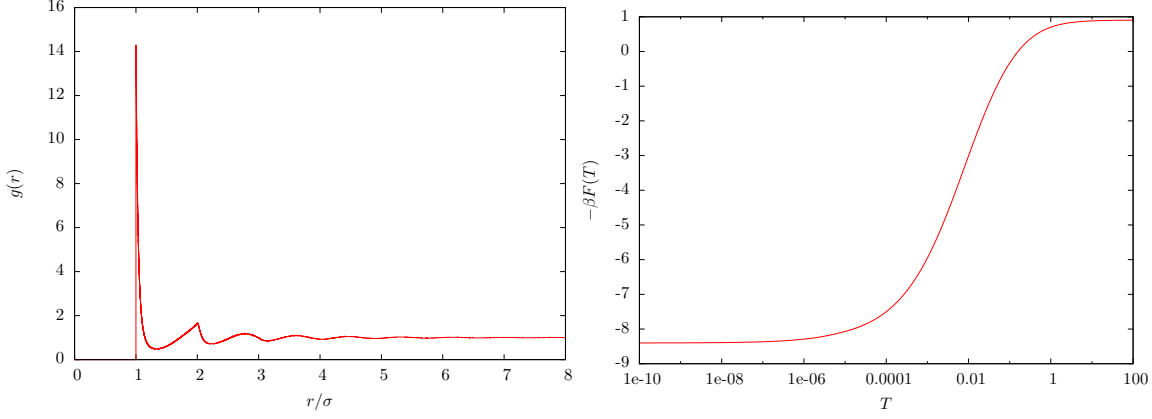


Figure 2.1: Left panel: pair correlation function g as a function of r/σ in the HNC approximation at density $\rho\sigma^3 = 1.1$ and temperature $k_B T/\varepsilon = 3.58 \times 10^{-4}$. Right panel: free energy $-\beta F$ as a function of temperature, at fixed density $\rho\sigma^3 = 1.1$.

Inserting this result into the approximate functional Γ_2 obtained by discarding the 2PI diagrams, we obtain the approximate equation of state of the liquid. We can notice that, in the isotropic and homogeneous case, a Fourier transform of one ring diagram reads, for example:

$$\text{Ring diagram} = \int_{123} \rho_1 h_{12} \rho_2 h_{23} \rho_3 h_{31} = \frac{V}{2} \frac{1}{3} \rho^3 \int_k h(k)^3, \quad (2.95)$$

so that the sum of all diagrams is a logarithm function in Fourier space, which leads to the following analytic expression:

$$\begin{aligned} \Gamma_2^{\text{HNC}}[\rho, h] = & V\rho [\ln \rho - 1] + \frac{V}{2} \rho^2 \int_r ([1 + h(r)] \ln[1 + h(r)] - h(r)) \\ & - \frac{V}{2} \int_k \left(\ln[1 + \rho h(k)] - \rho h(k) + \frac{1}{2} \rho^2 h(k)^2 \right). \end{aligned} \quad (2.96)$$

When this functional is evaluated at h^* , the solution of the variational equation, and the inverse Legendre transformation is performed, we obtain the Γ_1 functional, which is related to the free-energy of the liquid by:

$$\beta F = \Gamma_1[\rho] = \Gamma_2[\rho, h^*] - \frac{1}{2} w_{12} \rho_1 \rho_2 (1 + h_{12}^*), \quad (2.97)$$

$$\begin{aligned} \Rightarrow \beta F^{\text{HNC}} = & V\rho [\ln \rho - 1] + \frac{V}{2} \rho^2 \int_r ([1 + h(r)] (\ln[1 + h(r)] - w(r)) - h(r)) \\ & - \frac{V}{2} \int_k \left(\ln[1 + \rho h(k)] - \rho h(k) + \frac{1}{2} \rho^2 h(k)^2 \right). \end{aligned} \quad (2.98)$$

We show in the right frame of Fig.(2.1) the resulting free-energy as a function of temperature, at fixed density $\rho\sigma^3 = 1.1$. When $T \rightarrow 0^+$, it converges to the entropy of hard spheres, while increasing towards an ideal gas value for large temperatures.

Chapter 3

Dynamics near the glass transition: a field theory approach

Independently from an active community that attempts to improve Mode-Coupling Theory, it is believed that a convenient way to formulate the dynamics of colloids is by resorting to field theory, i.e. finding a diagrammatic approach inspired from quantum field theory. This step forward would allow us to use all the powerful diagrammatic tools developed in this context, such as those described in Chapter 2.

The search for a good field theory for studying the dynamics near the glass transition has a long history by now, and was pioneered by Das and Mazenko for coarse grained models [47]. However application to realistic models such as colloidal glasses has been delayed until a Langevin equation for the time-dependent density was derived by Dean [53]. This provided a starting point to formulate field theories for colloidal glasses, but they were soon shown by Miyazaki and Reichman [117] to be inconsistent with the time-reversibility of the dynamics. A first attempt by Andreanov, Biroli and Lefèvre to go beyond that problem gave unsatisfactory results [3], due to the difficulty to correctly deal with the entropic $\rho \ln \rho$ term inherent to the description of the ideal gas. Finally Kawasaki and Kim [86] managed to settle this last issue, but at the cost of a very heavy formalism, leaving little hope to extend their approach to higher orders.

In this chapter we briefly review the field-theoretic methods described above, and introduce an original way to formulate a field theory, that allows us to overcome some of their limitations, and more importantly provide a compact formalism. This work corresponds to publication **P5**.

3.1 Field theory for supercooled liquids

A system of N harmonic spheres is placed in a solvent at temperature T , that plays the role of a thermal bath. Each particle of our system is therefore a Brownian particle, that moves according to Brownian dynamics, more easily written in terms of Langevin equations. The space position of particle i at time t , will be denoted by $x_i(t)$, and we suppose that each trajectory satisfies the following

over-damped Langevin equation:

$$\left\{ \begin{array}{l} \frac{dx_i(t)}{dt} = F_i(t) + \zeta_i(t), \\ F_i(t) = -\nabla_{x_i} \sum_{j \neq i} v(x_i(t) - x_j(t)), \\ \langle \zeta_i(t) \zeta_j(t) \rangle = 2T \delta_{ij} \delta(t - t). \end{array} \right. \quad (3.1)$$

The field ζ is a three-dimensional Gaussian white noise of variance $2T$, as indicated in Eq.(3.1). This particular value of the variance ensures that the system converges towards equilibrium at long times, as given by the Boltzmann weight of Eq.(2.50), i.e. $\exp\left(-\beta \sum_{i < j} v(x_i - x_j)\right)$.

This type of Brownian dynamics are much simpler to analyze than the usual Hamiltonian dynamics since no velocities are involved, and the presence of a fluctuating noise allows us for more direct statistical descriptions. However, apart from differences between the short time evolutions of Hamiltonian and Brownian dynamics, the glassy features at long times are largely independent of the choice of dynamics [153].

3.1.1 Formulation in terms of the density and field-theoretic formulation

We are not interested in being able to follow the trajectory of each individual particle of the system, but rather in being able to accurately predict collective quantities, such as correlation functions of the fluctuations of density, as described in the introduction. In analogy with the equilibrium theory of liquids, we can define the time-dependent microscopic density of the system as:

$$\hat{\rho}(x, t) = \sum_{i=1}^N \delta(x - x_i(t)), \quad (3.2)$$

and seek for an evolution equation for $\hat{\rho}$ rather than for all the x_i 's. Dean [53] showed that the N Langevin equations written in Eq.(3.1) exactly give the following equation of evolution for $\hat{\rho}$:

$$\left\{ \begin{array}{l} \partial_t \hat{\rho}(x, t) = \nabla_x \cdot \left(\hat{\rho}(x, t) \int_y \hat{\rho}(y, t) \nabla_x v(x - y) \right) + T \nabla_x^2 \hat{\rho}(x, t) + \nabla_x \cdot \left(\sqrt{\hat{\rho}(x, t)} \eta(x, t) \right), \\ \langle \eta(x, t) \eta(y, t) \rangle = 2T \delta(x - y) \delta(t - t). \end{array} \right. \quad (3.3)$$

Of course these dynamics conserves the number of particles, since they can be written as:

$$\left\{ \begin{array}{l} \partial_t \hat{\rho}(x, t) + \nabla_x j_L(x, t) = 0, \\ j_L(x, t) = -\hat{\rho}(x, t) \int_y \hat{\rho}(y, t) \nabla_x v(x - y) - T \nabla_x \hat{\rho}(x, t) - \sqrt{\hat{\rho}(x, t)} \eta(x, t). \end{array} \right. \quad (3.4)$$

The $-T \nabla_x \hat{\rho}(x, t)$ term expresses Fick's law of diffusion, while each particle is additionally driven by the force field $-\int_y \nabla_x v(x - y) \hat{\rho}(y, t)$ created by the others particles. The current j_L can alternatively be put under the form:

$$\left\{ \begin{array}{l} j_L(x, t) = -\hat{\rho}(x, t) \nabla_x \frac{\delta \mathcal{F}[\hat{\rho}]}{\delta \hat{\rho}(x, t)}, \\ \mathcal{F}[\hat{\rho}] = T \int_x \hat{\rho}(x, t) \left[\ln \left(\frac{\hat{\rho}(x, t)}{\rho_0} \right) - 1 \right] + \frac{1}{2} \int_{x, y} \hat{\rho}(x, t) v(x - y) \hat{\rho}(y, t). \end{array} \right. \quad (3.5)$$

By insisting on working with a collective field, we turned the equations on x_i with additive noise into an equation for $\hat{\rho}$ with a multiplicative noise. This equation must thus be understood in the Itô sense [156]: at each new time step, the new value of the multiplicative noise is computed with the values of the density at the previous time step. Note that this expression superficially seems to coincide with a phenomenological equation derived by Kawasaki [85], where the pair potential has to be replaced by the two-body direct correlation function of the liquid. It was later shown by Kawasaki and Kim [87] that the use of Eq.(3.3) provides a correct treatment of the static quantities in a dynamical calculation, whereas using of a phenomenological equation does not.

Another difficulty is in the evaluation of the density profile at the beginning of the dynamics, that requires an input at time $t = 0$. To clarify this, the experiment that we have in mind is the following: at time $t = -\infty$, we prepare a system of harmonic spheres in a bath at temperature T , then let them evolve freely towards equilibrium. At $t = 0$, equilibrium is achieved, and we start monitoring the dynamics, which are modeled by our equation (3.3). In this interpretation, the initial value of $\hat{\rho}(x, t)$ must be obtained from an equilibrium distribution. This distribution is known, at least formally, from the discussion in the previous section. Indeed, exactly at $t = 0$, there will be fluctuations of the space dependent field $\hat{\rho}(x, t = 0)$ around its equilibrium value ρ_0 , which is constant in time and space because of translational and time-translational invariance. Defining the density fluctuation field $\delta\rho$ as:

$$\delta\rho(x, t) = \hat{\rho}(x, t) - \rho_0, \quad (3.6)$$

we thus have to know the probability distribution of $\delta\rho(x, 0)$. It is given by the Γ_1 functional of the liquid state theory described in the previous subsection. Indeed, expanding Γ_1 around a flat profile of density, we get:

$$\begin{aligned} \Gamma_1[\delta\rho] &= \Gamma_1[\rho_0] + \sum_{N=1}^{\infty} \int_{x_1, \dots, x_N} \frac{\delta\Gamma_1[\rho]}{\delta\rho(x_1) \cdots \delta\rho(x_N)} \delta\rho(x_1) \cdots \delta\rho(x_N) \\ &= \Gamma_1[\rho_0] + \int_x (\rho_0 + \delta\rho(x)) \left[\ln \left(1 + \frac{\delta\rho(x)}{\rho_0} \right) - 1 \right] \\ &\quad - \sum_{N=1}^{\infty} \int_{x_1, \dots, x_N} c^{(N)}(x_1, \dots, x_N) \delta\rho(x_1) \cdots \delta\rho(x_N). \end{aligned} \quad (3.7)$$

Now performing the inverse Legendre transformation to come back to the free-energy of the liquid simply cancels the $c^{(1)}$ term, in order to obtain the following probability of observing a density profile at equilibrium:

$$P[\delta\rho(x, t = 0)] \propto \exp \left(\begin{aligned} & - \int_x (\rho_0 + \delta\rho(x)) \left[\ln \left(1 + \frac{\delta\rho(x)}{\rho_0} \right) - 1 \right] \\ & + \sum_{N=2}^{\infty} \int_{x_1, \dots, x_N} c^{(N)}(x_1, \dots, x_N) \delta\rho(x_1) \cdots \delta\rho(x_N) \end{aligned} \right). \quad (3.8)$$

By evaluating this functional in the HNC approximation, where all $c^{(N)}$'s are set to zero for $N \geq 3$, we get the Ramakrishnan-Yussouf [134] expression for the probability of observing a density profile.

We show now for future use a standard procedure to turn the dynamical equation Eq.(3.3) into a diagrammatic computational scheme similar to the one described in the first section of this chapter. In order to obtain a particular density profile between time 0 and time t_f , we first have to draw an initial density profile out of the distribution in Eq.(3.8), then we have at each time step to draw a value of the noise out of its distribution $P[\eta]$, which is Gaussian, and finally we must find the correct

value of the density profile that satisfies the Langevin equation given the value of the noise that was chosen. Grouping all these contributions together, we can write down the probability of observing any density profile between time 0 and t_f (probability which is equal to one by definition !) as:

$$1 = Z = \int \mathcal{D}\rho_0 P[\rho_0] \int \mathcal{D}\eta P[\eta] \int \mathcal{D}\rho \prod_{t=0^+}^{t_f} \prod_x \delta(\text{Langevin equation at time } t \text{ and point } x) \quad (3.9)$$

$$= \int \mathcal{D}\rho \mathcal{D}\bar{\rho} \mathcal{D}\eta \mathcal{D}\rho_0 P[\rho_0] P[\eta] \exp \left(- \int_{t=0}^{t_f} \int_x \bar{\rho}(x, t) \times \text{Langevin equation at time } t \right) \quad (3.10)$$

$$= \int \mathcal{D}\rho_0 P[\rho_0] \int \mathcal{D}\rho \mathcal{D}\bar{\rho} \exp \left(- \int_{t,x} \left[\begin{array}{l} \bar{\rho}(x, t) \partial_t \rho(x, t) - T \bar{\rho}(x, t) \nabla_x^2 \rho(x, t) \\ - \bar{\rho}(x, t) \nabla_x \cdot \left(\rho(x, t) \int_y \rho(y, t) \nabla_x v(x - y) \right) \end{array} \right] \right) \\ \int \mathcal{D}\eta \exp \left(- \frac{1}{4T} \int_{t,x} \left[\eta^2(x, t) - 4T \bar{\rho}(x, t) \nabla_x \cdot \left(\sqrt{\rho(x, t)} \eta(x, t) \right) \right] \right). \quad (3.11)$$

In order to go from the first to the second line, we used the integral representation of the delta function, as well as a change of variables in the delta function, which has determinant 1 when the equation is understood in the Itô sense. After an integration by parts, the integral over the noise is Gaussian, and we obtain :

$$\left\{ \begin{array}{l} Z = \int \mathcal{D}\rho_0 e^{-\beta \mathcal{F}_{\text{equ}}[\rho_0]} \int \mathcal{D}\rho \mathcal{D}\bar{\rho} e^{-S[\rho, \bar{\rho}]} \\ S[\rho, \bar{\rho}] = \int_{t=0}^{t_f} \int_x \left[\bar{\rho}(x, t) \partial_t \rho(x, t) - \bar{\rho}(x, t) \nabla_x \cdot \left(\rho(x, t) \nabla_x \frac{\delta \beta \mathcal{F}[\rho]}{\delta \rho(x, t)} \right) - T \rho(x, t) (\nabla_x \bar{\rho}(x, t))^2 \right], \\ \beta \mathcal{F}_{\text{equ}}[\rho] = \int_x \rho(x) \left[\ln \frac{\rho(x)}{\rho} - 1 \right] + \sum_{N=2}^{\infty} \frac{1}{N!} \int_{x_1, \dots, x_N} c^{(N)}(x_1, \dots, x_N) \rho(x_1) \cdots \rho(x_N), \\ \beta \mathcal{F}[\rho] = \int_x \rho(x, t) \left[\ln \frac{\rho(x, t)}{\rho} - 1 \right] + \frac{1}{2} \int_{x,y} \rho(x, t) \beta v(x - y) \rho(y, t). \end{array} \right. \quad (3.12)$$

This formalism was first formulated by Martin, Siggia, and Rose [104], and put to work by De Dominicis [50] and Janssen [82, 83]. Now we find ourselves in the position of formulating a statistical field theory in the form described in the first chapter.

3.1.2 Diagrammatic structure of the theory

Following the line described in the first section, we look at the saddle point of the functional integral, defined as:

$$\left\{ \begin{array}{l} 0 = (-\partial_t - \nabla_x^2) \bar{\rho}(x, t) - \nabla_x \cdot \left(\rho(x, t) \frac{\delta \beta \mathcal{F}[\rho]}{\delta \rho(x, t)} \right) - T (\nabla_x \bar{\rho})^2 \\ 0 = (\partial_t - \nabla_x^2) \rho(x, t) - \nabla_x \cdot \frac{\delta \mathcal{F}[\rho]}{\delta \rho(x, t)} \cdot \nabla_x \bar{\rho}(x, t) - \int_y \bar{\rho}(y, t) \partial_y \rho(y, t) \cdot \partial_y \frac{\delta^2 \mathcal{F}[\rho]}{\delta \rho(x, t) \delta \rho(y, t)}. \end{array} \right. \quad (3.13)$$

Time translation invariance, isotropy and translation invariance enforce, if they are not spontaneously broken, that averages of one point quantities are constant, therefore leaving us with only $\rho(x, t) = \rho_0$ and $\bar{\rho}(x, t) = 0$. Now we gather the two fluctuations of the fields around their mean values into a vector φ defined by:

$$\varphi(x, t) = \begin{pmatrix} \delta \bar{\rho}(x, t) \\ \delta \rho(x, t) \end{pmatrix} \quad (3.14)$$

and obtain a field theory described by:

$$S[\varphi] = \frac{1}{2} \int_{k,t} \varphi(k,t) G_0^{-1}(k,t) \varphi(-k,t) + S_{\text{ng}}[\varphi], \quad (3.15)$$

$$G_0^{-1}(k,t) = \begin{pmatrix} -2T\rho_0 k^2 & \partial_t + k^2(1 + \beta\rho_0 v(k)) \\ -\partial_t + k^2(1 + \beta\rho_0 v(k)) & 0 \end{pmatrix}, \quad (3.16)$$

$$S_{\text{ng}}[\varphi] = \int_{k_1, k_2, k_3} \delta_{k_1+k_2+k_3} \left(\begin{aligned} & T k_2 \cdot k_3 \delta\rho(k_1, t) \delta\bar{\rho}(k_2, t) \delta\bar{\rho}(k_3, t) \\ & + \frac{1}{2} [k_1 \cdot k_3 \beta v(k_1) + k_2 \cdot k_3 \beta v(k_2)] \delta\rho(k_1, t) \rho(k_2, t) \delta\bar{\rho}(k_3, t) \end{aligned} \right) \quad (3.17)$$

3.1.3 Structure of the perturbative expansion

In a perturbative expansion as described in the first section of this chapter, the main quantity to compute is the bare propagator $G^{(0)}$, which is the inverse of the quadratic term in the action. In our case, we find:

$$G^{(0)}(k,t) = \begin{pmatrix} 0 & \theta(-t) \\ \theta(t) & T\rho_0 k^2 \end{pmatrix} e^{-k^2(1-\rho_0 w(k))|t|} \quad (3.18)$$

This form of propagator is crucial to obtain a causal structure, as was pointed out by De Dominicis. Indeed, if we look now at the diagrammatic structure of our theory, we see that we will have two kind of vertices to build diagrams, pictured as follows:

$$\delta\bar{\rho}(k, t_1) \equiv \leftarrow \bigcirc \quad (3.19)$$

$$\delta\rho(k, t_1) \equiv \bigcirc \rightarrow \quad (3.20)$$

$$\int_{k_1, k_2, k_3} \delta_{k_1+k_2+k_3} T k_2 \cdot k_3 \delta\rho(k_1, t) \delta\bar{\rho}(k_2, t) \delta\bar{\rho}(k_3, t) \equiv \text{---} \bullet \begin{array}{c} \curvearrowright \\ \curvearrowleft \end{array} \quad (3.21)$$

$$- \int_{k_1, k_2, k_3} \delta_{k_1+k_2+k_3} \frac{1}{2} [k_1 \cdot k_3 w(k_1) + k_2 \cdot k_3 w(k_2)] \rho(k_1, t) \rho(k_2, t) \delta\bar{\rho}(k_3, t) \equiv \begin{array}{c} \curvearrowright \\ \bullet \rightarrow \end{array} \quad (3.22)$$

$$G_{11}(k, t) \equiv 0 \equiv \bigcirc \rightarrow \leftarrow \bigcirc \quad (3.23)$$

$$G_{12}(k, t) \equiv \theta(t_1 - t_2) e^{-k^2(1-\rho_0 w(k))|t_2-t_1|} \equiv \bigcirc \rightarrow \bigcirc \quad (3.24)$$

$$G_{22}(k, t) \equiv T\rho_0 k^2 e^{-k^2(1-\rho_0 w(k))|t_2-t_1|} \equiv \bigcirc \text{---} \bigcirc \quad (3.25)$$

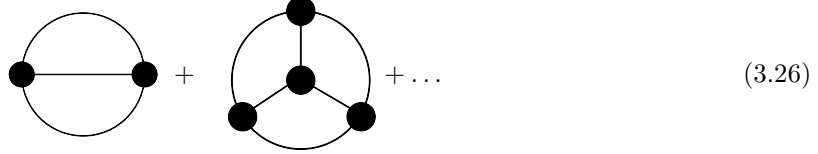
Given the value of the bare propagator, we see that joining one $\delta\rho$ line with a $\delta\bar{\rho}$ line gives a causal step function. Thus the arrows of the lines indicate the arrow of time, and if a diagram contains two arrows that run in opposite directions, or make a loop, the diagram is equal to zero.

Inevitably, diagrams of the free-energy are then all equal to zero, because by definition they are closed, and we recover the fact that $Z = 1$ in this dynamical theory.

We also see that the causal structure of the propagators is conserved when we add diagrams to the Gaussian estimate $G^{(0)}$: indeed a diagram that contributes to renormalize G_{11} has conflicting arrow of times and is therefore equal to zero, hence the property $G_{11} = 0$ holds non perturbatively. And a diagram that contributes to $G_{12}(k, t_2 - t_1)$ forces t_2 to be greater than t_1 , and thus G_{12} is always proportional to a Heaviside function.

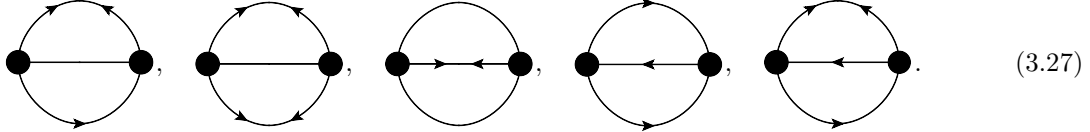
3.1.4 Symmetries and approximations

Now that we have a field-theoretic formulation, we can come back to the prescription of Chapter 2, and build up self consistent equations for the correlation functions. We use the variational principle in Eq.(2.48) to obtain the two-point vertex function Σ as the derivative of the sum of all 2PI diagrams of the theory. Since our formulation contains only cubic interactions, the first terms in this sum of diagrams will be of the form:



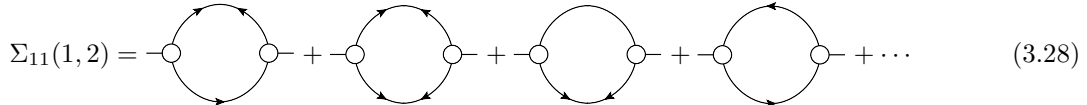
$$\text{Diagram 1} + \text{Diagram 2} + \dots \quad (3.26)$$

where the double lines represent the full propagators. We show here all the diagrams corresponding to the first term of Eq.(3.26):



$$\text{Diagram 1}, \text{Diagram 2}, \text{Diagram 3}, \text{Diagram 4}, \text{Diagram 5} \quad (3.27)$$

Note that since we have performed the second Legendre transform, the propagators on the lines of these diagrams are arbitrary functions; they are not necessarily causal. To obtain a self consistent equation on the propagators, we have to differentiate with respect to G , which leads to an expression for the Σ functional described in Chapter 2 via Eq.(2.48). In our case, we have two fields, so that the propagator and two-point vertex functions Σ are 2×2 matrices. Differentiating the diagrams in Eq.(3.27) with respect to G_{11} for example leads to:



$$\Sigma_{11}(1, 2) = \text{Diagram 1} + \text{Diagram 2} + \text{Diagram 3} + \text{Diagram 4} + \text{Diagram 5} + \dots \quad (3.28)$$

Note that it is customary to represent the vertex functions with external lines to recall which vertex function is considered, but these lines must be omitted when the diagram is computed. These are called amputated diagrams in the field-theoretic language.

When evaluated at the physical propagators, which have been proved to be causal, we see that all these contributions will disappear. We can see that this property is conserved whatever the number of diagrams we keep in our expansion is, so that $\Sigma_{11} = 0$ non-perturbatively as a consequence of causality. In the same way we will find that Σ_{12} is non-zero but is proportional to a step function of the difference between its two time arguments, and Σ_{22} is generically non zero. These causality properties for G and Σ are non-perturbative features, and have to be conserved by a truncation of the Γ_2 functional in order to obtain a consistent approximation for the propagators.

Another important physical constraint imposed on dynamical theories is the time-reversal invariance: i.e. the invariance of the dynamical equations with respect to a change $t \rightarrow -t$. It has been shown by Janssen[83] to correspond, in the formalism that we present here, to a non-linear symmetry

relating the density field and the response field:

$$\left\{ \begin{array}{l} t \rightarrow -t \\ \delta\rho(x, t) \rightarrow \delta\rho^R(x, t) = \delta\rho(x, -t), \\ \delta\bar{\rho}(x, t) \rightarrow \delta\bar{\rho}^R(x, t) = -\delta\bar{\rho}(x, -t) + \frac{\delta\beta\mathcal{F}[\rho]}{\delta\rho(x, -t)} \end{array} \right. \quad (3.29)$$

Because of the purely entropic ideal gas term in $\mathcal{F}[\rho]$, this symmetry is non-linear in the sense that it relates the fields to their higher order cumulants. While a truncation of the 2PI functional Γ_2 can easily be shown to automatically conserve linear symmetries of the action (if evaluated at propagators that verify themselves these symmetries), this is not the case automatically for non-linear symmetries. Thus an arbitrary truncation will surely violate micro reversibility [117], which is a crucial symmetry in our case: indeed we want to obtain an approximation that is able to predict a transition from an ergodic phase to a non-ergodic one. If we use an approximation that explicitly breaks time-reversal symmetry, a possible transition may be an artifact of this approximation. To be sure that we find (or do not find !) *spontaneous* symmetry breaking, we have to make sure time-reversal is properly enforced, as well as causality.

3.1.5 Linearizing the time-reversal

There are currently two different ways to linearize the time-reversal symmetry. Within the MSR formalism, the original idea was introduced by Andreanov Biroli and Lefèvre in [3], but was properly implemented later by Kawasaki and Kim in [87]. One introduces a Lagrange multiplier θ in the path integral, which will constrain all the non-linear contributions coming from $\frac{\delta\mathcal{F}[\rho]}{\delta\rho}$ to be equal to θ :

$$Z = \int \mathcal{D}\rho \mathcal{D}\bar{\rho} \delta\left(\theta - \frac{\delta\beta\mathcal{F}[\rho]}{\delta\rho} + \frac{\delta\rho}{\rho_0}\right) e^{-S[\rho, \bar{\rho}]}, \quad (3.30)$$

$$= \int \mathcal{D}\rho \mathcal{D}\bar{\rho} \mathcal{D}\theta \mathcal{D}\bar{\theta} e^{-S_{\text{KK}}[\rho, \bar{\rho}, \theta, \bar{\theta}]}, \quad (3.31)$$

$$S_{\text{KK}}[\varphi] = \frac{1}{2} \int_{k, t} \varphi(k, t) G_0^{-1}(k, t) \varphi(-k, t) + S_{\text{ng}}[\varphi], \quad (3.32)$$

$$G_0^{-1}(k, t) = \begin{pmatrix} 0 & -i\partial_t + k^2(1 - \rho_0 w(k)) & 0 & 0 \\ i\partial_t + k^2(1 - \rho_0 w(k)) & 2\rho_0 k^2 & \rho_0 k^2 & 0 \\ 0 & \rho_0 k^2 & 0 & -1 \\ 0 & 0 & -1 & 0 \end{pmatrix}, \quad (3.33)$$

$$S_{\text{ng}}[\varphi] = - \int_{x, t} \left[\begin{array}{l} \delta\bar{\rho}(x, t) \nabla_x \cdot \left(\delta\rho(x, t) \nabla_x \left[\theta(x, t) + \frac{\delta\rho(x, t)}{\rho_0} - (w \otimes \delta\rho)(x, t) \right] \right) \\ - \delta\rho(x, t) (\nabla_x \delta\bar{\rho}(x, t))^2 + \bar{\theta}(x, t) \left(\sum_{n=2}^{\infty} \frac{(-1)^n}{(n-1)} \frac{\delta\rho(x, t)^n}{\rho_0^{n-1}} \right) \end{array} \right], \quad (3.34)$$

where \otimes denotes space convolution. The time reversal is now a linear transformation of the fields:

$$\left\{ \begin{array}{ll} t & \rightarrow -t \\ \rho(x, t) & \rightarrow \rho^R(x, t) = \rho(x, -t) \\ \bar{\rho}(x, t) & \rightarrow \rho^R(x, t) = -\bar{\rho}(x, -t) + \frac{1}{\rho_0} \delta\rho(x, -t) - (w \otimes \delta\rho)(x, -t) + \theta(x, -t) \\ \theta(x, t) & \rightarrow \theta^R(x, t) = \theta(x, -t) \\ \bar{\theta}(x, t) & \rightarrow \bar{\theta}^R(x, t) = \bar{\theta}(x, -t) - i\partial_t \rho(x, -t) \end{array} \right. \quad (3.35)$$

and will therefore automatically be conserved by a truncation of the 2PI functional Γ_2 . However the cost has been to introduce an infinite number of interaction vertices in the action, that are all related to the non-interacting system. Thus, to each order of the calculation, one has to calculate an infinite number of diagrams in order to be able to fully describe the correct non-interacting system.

Note that these symmetry considerations on the time-reversal do not apply if one works with the Itô discretization, but only in the Stratonovich discretization [156]. Luckily, for the precise Langevin equation under scrutiny, the two discretizations are identical !

By cleverly taking into account the ideal gas contributions non-perturbatively, Kawasaki and Kim [87] were able to derive back the MCT equation. The same analysis were later performed by Nishino and Hayakawa [125] for the fluctuating non-linear hydrodynamics. However, the cost of taking correctly into account the ideal gas is a very heavy formalism, leaving little hope to extend the calculation to next orders properly. It would be better to have a theory that directly starts from non-interacting particles and treats the interactions as a perturbation. In the following sections of this chapter we present a first step towards such a theory, that is provided by a mapping of the particles onto effective bosons.

3.2 A way around: effective quantum mechanical formulation

3.2.1 Master equation and Doi-Peliti formalism

Coming back to a discretized version of the dynamics of our system, we now consider that our N particles are dispatched on an infinite, 3D, square lattice with mesh size a . The possible positions of the spheres are denoted $x_i = a(pe_1 + qe_2 + re_3)$, where $\{p, q, r\}$ are positive or negative numbers and e_1, e_2, e_3 are unitary vectors which form an orthonormal basis. The ensemble of vectors belonging to the lattice is called \mathcal{L} in the following.

The equivalent of the microscopic density that we are interested in is now the set of occupation numbers of the lattice sites. We call n_x the occupation number of the site located at x . A microscopic configuration of the system \mathcal{C} is then the set of all numbers of occupations :

$$\mathcal{C} = \{n_x, x \in \mathcal{L}\} \quad (3.36)$$

We call $E_p(\mathcal{C})$ the total potential energy of a given configuration \mathcal{C} , defined by :

$$E_p(\mathcal{C}) = \frac{1}{2} \sum_{y \neq z} n_y v(y - z) n_z, \quad (3.37)$$

where v is still the pair potential of our system, that can be for example the pair potential of harmonic spheres given in Eq.(1.20). We choose the following dynamic rules : within a time interval dt , a particle can jump from a site x to another site y (changing the microscopic configuration from \mathcal{C} to \mathcal{C}') with probability $\exp\left(-\frac{\beta}{2}[E_p(\mathcal{C}') - E_p(\mathcal{C})]\right) n_x dt$. We consider the evolution with time of the probability of observing a particular configuration \mathcal{C} at time t : $P(\mathcal{C}, t)$. We call \mathcal{C}' the configuration that differs from \mathcal{C} only by a jump of one particle to a closest neighbor :

$$\begin{aligned} \mathcal{C} &= \{\dots, n_x, \dots, n_{x+e}, \dots\}, \\ \mathcal{C}' &= \{\dots, n_x - 1, \dots, n_{x+e} + 1, \dots\}, \\ &\text{with } e = \pm a e_i, i \in \{1, 2, 3\} \end{aligned} \quad (3.38)$$

Note that this type of dynamics is compatible with the hard-sphere case, where $e^{-\beta v}$ is equal to 0 or 1 depending whether the configuration has overlaps or not. The only restriction is that the initial configuration must be an authorized one. In that case, the rate to go from the current configuration to a forbidden one is always 0, and the hard-sphere constraint is always satisfied.

These dynamics obviously satisfy detailed balance, and thus lead to a unique stationary distribution, which is the Boltzmann one:

$$P(\mathcal{C}, t) \underset{t \rightarrow \infty}{\sim} P_{\text{eq}}(\mathcal{C}) = e^{-\beta E_p(\mathcal{C})} \quad (3.39)$$

The continuum limit (letting a go to 0 while properly rescaling the physical quantities of interest) of these dynamics can be shown to be equivalent to the Langevin approach presented above [2]. However, we are interested in finding an alternative formulation, in which the non-interacting particles are exactly treated and time-reversal invariance is linear.

The microscopic dynamics described here corresponds to an evolution equation for $P(\mathcal{C}, t)$ that reads:

$$\left\{ \begin{array}{l} \partial_t P(\mathcal{C}, t) = W P(\mathcal{C}, t) \\ W = \sum_{x \in \mathcal{L}} \sum_e \left[(n_{x+e} + 1) e^{-\frac{\beta}{2}(E_p(\mathcal{C}) - E_p(\mathcal{C}'))} P(\mathcal{C}', t) - n_x e^{\frac{\beta}{2}(E_p(\mathcal{C}') - E_p(\mathcal{C}))} P(\mathcal{C}, t) \right], \end{array} \right. \quad (3.40)$$

We follow now the work of Doi [57], popularized in the context of reaction-diffusion processes by Peliti [131]. It consists in introducing a Fock space corresponding to the states \mathcal{C} and making use of the ladder operators of quantum mechanics to obtain the evolution of our system in a second quantized form, i.e. in terms of occupation numbers, which are the discrete versions of the microscopic densities defined in Eq.(3.2). We introduce the lowering and raising operators \hat{a}_x and \hat{a}_x^+ , which satisfy bosonic commutation relations:

$$\begin{aligned} [\hat{a}_x, \hat{a}_y] &= 0 \\ [\hat{a}_x^+, \hat{a}_y^+] &= 0 \\ [\hat{a}_x, \hat{a}_y^+] &= \delta_{x,y} \end{aligned} \quad (3.41)$$

Defining $\hat{n}_x = \hat{a}_x^+ \hat{a}_x$, and choosing convenient normalizations we then construct the Fock space of states from the vacuum state $|0\rangle$ with no particles in it:

$$\hat{a}_x |0\rangle = 0 \quad \forall x. \quad (3.42)$$

Starting from the vacuum state $|0\rangle$, the creation operators \hat{a}_x^+ generate all the microscopic states \mathcal{C} , that have their corresponding kets $|\mathcal{C}\rangle$:

$$|\mathcal{C}\rangle \equiv |\dots, n_x, \dots\rangle = \prod_x (\hat{a}_x^+)^{n_x} |0\rangle. \quad (3.43)$$

Application of the operators \hat{a}, \hat{a}^+ and \hat{n} on these states, and on their corresponding bra's are given by the following relations (note that the normalizations are different from usual conventions for the

quantum harmonic oscillator):

$$\begin{aligned}
\hat{n}_x | \dots, n_x, \dots \rangle &= n_x | \dots, n_x, \dots \rangle \\
\hat{a}_x^+ | \dots, n_x, \dots \rangle &= | \dots, n_x + 1, \dots \rangle \\
\hat{a}_x | \dots, n_x, \dots \rangle &= n_x | \dots, n_x - 1, \dots \rangle \\
\langle \dots, n_x, \dots | \hat{a}_x &= \langle \dots, n_x + 1, \dots | (n_x + 1) \\
\langle \dots, n_x, \dots | \hat{a}_x^+ &= \langle \dots, n_x - 1, \dots | \\
\langle 0 | \hat{a}_x^+ &= 0 \quad \forall x.
\end{aligned} \tag{3.44}$$

In this way, the states are normalized so that:

$$\langle \mathcal{C} | \mathcal{C}' \rangle = \delta_{\mathcal{C}, \mathcal{C}'} = \prod_x \delta_{n_x, n'_x} \tag{3.45}$$

We can now re-write the master equation Eq.(3.40) in the Fock space, by defining a wave function $|\Psi\rangle$ that contains all the information on the statistical state of the system:

$$|\Psi\rangle_t = \sum_{\mathcal{C}} P(\mathcal{C}, t) |\mathcal{C}\rangle \tag{3.46}$$

We can then rewrite the master equation as:

$$\partial_t |\Psi\rangle_t = \hat{W} |\Psi\rangle_t, \tag{3.47}$$

$$\hat{W} = \sum_{x \in \mathcal{L}} \sum_e e^{\frac{\beta V(e)}{2}} \left[\hat{a}_x^+ \hat{a}_{x+e} e^{\frac{\beta}{2} \Delta \hat{E}_p} - \hat{a}_x^+ \hat{a}_x e^{-\frac{\beta}{2} \Delta \hat{E}_p} \right], \tag{3.48}$$

$$\Delta \hat{E}_p = \sum_{y \neq x} (\hat{n}_{y+e} - \hat{n}_y) v(x - y), \tag{3.49}$$

which is functionally solved in time as:

$$|\Psi\rangle_t = e^{\hat{W}t} |\Psi\rangle_{t=0}. \tag{3.50}$$

The average of an observable $A(\mathcal{C})$ that depends on occupation numbers, such as E_p in Eq.(3.37) is defined as:

$$\langle A \rangle_t = \sum_{\mathcal{C}} A(\mathcal{C}) P(\mathcal{C}, t). \tag{3.51}$$

To compute this kind of object, we introduce the projection state:

$$\langle P | = \sum_{\mathcal{C}} \langle \mathcal{C} | = \langle 0 | \prod_x e^{a_x}, \tag{3.52}$$

which has the following properties:

$$\langle P | \hat{a}_x^+ = \langle P |, \tag{3.53}$$

$$\langle P | (\hat{a}_x^+ - 1) = 0, \tag{3.54}$$

$$\langle P | \Psi \rangle_t = \sum_{\mathcal{C}, \mathcal{C}'} P(\mathcal{C}', t) \langle \mathcal{C} | \mathcal{C}' \rangle = \sum_{\mathcal{C}} P(\mathcal{C}, t) = 1 \quad \forall t, \tag{3.55}$$

$$\langle P | \mathcal{C} \rangle = 1 \quad \forall \mathcal{C}, \tag{3.56}$$

and thus compute the average of an observable, as:

$$\langle A \rangle_t = \langle P | \hat{A} | \Psi \rangle_t, \tag{3.57}$$

where \hat{A} is the canonically quantized operator obtained by replacing all n_x in A by \hat{n}_x .

3.2.2 Passage to a field theory

Given a set of states $|\phi\rangle$ that form a representation of the identity,

$$\text{Id} = \sum_{\phi} |\phi\rangle\langle\phi|, \quad (3.58)$$

we can construct a path integral similar to the Feynman path integral by splitting the time interval $[0, t]$ into N slices of size $\Delta t = t/N$ and write:

$$\begin{aligned} \langle A \rangle_t &= \langle P | \hat{A} e^{\hat{H}\Delta t} \dots e^{\hat{H}\Delta t} | \Psi \rangle_{t=0} \\ &= \sum_{\phi_0, \dots, \phi_N} \langle P | \hat{A} | \phi_N \rangle \langle \phi_N | e^{\hat{H}\Delta t} | \phi_{N-1} \rangle \dots \langle \phi_1 | e^{\hat{H}\Delta t} | \phi_0 \rangle \langle \phi_0 | \Psi \rangle_{t=0} \\ &= \sum_{\phi_0, \dots, \phi_N} \langle P | \hat{A} | \phi_N \rangle \prod_{i=1}^N \langle \phi_i | \phi_{i-1} \rangle \langle \phi_0 | \Psi \rangle_{t=0} e^{\Delta t \sum_{i=1}^N \frac{\langle \phi_i | \hat{H} | \phi_{i-1} \rangle}{\langle \phi_i | \phi_{i-1} \rangle}} \end{aligned} \quad (3.59)$$

We specify now the complete set of states that we use to construct the path integral. We construct coherent states:

$$|a\rangle = |\dots, a_x, \dots\rangle = e^{-\frac{1}{2} \sum_x |a_x|^2} e^{\sum_x a_x \hat{a}_x^+} |0\rangle, \quad (3.60)$$

$$\langle a| = \langle \dots, a_x, \dots| = e^{-\frac{1}{2} \sum_x |a_x|^2} \langle 0| e^{\sum_x \bar{a}_x \hat{a}_x}. \quad (3.61)$$

The action of \hat{a} and \hat{a}^+ on these states are:

$$\begin{aligned} \hat{a}_x |a\rangle &= e^{-\frac{1}{2} \sum_x |a_x|^2} \prod_{y \neq x} e^{a_y \hat{a}_y^+} \hat{a}_x e^{a_x \hat{a}_x^+} |0\rangle \\ &= e^{-\frac{1}{2} \sum_x |a_x|^2} \prod_x e^{a_x \hat{a}_x^+} (a_x + \hat{a}_x) |0\rangle \\ &= a_x |a\rangle. \end{aligned} \quad (3.62)$$

$$\begin{aligned} \langle a | \hat{a}_x^+ &= e^{-\frac{1}{2} \sum_x |a_x|^2} \langle 0 | (\bar{a}_x + \hat{a}_x^+) \prod_x e^{\bar{a}_x \hat{a}_x} \\ &= \langle a | \bar{a}_x. \end{aligned} \quad (3.63)$$

The normalisation is given by:

$$\langle a | a \rangle = 1, \quad (3.64)$$

$$\langle a' | a \rangle = \exp \left(-\frac{1}{2} \sum_x [|a'_x|^2 + |a_x|^2] \right) \exp \left(\sum_x \bar{a}'_x a_x \right), \quad (3.65)$$

$$= \exp \left(\frac{1}{2} \sum_x [|a'_x|^2 - |a_x|^2] \right) \exp \left(\sum_x \bar{a}'_x [a_x - a'_x] \right). \quad (3.66)$$

Finally these states form a complete set of the space, as we wanted. To show it, first we remark that (defining $a = u + iv$):

$$\begin{aligned} \int \frac{dudv}{\pi} \bar{a}^n a^m e^{-|a|^2} &= \frac{1}{\pi} \int_{r=0}^{\infty} \int_{\theta=0}^{2\pi} dr d\theta r e^{-r^2} r^{n+m} e^{i(n-m)\theta} \\ &= 2\delta_{n,m} \int_0^{\infty} r^{2n+1} e^{-r^2} dr = n! \delta_{n,m}. \end{aligned} \quad (3.67)$$

It is easy to verify, by resorting to Eq. (3.67), that we have the unity representation:

$$\text{Id} = \int \prod_x \left(\frac{d\text{Re}z_x d\text{Im}z_x}{\pi} \right) |a\rangle\langle a|. \quad (3.68)$$

An important remark is that:

$$\langle P| = e^{\frac{M}{2}} \langle a = 1|, \quad (3.69)$$

where M is the number of lattice sites.

Coming back to Eq. (3.59), we define $t_i = i\Delta t$ and we use those coherent states to get:

$$\langle A \rangle_t = \int \prod_{i,x} \frac{d\Re a_{x,t_i} d\Im a_{x,t_i}}{\pi} \left[\langle P|\hat{A}|a_t\rangle \langle a_0|\Psi \rangle_{t=0} \prod_{i=1}^N \langle a_{t_i}|a_{t_{i-1}}\rangle \right] e^{\Delta t \sum_{i=1}^N \frac{\langle a_{t_i}|\hat{W}|a_{t_{i-1}}\rangle}{\langle a_{t_i}|a_{t_{i-1}}\rangle}} \quad (3.70)$$

We have:

$$\begin{aligned} \prod_{i=1}^N \langle a_{t_i}|a_{t_{i-1}}\rangle &= \prod_{i=1}^N e^{\frac{1}{2} \sum_x (|a_{x,t_i}|^2 - |a_{x,t_{i-1}}|^2)} e^{\sum_{i=1}^N \sum_x \bar{a}_{x,t_i} (a_{x,t_i} - a_{x,t_{i-1}})} \\ &= \exp \left(\frac{1}{2} \sum_x [|a_{x,t}|^2 - |a_{x,0}|^2] \right) \exp \left(\sum_{i=1}^N \sum_x \bar{a}_{x,t_i} (a_{x,t_i} - a_{x,t_{i-1}}) \right) \end{aligned} \quad (3.71)$$

There is still the term $\langle P|\hat{A}|a_t\rangle$ to calculate. The properties of our coherent states and of the projection state are such that, if in \hat{A} , all \hat{a}^+ operators are placed on the left and all \hat{a} operators on the right, this average will be easy to calculate. The operation of putting \hat{a}^+ on the left and \hat{a} on the right is called normal ordering [25]. Defining as \tilde{A} the normal ordered form of \hat{A} , we will have:

$$\begin{aligned} \langle P|\hat{A}|a_t\rangle &= e^{\frac{N}{2}} \langle 1|\hat{A}|a_t\rangle \\ &= e^{\frac{N}{2}} \tilde{A}(1, a_t) e^{\frac{1}{2} \sum_x (1 - |a_{x,t}|^2)} e^{\sum_x (a_{x,t} - 1)} \\ &= \tilde{A}(1, a_t) \exp \left(\sum_x \left[a_{x,t} - \frac{1}{2} |a_{x,t}|^2 \right] \right), \end{aligned} \quad (3.72)$$

where $\tilde{A}(1, a_t)$ is a short-hand notation for the function of the \bar{a} 's and the a 's obtained by replacing all \hat{a}^+ operators by their corresponding eigenvalues \bar{a} and all \hat{a} operators by their eigenvalues a , and finally setting all \bar{a} to unity. Finally, after taking the continuum limit, we arrive at:

$$\langle A \rangle_T = \int \mathcal{D}\bar{a} \mathcal{D}a \tilde{A}(1, a(x, T)) \langle a(x, 0)|\Psi \rangle_{t=0} e^{-S[\bar{a}, a]}, \quad (3.73)$$

$$S[\bar{a}, a] = \int_x (|a(x, 0)|^2 - a(x, T)) + \int_0^T \int_x \left(\bar{a}(x, t) \partial_t a(x, t) - \tilde{W}(\bar{a}(x, t), a(x, t)) \right). \quad (3.74)$$

We thus have found a field theory representation of our stochastic process. In the same way as above, we have had to normal order the operator \hat{W} to be able to easily calculate the matrix elements $\langle a_{t_i}|\hat{W}|a_{t_{i-1}}\rangle$, and we denoted the resulting function of \bar{a} and a by $\tilde{W}(\bar{a}(x, t), a(x, t))$. Note that the \bar{a} 's always have to be calculated at an earlier time than the a 's, a distinction which has disappeared when taking the continuum limit, but has to be remembered when calculating functions at equal times in this formalism. This is the equivalent of the Itô's interpretation of the Langevin equation.

3.2.3 Cole-Hopf transformation

Since the representation in terms of a master equation is fully equivalent to the Langevin equation in Eq.(3.3), all this procedure is for now only a complicated way to reformulate an existing theory. A Cole-Hopf change of variables (first introduced to deal with the Burgers equation in fluid mechanics [42, 75]) defined by:

$$\begin{cases} \bar{a}(x, t) & \rightarrow \exp(\bar{\rho}(x, t)) \\ a(x, t) & \rightarrow \rho(x, t) \exp(-\bar{\rho}(x, t)) \end{cases} \quad (3.75)$$

will lead exactly to the action Eq.(3.17). The terms involving the pair potential that come from the evolution operator \hat{W} will be obvious since they will depend only on $\bar{a}a$ which becomes ρ in this change of variables. Let us look at the other bulk terms. We see that they transform exactly into the ideal gas part of the action in Eq.(3.17):

$$\int_0^T \int_x \bar{a}(x, t) (\partial_t - \nabla_x^2) a(x, t) \rightarrow \int_0^T \int_x [\bar{\rho}(x, t) (\partial_t - \nabla_x^2) \rho(x, t) - \rho(x, t) (\nabla_x \bar{\rho}(x, t))^2] \quad (3.76)$$

up to boundary terms. This change of formulation, although mathematically equivalent to the Langevin formulation is very convenient since we see that the ideal gas part of the problem is now represented by a quadratic action, which is trivially solvable, whereas in the Langevin representation, an analysis in terms of causality of the diagrams must be performed. What about the time reversal ?

The transformation Eq.(3.29) when considered for the case of non-interacting particles simply becomes:

$$\begin{cases} a(x, -t) & \rightarrow \bar{a}(x, t) \\ \bar{a}(x, -t) & \rightarrow a(x, t) \end{cases}, \quad (3.77)$$

which is a linear transformation. However the interacting part of the free-energy involved in the transformation makes the symmetry look more complicated, giving:

$$\begin{cases} a(x, -t) & \rightarrow \bar{a}(x, t) \\ \bar{a}(x, -t) & \rightarrow a(x, t) \exp\left(\int_y \beta v(x-y) \bar{a}(y, t) a(y, t)\right) \end{cases} \quad (3.78)$$

We see that in this new formulation, all the difficulty of conserving the time-reversal is now contained in the interacting part of the problem. In a sense this second quantized form has solved one of our problems, the ideal gas contribution, but not yet the other one: the non-linear expression of the time-reversal.

3.2.4 An alternative linearization of the time-reversal

In order to render time-reversal a linear invariance, we can make use of the well-known similarity transformation [156], that corresponds in our formalism to a rotation in the Fock space:

$$|\Psi\rangle \rightarrow \hat{P}_{\text{eq}}^{1/2} |\Psi\rangle, \quad (3.79)$$

where \hat{P}_{eq} is the canonical quantized form of $P_{\text{eq}}(\mathcal{C})$, i.e.:

$$\hat{P}_{\text{eq}} = \exp\left(\frac{1}{2} \sum_{x \neq y} \hat{n}_x w(x-y) \hat{n}_y\right). \quad (3.80)$$

This has the effect of modifying the evolution operator as follows:

$$\hat{W} \rightarrow \hat{W}_{\text{sym}} \equiv \hat{P}_{\text{eq}}^{-1/2} \hat{W} \hat{P}_{\text{eq}}^{1/2}, \quad (3.81)$$

$$\hat{W}_{\text{sym}} = \sum_{x \in \mathcal{L}} \sum_e \left[\hat{a}_x^+ \hat{a}_{x+e} - \hat{a}_x^+ \hat{a}_x e^{-\frac{\beta V(e)}{2}} e^{-\frac{\beta}{2} \Delta \hat{E}_p} \right]. \quad (3.82)$$

Taking the continuum limit, which we define as:

$$\begin{cases} \hat{a}_x & \rightarrow \hat{a}(x) a^{3/2} \\ \hat{a}_x^+ & \rightarrow \hat{a}^+(x) a^{3/2} \\ \hat{n}_x & \rightarrow \hat{n}(x) a^3 \\ \sum_{y \neq x} a^3 & \rightarrow \int_y \end{cases} \quad (3.83)$$

and expanding the exponentials to second order in the lattice spacing leads to the following evolution equation:

$$\begin{cases} \partial_t |\Psi\rangle = \hat{W}_{\text{sym}} |\Psi\rangle \\ \hat{W}_{\text{sym}} = e^2 \int_x (\hat{a}^+(x, t) \partial_x^2 \hat{a}(x, t) - U_{\text{eff}}[\hat{n}](x, t)) \\ U_{\text{eff}}[\hat{n}](x, t) = \frac{1}{4} \hat{n}(x, t) \int_{y, z} \partial_y \hat{n}(y, t) \cdot \partial_z \hat{n}(z, t) w(x-y) w(x-z) - \frac{1}{2} \hat{n}(x, t) \int_y \partial_y^2 \hat{n}(y) w(x-y) \end{cases} \quad (3.84)$$

The appearance of the effective potential U_{eff} is at this stage very satisfying. Indeed this quantity can be seen as the local rate of escaping from a state, and therefore seems to be a good dynamical quantity in terms of which formulating our dynamical theory. Following the procedure described earlier, Eq.(3.82) leads to a field theory in the continuum in terms of the two fields \bar{a} and a that read:

$$Z = \int \mathcal{D}\bar{a} \mathcal{D}a e^{-S[\bar{a}, a]}, \quad (3.85)$$

$$S[\bar{a}, a] = \int_{x, t} [\bar{a}(x, t) (\partial_t - \nabla_x^2) a(x, t) + U_{\text{eff}}[\bar{a}(x, t) a(x, t)]]. \quad (3.86)$$

A drawback of this formulation is that the density $\bar{a}a$ is not the physical density, unless we place ourselves in the bulk of time: it is easily seen from Eq.(3.71) that the only modification due to the rotation that we performed is in the initial and final terms in the time discretization. The averages in the functional integral will thus correspond to the physical averages only if we send the initial time in the far past and the final observation time in the far future.

What has time-reversal become in this formalism ? Now, thanks to the symmetrization of the evolution operator, the dynamics can fully be interpreted as a quantum mechanical evolution (albeit in imaginary time), and time reversal is simply guaranteed by the symmetry of the action upon exchange of \bar{a} and a , i.e. we are back to the much simpler symmetry:

$$\begin{cases} \bar{a}(x, -t) & \rightarrow a(x, t) \\ a(x, -t) & \rightarrow \bar{a}(x, t) \end{cases}, \quad (3.87)$$

which is finally a linear symmetry. Thus the second of our problems is settled, and we can now safely perform a diagrammatic analysis of our theory. The strength of the interactions will be taken as an

expansion parameter, and since all the non-quadratic parts of the action depend only on $\bar{a}a$ through the effective potential U_{eff} , we are guaranteed never to break the time-reversal symmetry.

A last problem that has to be dealt with is the fact that we want to compute a density-density correlation function, which in our formalism is a four-point function. We dealt with that by constraining $\bar{a}a$ to be equal to ρ by a Lagrange multiplier $\lambda(x, t)$:

$$Z = \int \mathcal{D}\bar{a}\mathcal{D}a e^{-\int_{x,t} \bar{a}(x,t)(\partial_t - \nabla_x^2)a(x,t)} \int \mathcal{D}\rho \delta(\rho - \bar{a}a) e^{-\int_{x,t} U_{\text{eff}}[\rho(x,t)]} \quad (3.88)$$

$$= \int \mathcal{D}\bar{a}\mathcal{D}a\mathcal{D}\rho\mathcal{D}\lambda e^{-S[\bar{a},a,\rho,\lambda]}, \quad (3.89)$$

$$S[\bar{a}, a, \rho, \lambda] = \int_{x,t} \left(\bar{a}(x,t) (\partial_t - \nabla_x^2) a(x,t) + \lambda(x,t) [\rho(x,t) - \bar{a}(x,t)a(x,t)] + U_{\text{eff}}[\rho(x,t)] \right) \quad (3.90)$$

Introducing by hand the density has had the effect of adding a new cubic vertex in the action. Finally we are left with a four-field theory that contains two cubic interaction vertices, which is a much simpler situation than in the case of the Langevin representation, since in that case there is an infinity of interacting vertices in the action, that must be manipulated with care in order to take properly into account the non-interacting particles. The advantages of our formulation are two-fold:

- The ideal gas case is the natural starting point of the perturbative expansion, thus will be correct at all order of approximation, and the strength of the interactions will serve as an organizing device for the diagrammatic expansion
- The time-reversal is a “rapidity” symmetry between \bar{a} and a , and the introduction of the density $\rho = \bar{a}a$ ensures that these two fields will always play a symmetric role when truncations will be performed

3.3 A detour by the Fredrickson-Andersen model

The Fredrickson-Andersen (FA) model [64, 65] is a model of independent spins on a lattice that have two states, up and down, or zero and one, whose dynamics is constrained by a dynamical rule saying that a spin can flip only if one of its neighbors is in the up state. This model represents a coarse grained version of structural glasses. If one considers that the glass transition is a purely dynamical phenomenon, it must have a finite static correlation length. One then separates the system into cells of size of the order of this length, and consider these cells as independent at equilibrium. However, dynamically, one supposes that for a rearrangement to occur in one given cell (for a spin to flip), at least one of the neighboring cells must be in a mobile state (spin up). It is the idea of dynamical facilitation [135].

These models are called a kinetically constrained model, and although they usually have trivial thermodynamics, as a consequence of the kinetic constraints, their dynamics can reproduce various aspects of the glassy dynamics.

We study the FA model only as a toy model, in which the statics are trivial, and the dynamics present glassy features. We will see that in terms of field theory it will correspond to a simplification of the interaction terms when compared to the complicated case of interacting particles in Eq.(3.90). We will thus use this model as a benchmark for our method. The following is yet unpublished material.

3.3.1 The model: dynamics without the statics

We start from the standard action in the Doi-Peliti formalism for the FA model [159], and symmetrize it using the similarity transformation described in the previous section. We obtain as a starting point the following field theory:

$$S[\bar{a}, a] = \int_{x,t} \left[\bar{a} (\partial_t - \Delta) a + \zeta \bar{a} a + \bar{a}^2 a^2 - \sqrt{\zeta} \bar{a} a (\bar{a} + a) \right]. \quad (3.91)$$

Introducing the density, we get:

$$S[\bar{a}, a, \lambda, \rho] = \int_{x,t} \left[\bar{a} (\partial_t - \Delta) a + \zeta \bar{a} a + \rho^2 - \sqrt{\zeta} \rho (\bar{a} + a) + \lambda (\bar{a} a - \rho) \right]. \quad (3.92)$$

In the following, we will group the four fields in a vector $\varphi_i(1)$, defined by:

$$\varphi(1) \equiv \begin{pmatrix} a(x, t) \\ \bar{a}(x, t) \\ \lambda(x, t) \\ \rho(x, t) \end{pmatrix} \quad (3.93)$$

The propagators are defined as $G_{ij}(1, 2) \equiv \langle \varphi_i(1) \varphi_j(2) \rangle - \langle \varphi_i(1) \rangle \langle \varphi_j(2) \rangle$.

Consequences of time-reversal

As described in the previous section, the time-reversal symmetry of the action reads:

$$\begin{cases} a(x, t) \rightarrow \bar{a}(x, -t) \\ \bar{a}(x, t) \rightarrow a(x, -t) \\ \lambda(x, t) \rightarrow \lambda(x, -t) \\ \rho(x, t) \rightarrow \rho(x, -t) \end{cases} \quad (3.94)$$

This symmetry has consequences on the propagators, expressed in the Fourier space for space directions and real space for the time direction:

$$\begin{cases} G_{11}(k, \tau) = G_{22}(k, \tau) \\ G_{13}(k, \tau) = G_{23}(k, -\tau) \\ G_{14}(k, \tau) = G_{24}(k, -\tau) \\ G_{34}(k, \tau) = G_{34}(k, -\tau) \end{cases}, \quad (3.95)$$

We introduce a source term J for the fields, and define as in Chapter 2 the functional Γ , the Legendre transform of the logarithm of the partition function with respect to J . Defining as ϕ the means of the fields, the functional derivatives of Γ with respect to ϕ are defined as:

$$\Gamma_i^{(1)}(1) \equiv \frac{\delta \Gamma[\phi]}{\delta \phi_i(1)}, \quad (3.96)$$

$$\Gamma_{ij}^{(2)}(1, 2) \equiv \frac{\delta^2 \Gamma[\phi]}{\delta \phi_i(1) \delta \phi_j(2)}. \quad (3.97)$$

The time reversal has the same consequences on the two-point functions $\Gamma^{(2)}$ than on G :

$$\begin{cases} \Gamma_{11}^{(2)}(k, \tau) = \Gamma_{22}^{(2)}(k, \tau) \\ \Gamma_{13}^{(2)}(k, \tau) = \Gamma_{23}^{(2)}(k, -\tau) \\ \Gamma_{14}^{(2)}(k, \tau) = \Gamma_{24}^{(2)}(k, -\tau) \\ \Gamma_{34}^{(2)}(k, \tau) = \Gamma_{34}^{(2)}(k, -\tau) \end{cases}, \quad (3.98)$$

Averages of the field and mean-field approximation

The derivative of the action is:

$$\frac{\delta S[\varphi]}{\delta \varphi(1)} = \begin{pmatrix} [-\partial_t - \Delta_x + \zeta + \lambda(1)] \bar{a}(1) - \sqrt{\zeta} \rho(1) \\ [-\partial_t - \Delta_x + \zeta + \lambda(1)] a(1) - \sqrt{\zeta} \rho(1) \\ \bar{a}(1) a(1) - \rho(1) \\ 2\rho(1) - \sqrt{\zeta} [\bar{a}(1) + a(1)] - \lambda(1) \end{pmatrix} \quad (3.99)$$

The saddle-point is defined by the value of φ where this derivative is zero. We assume translational invariance, so that means of fields are independent of space and time, to obtain:

$$\begin{cases} a = \bar{a} = \sqrt{\zeta} \\ \lambda = 0 \\ \rho = \zeta \end{cases} \quad (3.100)$$

Shifting the fields by their mean field values, we find that the propagator of the theory is:

$$G_0(k, \omega) = \frac{1}{\omega^2 + \Omega^2} \begin{pmatrix} 0 & -i\omega + \Omega & \sqrt{\zeta}(-i\omega + \Omega) & \sqrt{\zeta}(-i\omega + \Omega) \\ i\omega + \Omega & 0 & \sqrt{\zeta}(i\omega + \Omega) & \sqrt{\zeta}(i\omega + \Omega) \\ \sqrt{\zeta}(i\omega + \Omega) & \sqrt{\zeta}(-i\omega + \Omega) & -2(\omega^2 + \Omega^2) + 2\zeta\Omega & -(\omega^2 + \Omega^2) + 2\zeta\Omega \\ \sqrt{\zeta}(i\omega + \Omega) & \sqrt{\zeta}(-i\omega + \Omega) & -(\omega^2 + \Omega^2) + 2\zeta\Omega & 2\zeta\Omega \end{pmatrix}, \quad (3.101)$$

which reads, in the real time domain:

$$G_0(k, \tau) = \begin{pmatrix} 0 & \theta(\tau) & \sqrt{\zeta}\theta(\tau) & \sqrt{\zeta}\theta(\tau) \\ \theta(-\tau) & 0 & \sqrt{\zeta}\theta(-\tau) & \sqrt{\zeta}\theta(-\tau) \\ \sqrt{\zeta}\theta(-\tau) & \sqrt{\zeta}\theta(\tau) & -2e^{\Omega|\tau|} + \zeta & -e^{\Omega|\tau|} + \zeta \\ \sqrt{\zeta}\theta(-\tau) & \sqrt{\zeta}\theta(\tau) & -e^{\Omega|\tau|} + \zeta & \zeta \end{pmatrix} e^{-\Omega|\tau|} \quad (3.102)$$

We see that, concerning the fields a , \bar{a} and λ , we have a causal structure of the bare propagator. In the very same way than the analysis performed in the case of the MSR formalism, an analysis of the diagrams that may renormalize G_{13} at all order of perturbation shows that all corrections to $G_{13}(k, \tau)$ remain proportional to $\theta(\tau)$. By symmetry, it is the same for G_{23} , and the analysis can be carried for G_{12} also, leading to the same result.

Since, for the Doi-Peliti construction we used, the action Eq. (3.92) must be understood in Itô's sense, we must conclude that G_{12} , G_{13} and G_{23} must be zero when evaluated at equal times.

We can compute evolution equations for the average fields by exploiting the fact that, when the source J is set to zero, we have:

$$\left\langle \frac{\delta S[\varphi]}{\delta \varphi(1)} \right\rangle = 0, \quad (3.103)$$

which gives four evolution equations:

$$\begin{cases} \sqrt{\zeta}\rho = (\zeta + \lambda)\bar{a} + G_{23}(1, 1) \\ \sqrt{\zeta}\rho = (\zeta + \lambda)a + G_{13}(1, 1) \\ \rho = \bar{a}a + G_{12}(1, 1) \\ \lambda = 2\rho - \sqrt{\zeta}(\bar{a} + a) \end{cases} \quad (3.104)$$

The rapidity symmetry imposes that $\bar{a} = a$ and $G_{13}(1, 1) = G_{23}(1, 1) = G_{12}(1, 1) = 0$ by causality so we are left with:

$$\begin{cases} a = \bar{a} = \sqrt{\zeta} \\ \lambda = 0 \\ \rho = \zeta \end{cases}, \quad (3.105)$$

i.e. the mean-field averages are exact at all order of perturbation.

Interaction vertices

Defining $\varphi = (a - \sqrt{\zeta}, \bar{a} - \sqrt{\zeta}, \lambda, \rho - \zeta)$, the field theory reads:

$$Z = \int \mathcal{D}\varphi e^{-\frac{1}{2} \int_{1,2} \varphi(1) G_0^{-1}(1,2) \varphi(2) - S_{\text{ng}}[\varphi]}, \quad (3.106)$$

$$G_0^{-1}(k, \tau) \equiv \begin{pmatrix} 0 & [-\partial_\tau + k^2 + \zeta] & \sqrt{\zeta} & -\sqrt{\zeta} \\ [\partial_\tau + k^2 + \zeta] & 0 & \sqrt{\zeta} & -\sqrt{\zeta} \\ \sqrt{\zeta} & \sqrt{\zeta} & 0 & -1 \\ -\sqrt{\zeta} & -\sqrt{\zeta} & -1 & 2 \end{pmatrix}, \quad (3.107)$$

$$S_{\text{ng}}[\varphi] = \int_{x,t} \varphi_3(x, t) \varphi_1(x, t) \varphi_2(x, t). \quad (3.108)$$

We see now that this model has the very same structure than the interacting particles, but without the interaction term coming from the pair potential, which involves the density field φ_4 . Here the absence of this term will greatly simplify the formalism. However, this suppresses the possibility of organizing the diagrammatic expansion in powers of the pair potential.

3.3.2 Building self-consistent equations for correlation functions

Following the prescription of Chapter 2, we will write self-consistent equations on the two-point functions by performing the double Legendre transformation. We define the vertex functions Σ :

$$\Sigma \equiv \begin{pmatrix} \Sigma_{11} & \Sigma_{12} & \Sigma_{13} & \Sigma_{14} \\ \Sigma_{21} & \Sigma_{22} & \Sigma_{23} & \Sigma_{24} \\ \Sigma_{31} & \Sigma_{32} & \Sigma_{33} & \Sigma_{34} \\ \Sigma_{41} & \Sigma_{42} & \Sigma_{43} & \Sigma_{44} \end{pmatrix} \quad (3.109)$$

By definition $G_0^{-1} - \Sigma$ is the inverse of the full (unknown) propagator G of the system. A self consistent equation for G is obtained by resorting to the stationary condition of the Legendre transform Eq.(2.48), which gives an expression of Σ as a function of G , and then inserting this expression in the Dyson equation:

$$(G_0^{-1} - \Sigma)G = 1 \quad (3.110)$$

Σ is bound to respect the symmetries of the action, so that it simplifies its matrix composition:

$$\Sigma \equiv \begin{pmatrix} \Sigma_{11} & \Sigma_{12} & \Sigma_{13} & \Sigma_{14} \\ \Sigma_{12}^+ & \Sigma_{11} & \Sigma_{13}^+ & \Sigma_{14}^+ \\ \Sigma_{13}^+ & \Sigma_{13} & \Sigma_{33} & \Sigma_{34} \\ \Sigma_{14}^+ & \Sigma_{14} & \Sigma_{34} & \Sigma_{44} \end{pmatrix}, \quad (3.111)$$

where the superscript \cdot^+ denotes time-reversed quantities.

Mori-Zwanzig equation

Before resorting to a diagrammatic expansion, we face the fact that we want to obtain equations that depend solely on the density-density correlation function, whereas we have a four-field field theory. Without making any approximation, we can obtain an equation similar to the Mori-Zwanzig equation Eq.(1.9) by simply rearranging the elements of the Dyson equation (3.110) that contain G_{44} .

Using the fact that the interaction vertices are independent of the density field, we have that Σ_{i4} and Σ_{4i} are equal to zero whatever the value of i is, which allows us to extract from Eq.(3.110) an exact relation between the propagators:

$$G_{34}(1, 2) = -\delta(1, 2) + 2G_{44}(1, 2) - \sqrt{\zeta} [G_{14}(1, 2) + G_{14}^+(1, 2)]. \quad (3.112)$$

We get another set of three equations that contain G_{44} plus corrections coming from the vertex functions:

$$[-\partial_\tau + \Omega(k)] G_{14}^+(k, \tau) + \sqrt{\zeta} (G_{34}(k, \tau) - G_{44}(k, \tau)) - [\]_{14} = 0, \quad (3.113)$$

$$[\partial_\tau + \Omega(k)] G_{14}(k, \tau) + \sqrt{\zeta} (G_{34}(k, \tau) - G_{44}(k, \tau)) - [\]_{24} = 0, \quad (3.114)$$

$$\sqrt{\zeta} [G_{14}(k, \tau) + G_{14}^+(k, \tau)] - G_{44}(1, 2) - [\]_{34} = 0. \quad (3.115)$$

with the notation $[\]_{ij} = \sum_k \int_3 \Sigma_{ik}(1, 3) G_{kj}(3, 2)$ and $\Omega(k) = k^2 + \zeta$. Combinations of Eqs. (3.112, 3.113-3.115) gives a equation that is closed on G_{44} if all vertex functions are neglected:

$$\begin{aligned} 2\zeta\Omega(k)\delta(\tau) &= [-\partial_\tau^2 + \Omega(k)^2] G_{44}(k, \tau) \\ &\quad - [2\zeta\Omega(k) + \partial_\tau^2 - \Omega(k)^2] [\]_{34} - \sqrt{\zeta} [\partial_\tau + \Omega(k)] [\]_{14} - \sqrt{\zeta} [-\partial_\tau + \Omega(k)] [\]_{24} \end{aligned} \quad (3.116)$$

We recover the free-diffusion behavior of G_{44} if $\Sigma = 0$, and the effect of the non-linearities of the theory are encoded in the matrix elements $[\]_{ij}$, that involve the vertex functions and all the propagators. We arrive at the same situation than in the Mode-Coupling context, where the exact memory kernel depends on all correlation functions of the system, and not only on the density-density one.

3.3.3 Mode-Coupling like equation

The 2PI diagrams that we must consider are built up from a cubic vertex, and thus have the same structure than those shown in Eq.(3.27)

$$\Sigma_{11} = \text{diagram 1} + \text{diagram 2}, \quad (3.117)$$

$$\Sigma_{12} = \text{diagram 3} + \text{diagram 4}, \quad (3.118)$$

$$\Sigma_{13} = \text{diagram 5} + \text{diagram 6}, \quad (3.119)$$

$$\Sigma_{14} = 0, \quad (3.120)$$

$$\Sigma_{33} = \text{diagram 7} + \text{diagram 8}, \quad (3.121)$$

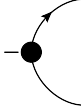
$$\Sigma_{34} = \Sigma_{44} = 0. \quad (3.122)$$

The diagrams above must be understood with the following convention:

$$\bar{a}(k, t_1) - \sqrt{\zeta} \equiv \leftarrow \bigcirc \quad (3.123)$$

$$a(k, t_1) - \sqrt{\zeta} \equiv \text{---} \bigcirc \quad (3.124)$$

$$\lambda(k, t_1) \equiv - \bigcirc \quad (3.125)$$

$$\int_{k_1, k_2, k_3} \delta_{k_1+k_2+k_3} \lambda(k_1, t) (\bar{a}(k, t_1) - \sqrt{\zeta}) (a(k, t_1) - \sqrt{\zeta}) \equiv - \bullet \quad (3.126)$$


$$G_{11}(k, t) \equiv \bigcirc \text{---} \bigcirc \quad (3.127)$$

$$G_{12}(k, t) \equiv \bigcirc \leftarrow \bigcirc \quad (3.128)$$

$$G_{13}(k, t) \equiv \bigcirc \text{---} - \bigcirc \quad (3.129)$$

$$G_{22}(k, t) \equiv \bigcirc \rightarrow \bigcirc \quad (3.130)$$

$$G_{23}(k, t) \equiv \bigcirc \rightarrow - \bigcirc \quad (3.131)$$

$$G_{33}(k, t) \equiv \bigcirc - - - \bigcirc \quad (3.132)$$

The natural thing to do in a field-theoretic context would be then to compute the first correction to mean-field in terms of all the propagators and look at the result for G_{44} . However, in order to understand the structure of the Mode-Coupling theory, we are interested in obtaining an equation solely on G_{44} , that leads us to perform another approximation allowing us to replace all the G_{ij} s with $(i, j) \neq (4, 4)$ in terms of G_{44} . This step is rather arbitrary in the context on the FA model, but will take its sense in the context of particle systems.

At the level of mean-field, all propagators are proportional to G_{44} , as can be seen in Eq.(3.102), and we will use these relations in order to eliminate them in favor of G_{44} :

$$G_{11}(k, \tau) = G_{22}(k, \tau) = 0, \quad (3.133)$$

$$G_{13}(k, \tau) = \frac{1}{2\sqrt{\zeta}\Omega(k)} [-\partial_\tau + \Omega(k)] G_{44}(k, \tau), \quad (3.134)$$

$$G_{23}(k, \tau) = \frac{1}{2\sqrt{\zeta}\Omega(k)} [\partial_\tau + \Omega(k)] G_{44}(k, \tau), \quad (3.135)$$

$$G_{12}(k, \tau) = \frac{1}{2\zeta\Omega(k)} [-\partial_\tau + \Omega(k)] G_{44}(k, \tau), \quad (3.136)$$

$$G_{33}(k, \tau) = -2\delta(\tau) + G_{44}(k, \tau), \quad (3.137)$$

$$G_{14}(k, \tau) = \frac{1}{2\sqrt{\zeta}\Omega(k)} [-\partial_\tau + \Omega(k)] G_{44}(k, \tau) \quad (3.138)$$

Furthermore, we observe that, when neglecting all vertex functions, we have the following relations:

$$G_{44}(k, \tau) = \zeta e^{-\Omega(k)|\tau|}, \quad (3.139)$$

$$\Rightarrow \begin{cases} G_{44}(k, \tau) = -\frac{1}{\Omega(k)} s(\tau) \partial_\tau G_{44}(k, \tau) \\ [\partial_\tau + \Omega(k)] G_{44}(k, \tau) = 2\theta(-\tau)\Omega(k)G_{44}(k, \tau) \\ [-\partial_\tau + \Omega(k)] G_{44}(k, \tau) = 2\theta(\tau)\Omega(k)G_{44}(k, \tau) \end{cases} \quad (3.140)$$

Which induce:

$$\begin{cases} G_{11}(k, \tau) = G_{22}(k, \tau) = 0, \\ G_{13}(k, \tau) = \frac{1}{\sqrt{\zeta}} \theta(\tau) G_{44}(k, \tau), \\ G_{23}(k, \tau) = \frac{1}{\sqrt{\zeta}} \theta(-\tau) G_{44}(k, \tau), \\ G_{12}(k, \tau) = \frac{1}{\zeta} \theta(\tau) G_{44}(k, \tau), \\ G_{33}(k, \tau) = -2\delta(\tau) + G_{44}(k, \tau), \\ G_{14}(k, \tau) = -\frac{1}{\sqrt{\zeta}\Omega(k)} \theta(\tau) G_{44}(k, \tau) \end{cases} \quad (3.141)$$

Replacing these relations in the diagrammatic expressions of the Σ_{ij} s, we obtain:

$$\begin{cases} \Sigma_{12}(k, \tau) = \frac{2}{\zeta} \theta(-\tau) \int_q G_{44}(k-q, \tau) G_{44}(q, \tau) \\ \Sigma_{ij}(k, \tau) = 0 \quad \text{if } (i, j) \neq (1, 2) \end{cases} \quad (3.142)$$

We thus see that:

$$\begin{aligned} [\]_{14} &= \int_{t'} \Sigma_{12}(k, t') G_{14}^+(k, t-t') \\ &= \frac{2}{\zeta^{3/2}} \int_{t'} \theta(-t') \theta(t'-t) \int_q G_{44}(k-q, t') G_{44}(q, t') G_{44}(k, t-t') \\ &= 0 \end{aligned} \quad (3.143)$$

$$\begin{aligned} [\]_{24} &= \int_{t'} \Sigma_{12}^+(k, t') G_{14}(k, t-t') \\ &= \frac{2}{\zeta^{3/2}} \int_{t'} \theta(t') \theta(t-t') \int_q G_{44}(k-q, t') G_{44}(q, t') G_{44}(k, t-t') \end{aligned} \quad (3.144)$$

$$= \frac{2}{\zeta^{3/2}} \int_0^t dt' \int_q G_{44}(k-q, t') G_{44}(q, t') G_{44}(k, t-t') \quad (3.145)$$

$$[\]_{ij} = 0 \quad \text{otherwise} \quad (3.146)$$

Inserting these relations in Eq. (3.116), we get:

$$2\zeta\Omega(k)\delta(\tau) = [-\partial_\tau^2 + \Omega(k)^2] G_{44}(k, \tau) + \frac{4}{\zeta} \int_0^t dt' \int_q G_{44}(k-q, t-t') G_{44}(q, t-t') \partial_{t'} G_{44}(k, t'), \quad (3.147)$$

which has the structure of a Mode-Coupling equation, albeit with a trivial kernel, which is due to the trivial statics of this particular model.

Suppose that the two-point correlation function can have a non-zero value at $t \rightarrow \infty$, which would signal a loss of ergodicity. Then we can obtain an equation on the non-ergodicity factor by Laplace transform. Defining:

$$G_{44}(k, t) = f(k) G_{44}(k, t=0) + g(k, t), \quad (3.148)$$

with g a function that decreases to 0 for $t \rightarrow \infty$, for all k . We get in that case:

$$\frac{f(k)}{1-f(k)} = \frac{4}{\zeta\Omega(k)^2} \int_q G_{44}(q, t=0) G_{44}(k-q, t=0) f(q) f(k-q). \quad (3.149)$$

At $t=0$, the correlation function takes its equilibrium value, which is:

$$G_{44}(k, t=0) = \zeta. \quad (3.150)$$

We obtain an equation for $f^* = f(k=0)$:

$$\frac{f^*}{1-f^*} = \frac{4}{\zeta} f^{*2}, \quad (3.151)$$

which has a trivial solution $f^* = 0$, but also, for $\zeta \leq 1$, two solutions:

$$f^* = \frac{1 \pm \sqrt{1-\zeta}}{2} \quad (3.152)$$

This analysis shows that by a well defined set of approximations, a Mode-Coupling like equation can be found. This procedure is directly applicable to the case of interacting particles, as we show below, but provides a very compact formalism when compared to the only existing field-theory approach, that of Kawasaki and Kim [86].

It was shown in [160, 149] that the slow dynamics of the FA model are governed by a zero-temperature fixed point, whereas the initial predictions of Fredrickson and Andersen [65] was a divergence at finite temperature of the relaxation time of the system.

The transition predicted by our theory is thus spurious. Indeed, this is a consequence of the absence of small parameter in the theory, that made our approximations quite unjustified. However, this encourages us to apply now this method to the case of particle systems, where the strength of the interaction can be used as an organizing device for the perturbation expansion.

3.4 Application to the dynamics of harmonic spheres

Now that we presented the approximation method in a simplified model, we present here its application in the case of the dynamics of harmonic spheres, or any equivalent pair potential that has a repulsive finite-range interaction. The steps of the derivation are essentially the same, but complicated by the appearance of a second interaction vertex that depends on the pair potential, and with a modification of the bare action. A conceptual difference with the derivation above is that the pair potential naturally serves as an expansion parameter around the ideal-gas contribution.

3.4.1 Diagrammatic structure and time-reversal

The time-reversal transformation is unchanged when compared to the FA case, so that Eqs.(3.95) and (3.98) hold. The mean values of the fields are now constrained, since the density is a conserved quantity, so that we have at all times:

$$\langle a(x, t) \rangle = \langle \bar{a}(x, t) \rangle = \sqrt{\rho_0}, \quad (3.153)$$

$$\langle \rho(x, t) \rangle = \rho_0, \quad (3.154)$$

$$\langle \lambda(x, t) \rangle = \langle \bar{\rho}(x, t) \rangle = 0. \quad (3.155)$$

Expanding the action Eq.(3.90) around these saddle point solutions, we get the expression of the inverse bare propagator for our system of particles:

$$G_0^{-1}(k, \tau) = \begin{pmatrix} 0 & \partial_\tau + k^2 & -\sqrt{\rho_0} & 0 \\ -\partial_\tau + k^2 & 0 & -\sqrt{\rho_0} & 0 \\ -\sqrt{\rho_0} & -\sqrt{\rho_0} & 0 & 1 \\ 0 & 0 & 1 & u(k) \end{pmatrix}, \quad (3.156)$$

with

$$u(k) = \frac{k^2}{2\rho_0} \left[(1 + \beta\rho_0 v(k))^2 - 1 \right]. \quad (3.157)$$

There is now an additional vertex in the theory, that contains the pair potential. Diagrammatically, the fields are defined as:

$$\bar{a}(k, t_1) - \sqrt{\rho_0} \equiv \leftarrow \bigcirc \quad (3.158)$$

$$a(k, t_1) - \sqrt{\rho_0} \equiv \bigcirc \rightarrow \quad (3.159)$$

$$\lambda(k, t_1) \equiv - \bigcirc \quad (3.160)$$

$$\rho(k, t) - \rho_0 \equiv \text{wavy line} \bigcirc, \quad (3.161)$$

the interaction vertices as:

$$\int_{k_1, k_2, k_3} \delta_{k_1+k_2+k_3} \lambda(k_1, t) (\bar{a}(k, t_1) - \sqrt{\zeta}) (a(k, t_1) - \sqrt{\zeta}) \equiv - \text{vertex with two incoming and one outgoing curved line} \quad (3.162)$$

$$\int_{k_1, k_2, k_3} \delta_{k_1+k_2+k_3} (\rho(k_1, t) - \rho_0) (\rho(k_2, t_1) - \sqrt{\rho_0}) (a(k_3, t_1) - \sqrt{\rho_0}) \equiv \text{vertex with two incoming wavy lines and one outgoing straight line} \quad (3.163)$$

and the propagators as:

$$G_{11}(k, t) \equiv \bigcirc \text{---} \bigcirc \quad (3.164)$$

$$G_{12}(k, t) \equiv \bigcirc \leftarrow \bigcirc \quad (3.165)$$

$$G_{13}(k, t) \equiv \bigcirc \text{---} - \bigcirc \quad (3.166)$$

$$G_{14}(k, t) \equiv \bigcirc \text{---} \text{wavy line} \bigcirc \quad (3.167)$$

$$G_{22}(k, t) \equiv \bigcirc \rightarrow \bigcirc \quad (3.168)$$

$$G_{23}(k, t) \equiv \bigcirc \rightarrow - \bigcirc \quad (3.169)$$

$$G_{24}(k, t) \equiv \bigcirc \rightarrow \text{wavy line} \bigcirc \quad (3.170)$$

$$G_{33}(k, t) \equiv \bigcirc \text{---} - \bigcirc \quad (3.171)$$

$$G_{34}(k, t) \equiv \bigcirc \text{---} \text{wavy line} \bigcirc \quad (3.172)$$

$$G_{44}(k, t) \equiv \bigcirc \text{wavy line} \bigcirc. \quad (3.173)$$

3.4.2 Mori-Zwanzig equation

Now we can write the equivalent of Eq.(3.116), i.e. the Mori-Zwanzig equation for the density density correlation function by the very same procedure to obtain:

$$\delta(\tau) = \frac{1}{2\rho_0 k^2} \left(-\partial_\tau^2 + \Omega(k)^2 \right) G_{44}(k, \tau) - [\]_{44} - \frac{-\partial_\tau^2 + k^4}{2\rho_0 k^2} [\]_{34} - \frac{\partial_\tau + k^2}{2\sqrt{\rho_0} k^2} [\]_{24} - \frac{-\partial_\tau + k^2}{2\sqrt{\rho_0} k^2} [\]_{14}, \quad (3.174)$$

where $\Omega(k)$ is now $k^2(1 + \beta\rho_0 v(k))$ and $[\]_{ij}$ is still the i, j matrix element of ΣG . By replacing these matrix elements by their actual values we obtain the expression:

$$\begin{aligned} \delta(\tau) = & \frac{1}{2\rho_0 k^2} (-\partial_\tau^2 + \Omega(k)^2) G_{44}(k, \tau) \\ & - \int_t \left[\Sigma_{14}^+(k, t) + \frac{-\partial_\tau^2 + k^4}{2\rho_0 k^2} \Sigma_{13}^+(k, t) + \frac{-\partial_\tau + k^2}{2\sqrt{\rho_0} k^2} \Sigma_{11}(k, t) + \frac{+\partial_\tau + k^2}{2\sqrt{\rho_0} k^2} \Sigma_{12}^+(k, t) \right] G_{14}(k, \tau - t) \\ & - \int_t \left[\Sigma_{14}(k, t) + \frac{-\partial_\tau^2 + k^4}{2\rho_0 k^2} \Sigma_{13}(k, t) + \frac{-\partial_\tau + k^2}{2\sqrt{\rho_0} k^2} \Sigma_{12}(k, t) + \frac{+\partial_\tau + k^2}{2\sqrt{\rho_0} k^2} \Sigma_{11}(k, t) \right] G_{14}^+(k, \tau - t) \\ & - \int_t \left[\Sigma_{34}(k, t) + \frac{-\partial_\tau^2 + k^4}{2\rho_0 k^2} \Sigma_{33}(k, t) + \frac{-\partial_\tau + k^2}{2\sqrt{\rho_0} k^2} \Sigma_{13}(k, t) + \frac{+\partial_\tau + k^2}{2\sqrt{\rho_0} k^2} \Sigma_{13}^+(k, t) \right] G_{34}(k, \tau - t) \\ & - \int_t \left[\Sigma_{44}(k, t) + \frac{-\partial_\tau^2 + k^4}{2\rho_0 k^2} \Sigma_{34}(k, t) + \frac{-\partial_\tau + k^2}{2\sqrt{\rho_0} k^2} \Sigma_{14}(k, t) + \frac{+\partial_\tau + k^2}{2\sqrt{\rho_0} k^2} \Sigma_{14}^+(k, t) \right] G_{44}(k, \tau - t). \end{aligned} \quad (3.175)$$

As expected, the memory kernel depends on all correlation functions, and a substitution has to be performed in order to express them as a function of G_{44} . In Kawasaki and Kim, this substitution is performed in a loop-expansion scheme, substituting in the one-loop result, the 0-loop relations between propagators. This also what we did in the case of the FA model. However, here, we have the strength of the interaction as an organizing device, and we can keep only the lowest orders in $\varepsilon(k) = \beta\rho_0 v(k)$.

3.4.3 Calculation to lowest order in the potential

Let us first have a look at the lowest order diagrams. There are more of them than in the case of the FA model, but we will see that only one will contribute at lowest order.

$$\Sigma_{11} = \text{---} \bigcirc \text{---} + \text{---} \bigcirc \text{---}, \quad (3.176)$$

$$\Sigma_{12} = \text{---} \bigcirc \text{---} + \text{---} \bigcirc \text{---}, \quad (3.177)$$

$$\Sigma_{13} = \text{---} \bigcirc \text{---} + \text{---} \bigcirc \text{---}, \quad (3.178)$$

$$\Sigma_{14} = \text{---} \bigcirc \text{---}, \quad (3.179)$$

$$\Sigma_{33} = - \bigcirc \text{---} + - \bigcirc \text{---}, \quad (3.180)$$

$$\Sigma_{34} = - \bigcirc \text{---}, \quad (3.181)$$

$$\Sigma_{44} = \text{---} \bigcirc \text{---}. \quad (3.182)$$

All propagators verify a Mori-Zwanzig equation such as Eq.(3.175) that relates them to G_{44} at lowest order, with loop corrections that depend on Σ , in the same way as in the case of the FA model. The expression of the inverse propagator is rather complicated, but we will only need it at the lowest order in ε . Setting $\varepsilon = 0$ gives:

$$G_0(k, \tau) = \frac{1}{\rho_0} \begin{pmatrix} 0 & \theta(-\tau) & 0 & \sqrt{\rho_0}\theta(-\tau) \\ \theta(\tau) & 0 & 0 & \sqrt{\rho_0}\theta(\tau) \\ 0 & 0 & 0 & 0 \\ \sqrt{\rho_0}\theta(\tau) & \sqrt{\rho_0}\theta(-\tau) & 0 & 1 \end{pmatrix} G_{44}(k, \tau) \quad (3.183)$$

Using the lowest order diagrams combined with the lowest order expressions of the propagators in function of G_{44} , we get that all vertex corrections can be expressed as integrals of memory kernels multiplied by density-density correlation functions:

$$\Sigma_{ij}(k, \tau) = \int_q \mathcal{M}_{ij}(k, q, \tau) G_{44}(q, \tau) G_{44}(k - q, \tau), \quad (3.184)$$

with the memory kernels given by:

$$\mathcal{M}_{11}(k, q, \tau) = -\frac{\varepsilon(q)\varepsilon(k-q)}{4\rho_0^3} [q^4\varepsilon(q) + (k-q)^4\varepsilon(k-q)], \quad (3.185)$$

$$\mathcal{M}_{12}(k, q, \tau) = \frac{\theta(\tau)}{2\rho_0^3} [q^2\varepsilon(q) + (k-q)^2\varepsilon(k-q)]^2, \quad (3.186)$$

$$\mathcal{M}_{13}(k, q, \tau) = \frac{\theta(\tau)}{4\rho_0^{5/2}} [\varepsilon(k-q) - \varepsilon(q)] [q^2\varepsilon(q) - (k-q)^2\varepsilon(k-q)], \quad (3.187)$$

$$\mathcal{M}_{14}(k, q, \tau) = \frac{\theta(\tau)}{4\rho_0^{3/2}} [k \cdot q\varepsilon(k)\varepsilon(q) + k \cdot (k-q)\varepsilon(k)\varepsilon(k-q) - q \cdot (k-q)\varepsilon(q)\varepsilon(k-q)] \quad (3.188)$$

$$[q^2\varepsilon(q) + (k-q)^2\varepsilon(k-q)]. \quad (3.189)$$

$$\mathcal{M}_{33}(k, q, \tau) = \frac{1}{8\rho_0^2} [\varepsilon(q) + \varepsilon(k-q)]^2, \quad (3.190)$$

$$\mathcal{M}_{34}(k, q, \tau) = \frac{1}{4\rho_0} [k \cdot q\varepsilon(k)\varepsilon(q) + k \cdot (k-q)\varepsilon(k)\varepsilon(k-q) - q \cdot (k-q)\varepsilon(q)\varepsilon(k-q)] [\varepsilon(q) + \varepsilon(k-q)], \quad (3.191)$$

$$\mathcal{M}_{44}(k, q, \tau) = \frac{1}{2} [k \cdot q\varepsilon(k)\varepsilon(q) + k \cdot (k-q)\varepsilon(k)\varepsilon(k-q) - q \cdot (k-q)\varepsilon(q)\varepsilon(k-q)]^2, \quad (3.192)$$

$$(3.193)$$

We see that all vertex functions are proportional at least to ε^2 , even when evaluating the propagators at zero order in the potential. Therefore the relations between propagators that we used are correct to $\mathcal{O}(\varepsilon)$.

Finally, we see that we can drop, at order $\mathcal{O}(\varepsilon^2)$, all contributions except Σ_{12}, Σ_{13} and Σ_{33} . Upon substituting their expressions in Eq.(3.175), we also see that we can neglect the contribution from Σ_{33} since it is convoluted with G_{34} , which is $\mathcal{O}(\varepsilon)$. Only the two first lines of the loop corrections in Eq.(3.175) survive at this order, and we can also replace G_{14} and G_{14}^+ by expressions at the lowest order in the potential in function of G_{44} :

$$(\partial_\tau + k^2)G_{14}(k, \tau) = 2\sqrt{\rho_0}\theta(-\tau)\partial_\tau G_{44}(k, \tau), \quad (3.194)$$

$$(-\partial_\tau + k^2)G_{14}^+(k, \tau) = -2\sqrt{\rho_0}\theta(\tau)\partial_\tau G_{44}(k, \tau). \quad (3.195)$$

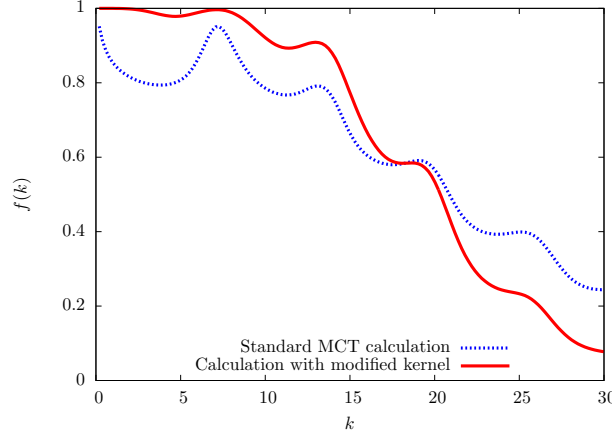


Figure 3.1: Non-ergodicity factor of harmonic spheres obtained by numerically solving Eq.(3.199) (solid line) and the original mode-coupling result Eq.(1.11) (dashed line), for density $\rho_0 = 1.01$ and reduced temperature $\beta\varepsilon = 10^{-4}$.

If $\tau > 0$ the Heaviside functions restrict the time interval to $[0, \tau]$ for the term containing $\Sigma_{12}G_{14}^+$ and cancels the term containing $\Sigma_{12}^+G_{14}$, and we finally obtain:

$$0 = (-\partial_\tau^2 + \Omega(k)^2) G_{44}(k, \tau) + \frac{k^2}{2\Omega(k)\rho_0^3} \int_0^\tau dt \int_q [q^2\varepsilon(q) + (k-q)^2\varepsilon(k-q)]^2 G_{44}(q, \tau-t) G_{44}(k-q, \tau-t) \partial_t G_{44}(k, t) \quad (3.196)$$

We note that G_{44} is equal to $\rho S(k, t)$, where $S(k, t)$ is the dynamical structure factor. By Laplace transforming Eq.(3.196) and focusing on the long-time limit, we get an equation for the non-ergodicity parameter:

$$\frac{f(k)}{1-f(k)} = \frac{\rho_0 k^2}{2\Omega(k)^3} \int_q [q^2\beta v(q) + (k-q)^2\beta v(k-q)]^2 S(q)S(k-q)f(q)f(k-q). \quad (3.197)$$

This equation has a flavor of the Mode-Coupling equation (1.11), but because we insisted on staying at the lowest order in the potential, we have that the direct correlation function is approximated by $c(k) = -\beta v(k)$, which is equivalent to setting $S(k) = 1/(1 + \beta\rho_0 v(k)) \Leftrightarrow \Omega(k) = k^2/S(k)$. This is the RPA approximation of liquid theory [74]. Restoring the renormalized values of the static quantities we end up with:

$$\frac{f(k)}{1-f(k)} = \frac{\rho S(k)}{2k^4} \int_q [q^2 c(q) + (k-q)^2 c(k-q)]^2 S(q)S(k-q)f(q)f(k-q). \quad (3.198)$$

Put under this form, the only difference with the true MCT equation is that in the kernel we have q^2 instead of $k \cdot q$ and $(k-q)^2$ instead of $k \cdot (k-q)$. We can simplify the integral by switching to bi-polar coordinates, i.e. defining $u = |q|, v = |k-q|$ and making the change of variables $q \rightarrow (u, v, \theta)$, where θ is the angle between k and q . The Jacobian of this transformation is uv/k , and we thus obtain:

$$\frac{f(k)}{1-f(k)} = \frac{\rho S(k)}{2k^5} \int_0^\infty du \int_{|k-u|}^{k+u} dv uv [u^2 c(u) + v^2 c(v)]^2 S(u)f(u)S(v)f(v) \quad (3.199)$$

Numerically solving this equation for harmonic spheres gives the result shown in Fig. 3.1. We see that f goes to one when k is small, which seems to constrain the form of the result in the vicinity

of $k = 0$. Indeed, it is a direct mathematical consequence of the form of the kernel: because of the replacement $k \cdot q \rightarrow q^2$, the small k behavior of the right hand side of Eq.(3.199) is singular, which forces the left hand side to be singular too, which means that $f(k = 0)$ must be equal to 1.

3.4.4 A new symmetry

This small k divergence is related to the appearance in the formalism of a new symmetry. Upon the transformation:

$$\begin{cases} \bar{a}(x, t) & \rightarrow \bar{a}(x, t)e^{i\theta} \\ a(x, t) & \rightarrow a(x, t)e^{i\theta} \end{cases}, \quad (3.200)$$

the original action is invariant. This gauge symmetry naturally enforces that $\langle \bar{a} \rangle = \langle a \rangle = 0$, a condition that we break in the beginning of our calculation. Even if this symmetry is not as crucial as time-reversal, and we could obtain reasonable results while breaking it, it is obvious that in order to have a consistent formalism, we need to find a way to properly include it in the formalism. The search for a 2PI action that would be operational in the symmetry-broken phase of Bose-Einstein condensate is of current interest in condensed matter, see in particular [92, 93], and we hope that such extension of the existing tools will be developed in the next years.

3.4.5 Discussion

The approach presented here has three main advantages:

- it takes into account the ideal gas part of the dynamics without having to resort to complicated non-perturbative manipulations as in [86]
- it possesses a small parameter when the pair potential of the liquid under scrutiny has an energy scale
- and it gives an operational result with few calculations when staying at the lowest order in the potential

It shows in a transparent way what kind of approximations are made in order to obtain a mode-coupling like equation. In particular it emphasizes the role of projection onto the density-density correlation functions, also present in the formulation of [86]: a more natural thing to do would be to keep all correlators and solve their self-consistent equations all at once, without performing substitutions. In the case of an expansion at the lowest order in the potential this procedure is well defined, however in most cases in the study of glasses, such expansion would not be possible, for example for hard-spheres an expansion in powers of the potential would clearly break down. Also the glass transition happens at quite low temperature, so that the parameter ε of the theory, which is $\beta v(k)$, is rarely small ! A possible exception could be provided by the Gaussian core model when studied at very high densities, where MCT has been found to be quite accurate [76, 78, 77].

In the case of the FA model, we have found that when solving the whole set of Dyson equations without focusing on the density-density sector, the ergodic phase with $f(k) = 0$ is always stable at finite temperature. Whether the situation is the same for the particles is much harder to analyse.

Another intriguing aspect is that it has been proved, when studying a schematic version of the Mode-Coupling equations, where space indices are dropped, that upon including successively higher order corrections, the transition is gradually shifted to larger and larger densities, and eventually

disappears when the whole series is re-summed [109], while the MCT fits still provide a good representation of the exact result for a limited time-interval. This is exactly the current experimental and numerical situation, and extending such results to the full dynamics of the system would be particularly satisfying.

There are two main drawbacks to the present theory:

- first the use of the similarity transformation forces one to consider a calculation in the bulk of time, therefore loosing track of the initial conditions, which are ordinarily used to recover the full static correlations of the system [3, 86].
- secondly, a $U(1)$ symmetry has been added in the problem, which is broken by hand by our approximation scheme, and is speculated to deteriorate the results at large wave-length.

The first drawback is easily dealt with thanks to the accumulation of knowledge in the field theory formulation of glassy dynamics, since we know on independent grounds how the static correlations get renormalized, but the second issue is more serious and prevents an attempt to go to next order in the calculation.

Chapter 4

The replica method for structural glasses

After focusing on the treatment of the glass transition by dynamical approaches, this chapter is devoted to the presentation of results obtained by using the replica method in the vicinity of the glass transition. Starting from assumptions on the structure of the system in the glass phase inspired by the RFOT scenario, and working in a static framework, one is able to derive self-consistent equations for the non-ergodicity factor [130], a quantity which is originally defined in terms of dynamical quantities.

The link between such equations in dynamical and static theories is still unclear, in particular because the assumptions made by RFOT on the metastable states of the system are not explicitly *a priori* related to a dynamical calculation, except in some mean-field disordered models [90, 46, 24]. A first attempt to relate the two approaches by Szamel [152], by characterizing metastable states by a vanishing current condition, is promising, but suffers from the same short-comings than MCT itself, in the sense that the truncation procedure is again rather arbitrary.

We adopt here a complementary approach, by staying in the hypotheses of RFOT, but insisting on obtaining a equivalent to the equation for the non-ergodicity parameter of Mode-Coupling theory Eq.(1.11). We showed that a part of the MCT kernel is recovered, while the other and most important can not be recovered within this approach, thus disentangling its static and dynamic parts. Moreover, the formalism set up to obtain this result can be further extended in a variety of directions to improve the quantitative efficiency of replica theory.

4.1 Focusing on the long time limit: the replica method

Motivated by the observations from dynamical calculations such as Mode-Coupling theory, or the calculation presented in Chapter 3, we will now make the assumption that there exists a well-defined transition from an ergodic liquid to a non-ergodic one, at a density $\rho_d(T)$. Above this density, adopting the point of view of the RFOT, the system is supposed to be stuck in one of many metastable states, and is not able to visit its whole phase-space anymore. The partition function is thus postulated to be separated in many pure states, parts of the phase space that are disconnected from one another. This picture is of course inspired from mean-field models, where it is exactly realized [116]. In finite dimension, the time needed in order to jump from one state to the other will be finite. A phenomenological theory of nucleation [89, 61, 27, 23] has been devised in order to correct the mean-field vision that

we describe here. However, until now, no theoretic calculation on realistic models such as harmonic spheres or hard spheres have been able to put quantitative background on these ideas, and we will stay at the level of these mean-field concepts.

4.1.1 Ergodicity breaking and complexity

By definition, ergodicity breaking, if it takes place, separates the phase space into “pure” states, i.e. states that can not be connected by any dynamical process in the thermodynamic limit, even in the $t \rightarrow \infty$ limit. Thus, we index these states by α that runs from 1 to \mathcal{N} , and we calculate the average of an observable A as follows:

$$\langle A \rangle = \frac{1}{Z} \sum_{\mathcal{C}} e^{-\beta H(\mathcal{C})} A(\mathcal{C}) = \sum_{\alpha=1}^{\mathcal{N}} \frac{\sum_{\mathcal{C} \in \alpha} e^{-\beta H(\mathcal{C})}}{Z} \frac{1}{\sum_{\mathcal{C} \in \alpha} e^{-\beta H(\mathcal{C})}} \sum_{\mathcal{C} \in \alpha} e^{-\beta H(\mathcal{C})} A(\mathcal{C}), \quad (4.1)$$

where \mathcal{C} is a microscopic state of the system (here the set of positions of the particles). Defining

$$Z_{\alpha} = \sum_{\mathcal{C} \in \alpha} e^{-\beta H(\mathcal{C})}, \quad (4.2)$$

$$w_{\alpha} = \frac{1}{Z} \sum_{\mathcal{C} \in \alpha} e^{-\beta H(\mathcal{C})}, \quad (4.3)$$

We thus define the average inside a state α :

$$\langle A \rangle_{\alpha} \equiv \frac{1}{Z_{\alpha}} \sum_{\mathcal{C} \in \alpha} A(\mathcal{C}) e^{-\beta H(\mathcal{C})}, \quad (4.4)$$

and an average over all states:

$$\overline{A_{\alpha}} \equiv \sum_{\alpha=1}^{\mathcal{N}} w_{\alpha} A_{\alpha}. \quad (4.5)$$

Finally any average will be denoted by $\overline{\langle \cdot \rangle_{\alpha}}$.

Defining f_{α} , the effective free-energy of state α , by:

$$f_{\alpha} = -\frac{k_B T}{N} \ln Z_{\alpha}, \quad (4.6)$$

where N is the number of particles in the system, and inserting this definition in the partition function we get:

$$Z = \sum_{\alpha=1}^{\mathcal{N}} e^{-N\beta f_{\alpha}}. \quad (4.7)$$

We define now the complexity as the extensive component of the number of metastable states. For a given free-energy level f , supposing that there are $\mathcal{N}(f)$ metastable states that have this precise free-energy, we introduce $\Sigma(f)$ as:

$$\Sigma(f) = \frac{1}{N} \ln \mathcal{N}(f). \quad (4.8)$$

By introducing a delta function in the partition function, we obtain:

$$Z = \sum_{\alpha=1}^{\mathcal{N}} \sum_f \delta(f - f_{\alpha}) e^{-N\beta f} \quad (4.9)$$

$$= \sum_f e^{-N\beta f} \underbrace{\sum_{\alpha=1}^{\mathcal{N}} \delta(f - f_{\alpha})}_{=\mathcal{N}(f)} \quad (4.10)$$

$$= \sum_f e^{-N\beta[f - T\Sigma(f)]}. \quad (4.11)$$

In the thermodynamic limit, the free-energy F of the system will be dominated by the free-energy that minimizes the argument of the exponential:

$$F \equiv \lim_{N \rightarrow \infty} -\frac{k_B T}{N} \ln Z \quad (4.12)$$

$$\Rightarrow \begin{cases} F = f^* - T\Sigma(f^*) \\ f^* \text{ defined as } \left. \frac{\partial \Sigma(f)}{\partial f} \right|_{f^*} = \frac{1}{T} \end{cases} \quad (4.13)$$

If the number of metastable states is sub-exponential, we will have $\Sigma = 0$, and the partition function will be dominated by the true free-energy minimum. But if we have $\Sigma \neq 0$, the free-energy of the glass in Eq.(4.13) will be smaller than the free energy of this isolated free-energy minimum, and thus the glass phase will be preferred thermodynamically.

We have now reduced the problem of detecting the glass transition to checking whether there exists or not a finite complexity. It is worth noting that, if there exists a transition from zero to non-zero complexity, this won't be associated to a true thermodynamic phase transition: indeed the entropic term $-T\Sigma(f^*)$ will act, thermodynamically, as a driving force that allows the system to visit all metastable states, thus restoring ergodicity.

However, dynamically, and in the thermodynamic limit, the time needed to perform these jump goes to infinity at the transition $\rho_d(T)$, and the system is effectively stuck forever in this particular state. This is the same situation that occurs in the ferromagnet-paramagnet transition, where the two possible ordered states are thermodynamically equivalent, but a fluctuation that would allow to change from one to the other is in practice never observed.

Of course Eq.(4.13) is useless since we still do not know the free-energy of the states f^* and the complexity $\Sigma(f)$, and we need a tool to go further. An adaptation of the replica method used in the study of mean-field models provides such a tool, as was realized by Monasson [118].

4.1.2 Order parameter for the glass transition

To continue the analogy with the ferromagnet-paramagnet transition, detecting the transition in that case with thermodynamical methods is easy, since we know exactly the structure of the two equivalent ordered states: all spins up or all spins down. Thus, we add a small external field which is coupled to the magnetization to explicitly break the symmetry between the two states, calculate the free-energy with this small symmetry breaking field, then let the strength of the field go to zero. If the system is in the disordered phase, letting go of the external field averages the magnetization to zero. However, if the system is in the ordered (ferromagnetic) state, the total magnetization will be equal to a non-

zero value even in the limit of zero external field. This provides a scalar order parameter for the ferromagnet-paramagnet transition: the magnetization.

In the case of the glass transition, we do not know the possible final states after the transition: they are infinitely numerous, and are frozen liquid configurations. Thus it is much harder to pin the system towards one of these states. However, one possible way is to introduce exact copies of the system, say for example m copies. The copies are indexed by $a = 1, \dots, m$. If the copies are uncorrelated, then the partition function of the replicated liquid is just Z^m . Now consider introducing a small attractive coupling between the copies. More precisely, particle i in copy a will interact with particle j in copy b (if $a \neq b$) via an attractive pair potential $\tilde{v}(x_i^a - x_j^b)$, that has a small amplitude ε .

Exactly as in liquid theory, we are interested in global quantities such as the density, and we can generalize the definitions of the density and correlation functions to the case of the replicated liquid, defining:

$$\hat{\rho}_a(x) = \sum_{i=1}^N \delta(x - x_i^a), \quad (4.14)$$

$$\rho_a(x) = \langle \hat{\rho}_a(x) \rangle. \quad (4.15)$$

Of course by translational invariance and because all copies are identical, in the vanishing coupling limit, $\rho_a(x) = \rho$. We have to look at a two-point quantity, as in the dynamical framework. We now search for a quantity playing the role of an order parameter for the glass transition, and we expect it to be a two-point quantity. We naturally turn to the generalization for copies of the pair correlation function defined in Eq.(2.60) for copies:

$$h_{ab}(x, y) \equiv \frac{\langle \hat{\rho}_a(x) \hat{\rho}_b(y) \rangle}{\rho^2} - 1 - \delta_{ab} \frac{1}{\rho} \delta(x - y), \quad (4.16)$$

and we show below that this is indeed the correct order parameter. Note that, for $a \neq b$, the coinciding point term is absent, because particle i of copy a interacts with all particles of copy b , including particle i , whereas within copy a , particle i does not interact with itself. At finite N , ergodicity is guaranteed and the small attraction will ensure that the two copies will be in the same state. Now perform the large system size limit $N \rightarrow \infty$:

- if $\rho < \rho_d$, ergodicity is maintained, and letting ε to zero will lead the two copies to de-correlate, i.e. $h_{ab} = 0$;
- if $\rho > \rho_d$, the two copies will be trapped into a metastable state α . Finally letting ε go to zero, the two copies will remain correlated and $h_{ab} \neq 0$.

We see that the h_{ab} function, provided it is calculated with vanishingly small attractive coupling, is a good order parameter for the glass transition.

The average in Eq.(4.16) is, in our static interpretation, first an average inside a state α , then an average over all states. The presence of the attractive coupling between the copies will force them into the same pure state α , leading to:

$$h_{ab}(x, y) = \frac{\langle \hat{\rho}_a(x) \hat{\rho}_b(y) \rangle_\alpha}{\rho^2} - 1 \quad \text{for } a \neq b. \quad (4.17)$$

Letting the interaction go to zero will allow them to de-correlate inside the state, leading to:

$$\lim_{\varepsilon \rightarrow 0} h_{ab}(x, y) = \frac{\langle \hat{\rho}(x) \rangle_\alpha \langle \hat{\rho}(y) \rangle_\alpha}{\rho^2} - 1 \quad (4.18)$$

Note that the average density inside a state is the same for all copies, but needs not be constant, since translational invariance is restored only after summation over all the states.

Independently, the time-dependent density-density correlation, which serves as a dynamic order parameter for the glass transition is defined in real-space by:

$$S(x, y, t) = \langle (\hat{\rho}(x, t) - \rho)(\hat{\rho}(y, 0) - \rho) \rangle. \quad (4.19)$$

The RFOT interpretation is that, at a volume fraction above the glass transition volume fraction, and in the long time limit, the system is stuck in a pure state α , and we have:

$$S(x, y, t) \xrightarrow{t \rightarrow \infty} \overline{\langle \hat{\rho}(x, t) \hat{\rho}(y, 0) \rangle_\alpha} - \rho^2 \quad (4.20)$$

But the system is at least able to de-correlate inside the state, giving:

$$S(x, y, t) \xrightarrow{t \rightarrow \infty} \overline{\langle \hat{\rho}(x) \rangle_\alpha} \overline{\langle \hat{\rho}(y) \rangle_\alpha} - \rho^2 = \rho^2 h_{ab}(x, y). \quad (4.21)$$

Now we get in Fourier space:

$$S(k, t) \xrightarrow{t \rightarrow \infty} \rho^2 h_{ab}(k). \quad (4.22)$$

Finally we see that h_{ab} is directly proportional to the non-ergodicity parameter [130] defined in Eq.(1.8) of Chapter 1:

$$f(k) = \frac{\rho h_{ab}(k)}{S(k)} \text{ with } a \neq b \quad (4.23)$$

We see that the static order parameter that we defined with the introduction of copies is the same physical observable as the one defined by dynamical means. It is thus interesting to investigate the degree of relevance of the set of approximations made to obtain this static description (separation of the partition function into pure states, form of the spectrum of free-energies, number of metastable states, ...), in order to sort out what is purely static from what is purely dynamic in the glass transition.

4.1.3 Computing the complexity with replicas

We have seen that introducing copies attracted to each other allows one to define an order parameter, but it also gives a way to compute the complexity and free energy of the system. Define first the partition function of the replicated liquid in the grand-canonical ensemble by introducing a chemical potential for each copy:

$$Z_m[\boldsymbol{\nu}, \mathbf{w}] = \text{Tr} e^{\frac{1}{2} w_{ab}(x, y) \hat{\rho}_{ab(x, y)}^{(2)} + \nu_a(x) \hat{\rho}_a(x)}, \quad (4.24)$$

where implicit summation over replica indices and integration over repeated space variables is assumed. The Tr operation is now $\text{Tr} = \frac{1}{N!^m} \int dx_1 \cdot dx_m$. The replicated two-point density and pair potential are defined as [113]:

$$\hat{\rho}_{ab}^{(2)}(x, y) = \sum_{i, j} \delta(x - x_i^a) \delta(y - x_j^b) - \delta_{ab} \delta(x - y) \sum_i \delta(x - x_i^a), \quad (4.25)$$

$$w_{ab}(x, y) = -\beta v(x, y) \delta_{ab} - \beta \tilde{v}(x, y) (1 - \delta_{ab}). \quad (4.26)$$

so that the potential energy component of the hamiltonian separates into a part that contains the liquid pair potential v , and a part that contains the interaction between copies. With these definitions, w_{ab} is conjugated to h_{ab} , for $a = b$, as well as $a \neq b$. We see at that point that a replica index always

appears with a space index, so that, depending on the context, we may group them in one subscript for simplicity.

If copies are attracted to each other, they fall in the same state. Then in the limit of vanishing coupling, they de-correlate inside this state. Moreover, the free-energy landscape felt by all copies is the same as that of the original one when the coupling is sent to zero, such that for the partition function Z_m of the replicated liquid can now be written, in the same way as in Eq.(4.13) as:

$$Z_m = \sum_f e^{-N\beta(mf - T\Sigma(f))}, \quad (4.27)$$

$$\Rightarrow \left\{ \begin{array}{l} F_m = f^*(m) - T\Sigma(f^*(m)), \\ \frac{\partial \Sigma}{\partial f} \Big|_{f^*(m)} = \frac{m}{T} \end{array} \right. \quad (4.28)$$

Performing now an analytic continuation for arbitrary values of m , the free energy and complexity can be calculated as [118]:

$$\left\{ \begin{array}{l} f^*(m) = \frac{\partial F_m}{\partial m} \Big|_{m=1}, \\ \Sigma(f^*(m)) = \frac{m^2}{T} \frac{\partial F_m/m}{\partial m} \Big|_{m=1}. \end{array} \right. \quad (4.29)$$

The program is now clear:

- compute the free-energy of an m -time replicated liquid in the presence of an attractive coupling
- take the large system size limit
- let the coupling go to zero
- make the free-energy analytic in m
- take a derivative with respect to m to get $\Sigma(f^*(m))$
- take the limit $m \rightarrow 1$

If the resulting complexity is non zero, the glass transition has been detected and we can compute the corresponding structure factor by computing the correlation function between two copies.

4.2 Replicated liquid theory

To realize our program, we only need tools issued from liquid theory, as described in chapter 2, since a replicated liquid can be seen as a mixture of m different species of particles. All results from chapter 2 have straightforward generalizations to multi-component systems. We saw that in order to obtain accurate and consistent approximations on the free-energy (that is needed to access the complexity) and pair correlation function (that we need to compute the non-ergodicity factor), it is better to start from the double Legendre transform of the partition function with respect to the chemical potential and the pair potential. Thus we start from the replicated version of this double Legendre transform

[121], given by:

$$\begin{aligned} \Gamma_m[\boldsymbol{\rho}, \mathbf{h}] = & \sum_a \int_x \rho_a(x) [\ln \rho_a(x) - 1] \\ & + \frac{1}{2} \sum_{a,b} \int_{x,y} \rho_a(x) \rho_b(y) [(1 + h_{ab}(x, y)) \ln(1 + h_{ab}(x, y)) - h_{ab}(x, y)] \\ & + \frac{1}{2} \sum_{n \geq 3} \frac{(-1)^n}{n} \text{Tr} \rho_{a_1}(x_1) h_{a_1 a_2}(x_1, x_2) \cdots \rho_{a_n}(x_n) h_{a_n a_1}(x_n, x_1) \\ & + \{2\text{PI diagrams}\}. \end{aligned} \quad (4.30)$$

$$(4.31)$$

The 2PI diagrams are diagrams composed of black nodes $\rho_a(x)$ and links $h_{ab}(x, y)$, such that when two links are removed from the diagrams, it doesn't disconnect in two separate parts. As in the one-component case, the third line of Eq.(4.31) can be seen as a sum of all ring diagrams, with appropriate weighting.

This functional must be extremalized with respect to the pair correlation h_{ab} , which gives a self consistent equation on h_{ab} , making use of the replicated version of Eq.(2.89) [74]:

$$w_{ab}(x, y) = \ln(1 + h_{ab}(x, y)) - h_{ab}(x, y) + c_{ab}(x, y) + \frac{\delta}{\delta h_{ab}(x, y)} \{2\text{PI diagrams}\}, \quad (4.32)$$

where the direct correlation functions c_{ab} are defined by a generalization of Eq.(2.87) to multicomponent mixtures:

$$c_{ab}(x, y) = h_{ab}(x, y) - \sum_c \int_z h_{ac}(x, z) \rho_c(z) c_{cb}(z, y). \quad (4.33)$$

We already see that the form of pair potential that we have chosen implies an asymmetry between h_{ab} with $a \neq b$ and h_{aa} . Otherwise, all replicas play the same role, and we define for the following:

$$\begin{cases} h(x, y) \equiv h_{aa}(x, y), \\ \tilde{h}(x, y) \equiv h_{ab}(x, y) \quad \text{with } a \neq b. \end{cases} \quad (4.34)$$

This is equivalent to a 1RSB structure in the context of mean-field disordered spin glasses [118]. We called the aa correlation function h , since we anticipate that in the ergodic phase, $\tilde{h} = 0$ and thus h_{aa} is the liquid correlation function. For the density fields $\rho_a(x)$, the chemical potentials are not supposed to be asymmetric, and we suppose that as a result $\rho_a(x) = \rho \quad \forall a$.

Now performing our program is quite easy starting from this set of equations:

- The thermodynamic limit has been taken, since Mayer diagrams, apart from a trivial volume dependence, will depend only on $\rho = N/V$, so that N and V can safely be sent to infinity ;
- Letting the couplings go to zero is trivially done by setting w_{ab} to zero for $a \neq b$ in Eq.(4.32) before evaluation of h_{ab} ;
- The equivalence between replicas assumed in Eq.(4.34) will render the free energy analytic in m , since the summations over replica indices will make the appearance of m explicit, and the free-energy will then only depend on m , h and \tilde{h} . For example we can perform the summations

over the replica indices in Eq.(4.33) to get:

$$\begin{cases} c(x, y) = h(x, y) - \rho \int_z h(x, z) c(z, y) - (m-1) \rho \int_z \tilde{h}(x, z) \tilde{c}(z, y) \\ \tilde{c}(x, y) = \tilde{h}(x, y) - \int_z \tilde{h}(x, z) c(z, y) - \rho \int_z h(x, z) \tilde{c}(z, y) - (m-2) \rho \int_z \tilde{h}(x, z) \tilde{c}(z, y) \end{cases} \quad (4.35)$$

- We can take the limit $m = 1$ that we are interested in:

$$\begin{cases} c(x, y) = h(x, y) - \rho \int_z h(x, z) c(z, y) \\ \tilde{c}(x, y) = \tilde{h}(x, y) - \int_z \tilde{h}(x, z) c(z, y) - \rho \int_z h(x, z) \tilde{c}(z, y) + \rho \int_z \tilde{h}(x, z) \tilde{c}(z, y) \end{cases} \quad (4.36)$$

- The replicated free-energy is calculated in the end by inserting h and \tilde{h} that result from Eq.(4.32) and Eq.(4.36) back into Eq.(4.31).

We do not have at our disposal, for the moment, an organizing device for the 2PI diagrams that would help us pick the relevant ones for our purposes, so that the natural thing to do is first to neglect them in order to get more intuition on the problem. This was done by Mézard and Parisi [113], and we review their results here, in the light of our analogy between the static order parameter \tilde{h} and the dynamical one $f(k)$ provided by Eq.(4.23).

4.2.1 Replicated Hyper-Netted-Chain approximation

Now if we neglect the 2PI diagrams, Eq.(4.32) gives two self consistent equations on h and \tilde{h} :

$$\begin{cases} \ln(1 + h(x, y)) = w(x, y) + h(x, y) - c(x, y) \\ \ln(1 + \tilde{h}(x, y)) = \tilde{h}(x, y) - \tilde{c}(x, y) \end{cases} \quad (4.37)$$

These equations must be supplemented with the replicated Ornstein-Zernike equations evaluated at $m = 1$ Eq.(4.36), that read in Fourier space:

$$\begin{cases} c(k) = h(k) - \rho h(k) c(k), \\ \tilde{c}(k) = \tilde{h}(k) - \rho h(k) \tilde{c}(k) - \rho \tilde{h}(k) c(k) + \rho \tilde{h}(k) \tilde{c}(k). \end{cases} \quad (4.38)$$

We see that the functions h and c do not depend on \tilde{h} and \tilde{c} , as expected since they must coincide with the corresponding liquid quantities when $\tilde{h} = \tilde{c} = 0$. They are given by the HNC equations, that have been already discussed in chapter 2.

The functions \tilde{h} and \tilde{c} satisfy a similar set of equations, that also involve h and c :

$$\begin{cases} \tilde{c}(x, y) = \tilde{h}(x, y) - \ln(1 + \tilde{h}(x, y)) \\ \tilde{c}(k) = \tilde{h}(k) - \rho h(k) \tilde{c}(k) - \rho \tilde{h}(k) c(k) + \rho \tilde{h}(k) \tilde{c}(k). \end{cases} \quad (4.39)$$

We can rewrite the second of these equations as:

$$\tilde{c}(k) = \frac{(1 - \rho c(k)) \tilde{h}(k)}{1 + \rho h(k) - \rho \tilde{h}(k)}, \quad (4.40)$$

and use the definition of the structure factor Eq.(2.65), the Ornstein-Zernike equation Eq.(2.87) and the link between h_{ab} for $a \neq b$ with the non-ergodicity factor Eq.(4.23) to obtain:

$$\tilde{c}(k) = \frac{1}{\rho S(k)} \frac{f(k)}{1 - f(k)}. \quad (4.41)$$

Since \tilde{c} and \tilde{h} are both related to f , we see that Eq.(4.38) is a self-consistent equation for the non-ergodicity parameter.

One may wonder if there is any resemblance between such result and the Mode-Coupling one. To make an explicit bridge between the two, we expand the logarithm term in powers of f , to get, to lowest order:

$$\frac{f(k)}{1 - f(k)} = \frac{S(k)}{2\rho} \int_q S(q)S(k-q)f(q)f(k-q), \quad (4.42)$$

which has the very same structure as the long-time limit of the Mode-Coupling equation Eq.(1.11), except that the kernel is missing here. We see that Mode-Coupling only keeps $\mathcal{O}(f^2)$ terms, whereas even a simple approximation like HNC retains an infinite number of those. However the HNC kernel to second order is trivial, and reminiscent of the result obtained by [3] by a dynamical field-theory calculation. The result of such equation is that $f(k) = 1$ for all densities. In contrast, if one keeps the full \ln term, we obtain the following self-consistent equation:

$$\frac{f(k)}{1 - f(k)} = \rho S(k) \mathcal{FT} \left\{ \frac{(S \otimes f)(r)}{\rho} - \ln \left(1 + \frac{(S \otimes f)(r)}{\rho} \right) \right\}, \quad (4.43)$$

where \otimes means convolution in real space, and $\mathcal{FT}\{g(r)\}$ is the Fourier transform of $g(r)$. We solved this equation numerically for the hard-sphere pair potential:

$$v(r) = \begin{cases} +\infty & \text{if } r < \sigma \\ 0 & \text{otherwise} \end{cases}, \quad (4.44)$$

which is the $T \rightarrow 0$ limit of the harmonic spheres potential Eq.(1.20). Similarly to the liquid HNC equations, the numerical scheme is the following:

- Start from a guess on $\tilde{c}(k)$;
- Deduce the corresponding $f(k)$ with Eq.(4.41);
- Inverse Fourier transform to obtain $f(r)$;
- Plug into Eq.(4.43) to get a new estimate of $f(k)$;
- Deduce the corresponding $\tilde{c}(k)$;
- Iterate this procedure until $\tilde{c}(k)$ does not change anymore between two steps.

As described in Chapter 2, the HNC equation was solved by gradually increasing the density and inserting the previous value for $c(k)$ in the next step. Here we can not do that since for all densities smaller than ρ_d , $\tilde{c}(k)$ sticks to 0. At each density we thus started with a Gaussian guess for $\tilde{c}(k)$ until a first non-zero value of the function is spontaneously generated. To stabilize the value of the critical density, we decrease the density and iterate again the scheme by using this obtained $f(k)$ as a starting point, until the solution spontaneously disappears. The obtained non-ergodicity factor is shown in Fig. 4.1.

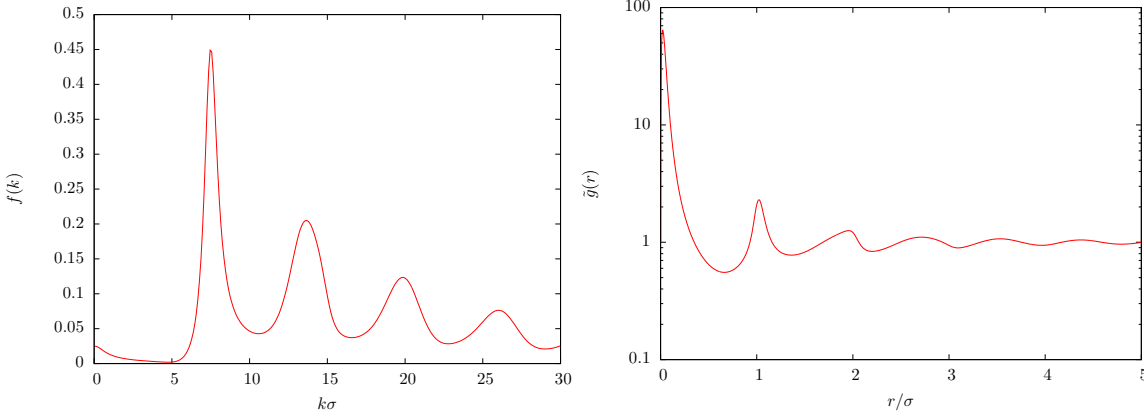


Figure 4.1: Left: Non-ergodicity factor computed from Eq.(4.43) for hard-spheres in 3 dimensions, computed at the transition. Right: Corresponding \tilde{g} function in real space.

The first great success of the replicated HNC approach is that, even within the quite radical set of approximations performed, it detects the presence of a dynamic transition around 0.61 in volume fraction for hard spheres in $3d$, with the concomitant appearance of a non-zero complexity. It is important to emphasize that this complexity is not an artifact of the computation, and that its appearance is a highly non-trivial feature. The qualitative behavior is generally good: the non-ergodicity factor has a strong peak around $k = 2\pi/\sigma$ and oscillates in phase with $S(k)$ while gradually, decreasing to zero at large k .

However, the obtained structure factor is too small to be realistic, and replicated HNC is clearly only a starting point, and calls for improvement.

4.2.2 Expansion in the non-ergodicity parameter

In order to make further progress, we must incorporate some 2PI diagrams into the free-energy. Now consider the 2PI diagrams in Eq.(2.86). Some of those do not contain any h_{ab} with $a \neq b$, and are thus standard liquid theory diagrams, but we can show that those which do contain such links must contain at least three of these. Indeed, one \tilde{h} link joins two nodes that have different replica indices, say a and b . All the nodes connected to the a node by a path of h links must also have replica index a , and the same applies to the b node. Thus all \tilde{h} links are nodal links: they separate the diagram into two parts, each of which has a different replica index. If a 2PI diagram would contain one or two \tilde{h} links, then differentiating once or twice with respect to \tilde{h} would cut the diagram into two parts, which is in contradiction with the fact that the diagram is 2PI. Thus we proved that all 2PI diagrams contain either zero, or three, or more \tilde{h} links. It will prove convenient to classify the diagrams by the number of \tilde{h} links they contain.

The 2PI diagrams of the free-energy are at least $\mathcal{O}(\tilde{h}^3)$, and thus when differentiated with respect to \tilde{h} , will give contributions at order $\mathcal{O}(\tilde{h}^2)$ to the missing kernel of Eq.(4.43). To make contact with the long-time limit of the MCT equation Eq.(1.11), we thus have to re-sum all $\mathcal{O}(\tilde{h}^3)$ 2PI diagrams.

Let us look at the diagrammatic structure of the $\mathcal{O}(\tilde{h}^3)$ diagrams of the free-energy. A diagram that contains three \tilde{h} links can have at most six parts composed of h links and ρ nodes that all have the same replica index. But since the diagram is a free-energy contribution, it must be 1PI, as explained in Chapter 2, i.e. it cannot be cut into two parts by cutting a line. Thus the only possibilities to order \tilde{h}^3 are the diagrams depicted in Fig. 4.2.

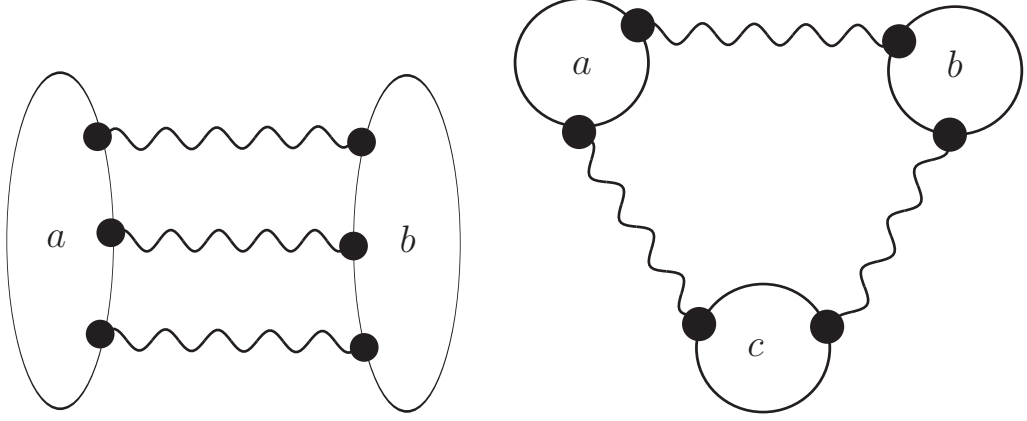


Figure 4.2: Diagrams that contribute to the free-energy at order \tilde{h}^3 . A wiggly line joining two replica indices a and b is a h_{ab} function, a black dot attached to a zone with replica index a is an integration point weighted by a density factor ρ_a .

Note that the ring diagram in Fig. 4.2 is already contained in the re-summation performed by the HNC approximation since it is 1PI but not 2PI. Thus we only have to calculate the diagram on the left to get the contribution that corrects the HNC result in Eq.(4.43). It is important to understand that there are two distinct re-summations involved in this calculation: first a re-summation of all the diagrams that are not 2PI, then a further re-summation of the diagrams that contain exactly three \tilde{h} links. In practice, we will first calculate the sum of all $\mathcal{O}(f^3)$ diagrams, and then add to that result all the other non-2PI diagrams of the replicated HNC equation.

4.3 Expansion at third order

The diagram that we have to compute is composed of two parts, each of which is a non-replicated liquid theory diagram. We will see that each part will be a $\Gamma_1^{(3)}[\rho](x, y, z)$ function of liquid theory, as was defined in Eq.(2.42) of Chapter 2, which are related to the third order direct correlation function of the liquid via Eq.(2.77).

Formally, we have to calculate the third derivative of the free-energy with respect to h_{ab} with $a \neq b$, and evaluate this derivative at zero \tilde{h} , to discard all the diagrams that are of higher order in \tilde{h} than \tilde{h}^3 . In the following we will need to distinguish the derivatives with respect to the density and with respect to the correlation functions. We define:

$$\Gamma_a^{(1,0)}(x_1) = \frac{\partial \Gamma_m[\boldsymbol{\rho}, \mathbf{h}]}{\partial \rho_a(x_1)}, \quad (4.45)$$

$$\Gamma_{ab}^{(0,1)}(x_1, y_1) = \frac{\partial \Gamma_m[\boldsymbol{\rho}, \mathbf{h}]}{\partial h_{ab}(x_1, y_1)}, \quad (4.46)$$

$$\Gamma_{a,cd}^{(1,1)}(x_1; x_2, y_2) = \frac{\partial^2 \Gamma_m[\boldsymbol{\rho}, \mathbf{h}]}{\partial \rho_a(x_1) \partial h_{cd}(x_2, y_2)}, \quad (4.47)$$

and so on. We will also need to define derivatives of $\ln Z_m$ with respect to the chemical potentials

and pair potentials:

$$W_a^{(1,0)}(x_1) = \left. \frac{\partial \ln Z_m[\boldsymbol{\nu}, \mathbf{w}]}{\partial \nu_a(x_1)} \right|_{\boldsymbol{\nu}^*, \mathbf{w}^*}, \quad (4.48)$$

$$W_{ab}^{(0,1)}(x_1, y_1) = \left. \frac{\partial \ln Z_m[\boldsymbol{\nu}, \mathbf{w}]}{\partial w_{ab}(x_1, y_1)} \right|_{\boldsymbol{\nu}^*, \mathbf{w}^*}, \quad (4.49)$$

$$W_{a,cd}^{(1,1)}(x_1; x_2, y_2) = \left. \frac{\partial^2 \ln Z_m[\boldsymbol{\nu}, \mathbf{w}]}{\partial \nu_a(x_1) \partial w_{cd}(x_2, y_2)} \right|_{\boldsymbol{\nu}^*, \mathbf{w}^*}, \quad (4.50)$$

and so on. The term we are interested in, with these notations is $\Gamma_{ab,cd,ef}^{(0,3)}(x_1, x_2; y_1, y_2; z_1, z_2)$ with $a \neq b$, $c \neq d$ and $e \neq f$, evaluated in the liquid phase. This derivative can be related to cumulants of the density and the second derivative $\Gamma^{(0,2)}$ by exploiting the properties of the double Legendre transform.

Considering, for simplicity, a discretized version of our theory, we have that $\boldsymbol{\rho}$ is an $m \times M$ matrix, where M is the number of points of the underlying lattice, and \mathbf{h} is an $m \times m \times M \times M$ object, and the same applies to $\boldsymbol{\nu}$ and \mathbf{w} . We can write the two pairs $\boldsymbol{\rho}, \mathbf{h}$ and $\boldsymbol{\nu}, \mathbf{w}$ in the form of two vectors:

$$\Psi \equiv (\boldsymbol{\rho}, \mathbf{h}), \quad (4.51)$$

$$\Phi \equiv (\boldsymbol{\nu}, \mathbf{w}), \quad (4.52)$$

with the convention that if $i > mM$ an index i must be understood as a group of two space coordinates (x_i, y_i) and two replica indices (a_i, b_i) , but if $i \leq mN$, it must be understood as one space coordinate and one replica index. The double Legendre transform Γ_m can then be written as:

$$\left\{ \begin{array}{l} \Gamma_m[\Psi] = \text{Tr } \Phi_1^* \Psi_1 - \ln Z_m[\Phi^*], \\ \text{with } \Phi^* \text{ such that } \left. \frac{\delta \ln Z_m[\Phi]}{\delta \Phi_1} \right|_{\Phi^*} = \Psi_1. \end{array} \right. \quad (4.53)$$

With these notations, we can make direct use of Eq.(2.42) which gives us:

$$\frac{\delta^3 \Gamma_m[\Psi]}{\delta \Psi_1 \delta \Psi_2 \delta \Psi_3} = -\text{Tr} \left(\frac{\delta^2 \Gamma_m[\Psi]}{\delta \Psi_1 \delta \Psi_1'} \frac{\delta^2 \Gamma_m[\Psi]}{\delta \Psi_2 \delta \Psi_2'} \frac{\delta^2 \Gamma_m[\Psi]}{\delta \Psi_3 \delta \Psi_3'} \frac{\delta^3 \ln Z_m[\Phi]}{\delta \Phi_1' \delta \Phi_2' \delta \Phi_3'} \right)_{\Phi^*}. \quad (4.54)$$

We are interested in the continuum space limit of this expression, evaluated in the liquid, and with 1, 2 and 3 that are all greater than mM . Then we get, with explicit space coordinates and replica indices and implicit summation and integration over repeated indices and variables:

$$\begin{aligned} & \Gamma_{ab,cd,ef}^{(0,3)}(x_1, y_1; x_2, y_2; x_3, y_3) \\ &= -\Gamma_{ab,a'}^{(1,1)}(x_1, y_1; x'_1) \Gamma_{cd,c'}^{(1,1)}(x_2, y_2; x'_2) \Gamma_{ef,e'}^{(1,1)}(x_3, y_3; x'_3) W_{a',c',e'}^{(3,0)}(x'_1; x'_2; x'_3) \\ & - 2\Gamma_{ab,a'b'}^{(0,2)}(x_1, y_1; x'_2, x'_3) \Gamma_{cd,c'}^{(1,1)}(x_2, y_2; x'_2) \Gamma_{ef,e'}^{(1,1)}(x_3, y_3; x'_3) W_{a'b',c',e'}^{(2,1)}(x'_1, y'_1; x'_2; x'_3) \\ & - \text{two permutations } \{(a, b); (x_1, y_1)\} \leftrightarrow \{(c, d); (x_2, y_2)\} \leftrightarrow \{(e, f); (x_3, y_3)\} \\ & - 4\Gamma_{ab,a'}^{(1,1)}(x_1, y_1; x'_1) \Gamma_{cd,c'd'}^{(0,2)}(x_2, y_2; x'_2, y'_2) \Gamma_{ef,e'f'}^{(0,2)}(x_3, y_3; x'_3, y'_3) W_{a',c'd',e'f'}^{(1,2)}(x'_1; x'_2, y'_2; x'_3, y'_3) \\ & - \text{two permutations } \{(a, b); (x_1, y_1)\} \leftrightarrow \{(c, d); (x_2, y_2)\} \leftrightarrow \{(e, f); (x_3, y_3)\} \\ & - 8\Gamma_{ab,a'b'}^{(0,2)}(x_1, y_1; x'_1, y'_1) \Gamma_{cd,c'd'}^{(0,2)}(x_2, y_2; x'_2, y'_2) \Gamma_{ef,e'f'}^{(0,2)}(x_3, y_3; x'_3, y'_3) W_{a'b',c'd',e'f'}^{(0,3)}(x'_1, y'_1; x'_2, y'_2; x'_3, y'_3). \end{aligned} \quad (4.55)$$

There are two types of objects that we need to compute in order to use this relation: cumulants of the microscopic densities that are generated by the differentiation of $\ln Z_m$ with respect to ν_a and

w_{ab} , and second derivatives of Γ_m with respect to ρ_a and h_{ab} . In the end, we want to evaluate these objects in the liquid phase where \tilde{h} is equal to zero. But we know that the free energy can be written as the HNC free energy plus 2PI contributions, that are $\mathcal{O}(\tilde{h}^3)$, i.e. contain more than three \tilde{h} links. Thus when taking one or two derivatives of the 2PI diagrams with respect to \tilde{h} , they still will contain at least one \tilde{h} link, and will all cancel out when evaluated at zero \tilde{h} . This proves that Eq.(4.55) when evaluated in the liquid phase can be computed by replacing the Γ_m functionals in the r.h.s. by Γ_m^{HNC} .

Thus the needed derivatives of Γ_m can be computed starting from Eq.(2.86) by dropping the 2PI diagrams, to obtain (with use of Eq.(4.33) to let the direct correlation function appear when possible):

$$\left\{ \begin{array}{l} \Gamma_{a,cd}^{(1,1)}(x_1; x_2, y_2) \Big|_{\text{liq}} = -\frac{1}{2}\rho (\delta_{ac}\delta(x_1, x_2) + \delta_{ad}\delta(x_1, y_2)), \\ \Gamma_{ab,cd}^{(0,2)}(x_1, y_1; x_2, y_2) \Big|_{\text{liq}} = \frac{1}{2}\rho^2 \delta_{ac}\delta_{bd}\Gamma_{\text{liq}}^{(2)}(x_1, x_2)\Gamma_{\text{liq}}^{(2)}(y_1, y_2). \end{array} \right. \quad (4.56)$$

Finally, computing the cumulants of the microscopic density evaluated in the liquid phase is straightforward, but depends on the replica structure that we consider. For example, if $a \neq b$ and $b = c$, we have:

$$\begin{aligned} \langle \hat{\rho}_a(x)\hat{\rho}_b(y)\hat{\rho}_c(z) \rangle \Big|_{\text{liq}} &= \langle \hat{\rho}(x) \rangle \Big|_{\text{liq}} \langle \hat{\rho}(y)\hat{\rho}(z) \rangle \Big|_{\text{liq}} \\ &= \rho(x)\rho(y)\rho(z) \left[1 + \frac{1}{\rho(y)}\delta(y, z) + h(y, z) \right] \end{aligned} \quad (4.57)$$

If $a = b = c$, we obtain the third order cumulant of the liquid phase, and if $a \neq b \neq c$, we get zero.

A differentiation of $\ln Z_m$ with respect to v_{ab} will also generate an average of microscopic densities:

$$W_{ab}^{(0,1)}(x, y) = -\frac{1}{2\beta} \langle \hat{\rho}_a(x)\hat{\rho}_b(y) - \hat{\rho}_a(x)\delta_{ab}\delta(x, y) \rangle, \quad (4.58)$$

so that the procedure described in Eq.(4.57) can also be applied to evaluate quantities such as the $W^{(i,j)}$ defined in Eqs.(4.48–4.50).

The $\mathcal{O}(\tilde{h}^3)$ term in the free-energy will be of the form:

$$\delta\Gamma_m[\rho, \mathbf{h}] = \frac{\rho^2}{3!} \text{Tr}' \Gamma_{ab,cd,ef}^{(0,3)}(x_1, y_1; x_2, y_2; x_3, y_3) h_{ab}(x_1, y_1) h_{cd}(x_2, y_2) h_{ef}(x_3, y_3), \quad (4.59)$$

where the Tr' operation means a summation over repeated indices and variables, but with the constraint $a \neq b$, $c \neq d$ and $e \neq f$. Within the ansatz that we make in Eq.(4.34), we see that we can interchange the role of replica indices (a, b) and (c, d) and (e, f) freely, as long as the role of space indices is exchanged as well, and the constraints $a \neq b \dots$ are respected. Thus, for a given configuration of replicas, say for example $(a = c = e) \neq (b = d = f)$, there will be several equivalent possibilities that will give the same contribution in the free-energy. In the example above the case $(a = c = f) \neq (b = d = e)$ give the same contribution. After performing the summation over replica indices, we will be left with a sum of topologically inequivalent (in terms of the structure of replica indices) terms, weighted by a multiplicity factor that will depend on m .

Gathering all the expressions of derivatives of $\ln Z_m$ and Γ_m , we obtain the following expression for the $\mathcal{O}(\tilde{h}^3)$ term of Γ_m :

$$\delta\Gamma_m[\rho, \mathbf{h}] = -m(m-1)\frac{\rho^2}{6} \int_{x_1, \dots, x_6} V(x_1, \dots, x_6) \tilde{h}(x_1, x_2) \tilde{h}(x_3, x_4) \tilde{h}(x_5, x_6) + \mathcal{O}((m-1)^2) + \mathcal{O}(f^4), \quad (4.60)$$

$$V(x_1, \dots, x_6) = \frac{1}{2} \Gamma_{\text{liq}}^{(3)}(x_1, x_3, x_5) \Gamma_{\text{liq}}^{(3)}(x_2, x_4, x_6) - \Gamma_{\text{liq}}^{(2)}(x_1, x_3) \Gamma_{\text{liq}}^{(2)}(x_2, x_5) \Gamma_{\text{liq}}^{(2)}(x_4, x_6), \quad (4.61)$$

where $\Gamma_{\text{liq}}^{(3)}$ is the liquid third derivative of the functional Γ_1 as defined in Chapter 2.

It is important to notice that with this calculation, we included all $\mathcal{O}(\tilde{h}^3)$ diagrams, including the ones that are not 2PI, that are already contained in the replicated HNC result. We thus have to subtract these terms, leading to:

$$\begin{aligned} \Gamma_m[\boldsymbol{\rho}, \mathbf{h}] = & \Gamma_m^{\text{HNC}}[\boldsymbol{\rho}, \mathbf{h}] - m(m-1) \frac{\rho^2}{12} \int_{x_1, \dots, x_6} c_{\text{liq}}^{(3)}(x_1, x_3, x_5) c_{\text{liq}}^{(3)}(x_2, x_4, x_6) \tilde{h}(x_1, x_2) \tilde{h}(x_3, x_4) \tilde{h}(x_5, x_6) \\ & - m(m-1) \frac{1}{6} \int_{x_1, \dots, x_4} c_{\text{liq}}^{(3)}(x_1, x_2, x_3) \tilde{h}(x_1, x_4) \tilde{h}(x_2, x_4) \tilde{h}(x_3, x_4) + \mathcal{O}((m-1)^2) + \mathcal{O}(f^4). \end{aligned} \quad (4.62)$$

From this expression we can deduce the $m \rightarrow 1$ limit of the equation on \tilde{h} , obtained by differentiation with respect to \tilde{h} , and we end up with:

$$\begin{aligned} \frac{f(k)}{1-f(k)} = & \rho S(k) \mathcal{FT} \left\{ \frac{(S \otimes f)(r)}{\rho} - \ln \left(1 + \frac{(S \otimes f)(r)}{\rho} \right) \right\} \\ & + \frac{S(k)}{2\rho} \int_q \left[\rho^2 c^{(3)}(-k, q) c^{(3)}(k, -q) + 2\rho c^{(3)}(-k, q) \right] S(q) f(q) S(k-q) f(k-q) \end{aligned} \quad (4.63)$$

This result incorporates exactly all diagrams up to order \tilde{h}^3 , plus all diagrams of replicated HNC, that can be of all orders in \tilde{h} . Thus it can be seen as an improvement over replicated HNC.

Our goal was to obtain an equation for the non-ergodicity parameter in order to make contact with the result of mode-coupling theory. To do that, we once again expand the \ln in powers of \tilde{h} and keep only second order, as we did in the case of replicated HNC, to finally get:

$$\frac{f(k)}{1-f(k)} = \frac{S(k)}{2\rho} \int_q \left[1 + \rho c_{\text{liq}}^{(3)}(k, -q) \right]^2 S(q) S(k-q) f(q) f(k-q) \quad (4.64)$$

When comparing to Eq.(1.11), we see that we recover exactly the term involving the third-order direct correlation function, which is rather unexpected in regards to the very different nature of the starting points of mode-coupling theory and replica theory.

4.3.1 Computing the liquid three-body correlations

Computing the liquid three-body direct correlation function has a long history, mainly due to the importance of the direct correlation functions in Density Functional Theory (DFT) of liquids [55]. In this theoretical framework, one calculates the thermodynamics of an inhomogeneous liquid as an expansion around the homogenous liquid. Thus $\mathcal{F}[\rho]$, the free-energy of the liquid with density profile $\rho(x)$, is expanded around the homogeneous density ρ . Defining $\delta\rho = \rho(x) - \rho$, $\mathcal{F}[\rho]$ is expanded in a functional Taylor series just as in Eq.(3.7) [74]. Truncating this expansion to order 2, one obtains the Ramakrishnan-Yussouf [134] functional. With this kind of expansion, one is able to detect the instability of the homogeneous phase with respect to a phase with broken translational-invariance, the crystal. It is thus crucial to be able to assess the convergence of such series as the one shown in Eq.(3.7), in order to have an accurate density functional theory of freezing [54].

In density functional theory, it was shown that including the $c^{(3)}$ term in the free-energy expansion can lead to an increase of accuracy of the predictions for freezing [144], but without any significant qualitative change. In the context of Mode-Coupling theory, the $c^{(3)}$ term is also present in the kernel, and several numerical works have shown that, except for special cases such as Silica [141], this term is always negligible when compared to the $c^{(2)}$ one [9, 8] contributions that are also present in the kernel.

In our case, the $c^{(3)}$ term is not compared to $c^{(2)}$ but simply to 1, and one could imagine that its effect becomes now non-negligible. However, since $c^{(3)}$ measures the deviation from the convolution form of the third-order structure factor, the numerical values of this function are small and oscillate around 0 with the value of the angle between its two arguments. As a consequence, we speculate that the kernel is equal to 1 plus very small corrections, leading to no significant improvement over the trivial result obtained from Eq.(4.42). In the same way, the inclusion of the $c^{(3)}$ terms in addition to the full HNC result should not change the result.

4.3.2 Conclusion

We have shown that replica theory allows for a prediction for the equivalent of the Mode-Coupling kernel that includes a three-body correlations term. In this way, we showed that this part of the Mode-Coupling kernel has a static origin. Moreover, the term containing the two-body direct correlation function can not be obtained within a static framework, and its origin has to be found in a purely dynamic context. The attempt of Chapter 3, as well as other related works, show that a dynamical calculation typically ends up with such term.

We have seen that, at least in the static context, it is important not to truncate the calculation at lowest orders in \tilde{h} , since it is not a small parameter of the theory: it has a strong peak at the origin, reflecting the fact that two copies are very likely to be found close from one another. This explains why the expansion in the logarithm in Eq.(4.43), that leads to Eq.(4.42), behaves non-physically, and maybe explains also why the results of the full replicated HNC are not in good quantitative agreement with numerical results. Indeed, if we look at a generic diagram kept in the replicated HNC approximation, it is less connected than a 2PI diagram. Since each diagram with a \tilde{h} link will give a strong contribution due to the presence of the peak at $r = 0$, the more \tilde{h} links a diagram will have, the bigger its contribution may be [130].

With these observations in mind this calculation can be extended in two different directions:

- In analogy with the density functional theory of freezing (DFT), one can try to incorporate all diagrams containing the third order direct correlation function (3 particle reducible diagrams), and neglect the higher-order direct correlation functions. The next step is to incorporate all diagrams containing the fourth-order direct correlation function, and neglect all the others, and so on. The convergence of such procedure is not guaranteed, but its efficiency in DFT gives some hope that it may improve the replicated HNC result.
- In analogy with the methods used to treat the Jamming transition within replica theory, that are presented in the next chapter, one can try to introduce a small parameter of the theory like the size of the cage seen by the particles, i.e. the mean amplitude of the vibrations of a particle around its position, averaged on a time scale comparable to the beta relaxation time. This parameter can be used as an organizing device for the diagrammatic expansion that we describe in this chapter.

Chapter 5

Jamming transition of harmonic spheres

In this chapter we present the results obtained when applying the ideas of replica theory as presented in Chapter 4 to the vicinity of the jamming point, with the goal to assess whether the jamming transition is the zero-temperature mechanism that controls the glass transition at finite temperature. We study harmonic spheres at very large volume fractions, around 0.64, and at very low or zero temperature, in order to study the jamming phase diagram of Fig. 1.5. It is found that for these very dense states, at very low temperature, replica theory can be cast into a computationally efficient approximation scheme, allowing us to argue, within a given set of approximations, that the jamming transition is a phenomenon conceptually different from the glass transition, in the line of the calculations on mean-field models of [95] and [103] and hard spheres [130], and numerical experiments on harmonic spheres [21, 20].

We predict, without assuming it, the existence of a jamming transition, solely from microscopic calculations, and successfully reproduce a large set of observed characteristics of the Jamming transition. This work corresponds to publications **P3**, **P4** (short report) and **P6** (long version).

5.1 Jammed states as the densest glassy states

Based on previous works cited above, we have in mind the schematic phase diagram reported in Fig. 5.1. In this picture, that we will derive in the following, the liquid undergoes an ideal glass transition at the Kauzmann temperature $T_K(\varphi)$ (note that in the following, we will mostly use the volume fraction $\varphi = \pi\rho\sigma^3/6$ instead of the density, because it is more suited to the study of hard-spheres and jamming).

The line $T_K(\varphi)$ vanishes at a volume fraction φ_K which also corresponds to the ideal glass transition for hard spheres [130]. The point φ_K *is not the jamming transition*: the ground state energy and pressure remain zero across φ_K . Above φ_K , the system enters, at zero temperature, a *hard sphere glassy state*. In this state, particles vibrate near well-defined (but random) positions, and the system is not jammed yet [130]. Jamming occurs when the glass reaches its close packing density, which we shall call “glass close packing” (GCP), following [130]. We *identify the jamming transition with* φ_{GCP} . Note that at this point this is only an assumption, although a reasonable one, and quantitative arguments will be derived in the following.

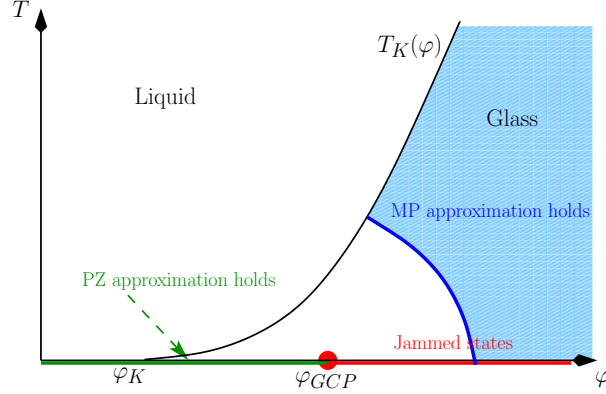


Figure 5.1: A schematic phase diagram for the glassy states of the model defined by Eq. (1.20) showing both the glass transition line at $T_K(\varphi)$ and the jamming point at $T = 0$ and $\varphi = \varphi_{GCP}$. The Parisi-Zamponi (PZ) approach only holds at $T = 0$ and $\varphi < \varphi_{GCP}$, while the Mézard-Parisi (MP) approach holds for large enough densities and temperatures. We developed a method to fill the gap between the PZ and MP analytical schemes to explore the vicinity of the jamming transition.

The main theoretical difficulty in the study of the jamming transition at φ_{GCP} is that it occurs deep inside the glass phase. Therefore, we first need to develop an accurate theoretical description of the glass phase. As discussed in detail in [18], previous theories of the glass phase fail (see Fig. 5.1). The Mézard-Parisi approach (denoted by MP in the following) [113, 114] holds only at high enough temperature or density, where a simple harmonic approximation for vibrations in the glass holds. The Parisi-Zamponi approach (denoted by PZ) [130] holds only in the hard sphere region, $T = 0$ and $\varphi < \varphi_{GCP}$. The central theoretical achievement that we describe here is an approximation scheme that can naturally interpolate between those of MP and PZ and is correct in the entire vicinity of the jamming transition, thus allowing us to fully explore the phase diagram of Fig. 5.1, and in particular the region of low temperature, $T \ll T_K(\varphi)$ and $\varphi \sim \varphi_{GCP}$. We theoretically obtain from a first principle calculation a large number of the observed behaviors of harmonic spheres in numerical experiments [126, 127, 58, 143, 165], and predict new results for the correlation functions of this system around the jamming transition.

Our approach is very different from, but complementary to, recent theoretical works on jamming. The aim of our work is to show, directly from the Hamiltonian, that the jamming transition exists, and determine from first principles its location and properties. Other approaches assume the existence of jammed states and try to obtain geometrical informations on them [41, 147], or develop a scaling picture of the jamming transition by showing that the transition is characterized by a diverging correlation length [162].

Before proceeding further, it is worth noting that even though the mean-field picture on which we will base our calculations is expected to be tempered, in finite dimensional models by nucleation processes [101, 35], we expect that the local and static properties that we intend to compute (such as the number of contacts, energy of a packing, etc.) will not be affected by these processes in the very low temperature and high density regime near the jamming transition.

For this reason, in this work we follow Mézard and Parisi [113, 114] and directly apply the mean-field concepts described above to three dimensional glass-formers.

5.1.1 Thermodynamics of the glass phase

In Chapter 4, we used the replica trick to detect the emergence of a non-zero complexity, signaling the appearance of an exponential number of metastable states, responsible for the slowing down of the dynamics. However, the idea of replicating the system can be pushed further, in order to compute the thermodynamics of the glass phase, as was shown by Monasson [118].

In the following we will use a “free-entropy” \mathcal{S} defined as

$$\mathcal{S} = \lim_{N \rightarrow \infty} \frac{1}{N} \ln Z \quad (5.1)$$

instead of the usual free-energy that goes to 0 when $T \rightarrow 0$.

Returning to Eq.(4.13), the ideal glass transition is reached at the Kauzmann temperature $T_K(\varphi)$, defined by the point where the saddle point of Eq.(4.13) for which the complexity vanishes:

$$\left\{ \begin{array}{l} \frac{\partial \Sigma(f)}{\partial f} \Big|_{f^*(T_K, \varphi)} = \frac{1}{T_K(\varphi)}, \\ \Sigma(f^*(T_K(\varphi), \varphi)) = \Sigma(f_{min}) = 0. \end{array} \right. \quad (5.2)$$

The free-entropy can be read off Eq.(4.13) by multiplying by $-\beta$, and has a simple expression for $T < T_K(\varphi)$, where the complexity sticks to zero:

$$\mathcal{S}_{\text{glass}}(T, \varphi) = -\beta f_{min}(T, \varphi). \quad (5.3)$$

We have shown in Chapter 4 that introducing m replicas coupled together allows for an explicit computation of the complexity. After introducing m replicas, Eq.(4.13) was modified to obtain Eq.(4.28), which contained an m dependance that allows for the computation of Σ . We rewrite here this equation in terms of the quantity \mathcal{S} :

$$\left\{ \begin{array}{l} \mathcal{S}(m; T, \varphi) = \Sigma(f^*(m; T, \varphi)) - m\beta f^*(m; T, \varphi), \\ \frac{\partial \Sigma}{\partial f}(f^*(m; T, \varphi)) = \frac{m}{T}, \\ \Sigma(f^*(m; T, \varphi)) = -m^2 \frac{\partial}{\partial m} \left(\frac{\mathcal{S}(m; T, \varphi)}{m} \right). \end{array} \right. \quad (5.4)$$

Eq.(5.3) shows that for $T < T_K$ the free energy of the glass is equal to $f_{min}(T)$, the point where $\Sigma(f) = 0$. Note also that this value of f depends only on the free-energy landscape, which is the same for all replicas, and it is thus independent of m . Inside the glass phase, if there are several copies, the free-energy will simply be equal to $m f_{min}(T)$.

The parameter m allows, without changing the temperature or density, to modify the value of f^* the saddle point in Eq.(5.4), i.e. to displace the Kauzmann temperature artificially. If we choose m^* it so that $f^*(m^*; T, \varphi) = f_{min}(T, \varphi)$, the complexity will be zero when evaluated at this free-energy, and the expression of the free-entropy will simply become:

$$\mathcal{S}(m^*; T, \varphi) = -m^* \beta f_{min}(T, \varphi), \quad (5.5)$$

and, recalling Eq.(5.3), the free-entropy of the glass will be obtained by dividing by m^* :

$$\mathcal{S}_{\text{glass}}(T, \varphi) = \frac{\mathcal{S}(m^*; T, \varphi)}{m^*} \quad \text{if } T < T_K. \quad (5.6)$$

Still, m^* is an unknown, but we remark that it is made to constrain that $f^* = f_{min}$. Since we expect the complexity to be a monotonic function of f , this is equivalent to say that m^* is made up so that $\Sigma(f^*) = \Sigma(f_{min}) = 0$. Thus m^* is calculated as the value of m that cancels the complexity. But the complexity can be calculated as the derivative of \mathcal{S}/m as shown in Eq.(5.4). Thus m^* is so that:

$$\left. \frac{\partial}{\partial m} \left(\frac{\mathcal{S}(m; T, \varphi)}{m} \right) \right|_{m^*} = 0, \quad (5.7)$$

and thus is the value of m that minimizes \mathcal{S}/m , which finally gives:

$$\mathcal{S}_{glass}(T, \varphi) = \min_m \frac{\mathcal{S}(m; T, \varphi)}{m}. \quad (5.8)$$

Now we see that, in order to compute the thermodynamics inside the ideal glass phase, one must be able to calculate the free entropy of a replicated liquid, and extremize it with respect to the number of copies.

5.1.2 Effective potential approximation

Computing the free-energy and complexity of the glass amounts to computing the free entropy of an m -time replicated liquid. One can use a replicated version of standard liquid theory approximations such as the replicated Hyper-Netted-Chain (HNC) [113, 31] presented in Chapter 4, but we have seen that these of approximations break down deep in the glass phase [130]. One can also follow Mézard and Parisi (MP) [114, 115] and start at high density, then perform cage expansions: at high densities the copies stay close to the originals, forming molecules of size A . One can then expand the replicated free entropy with respect to this parameter A . However, to be able to explicitly compute the various integrals appearing in the computation, one traditionally has to suppose that the attraction between copies is smooth, an assumption which breaks down for hard spheres, as discussed in [130]. To correctly treat the replicated hard sphere system, Parisi and Zamponi (PZ) [130] developed an effective potential approximation, which amounts to performing an expansion in powers of \sqrt{A} instead of A . We explain in the following the extension of the effective potential approximation to finite temperature harmonic spheres. By construction, we will see that we are bound to recover both high density MP results and zero temperature PZ results in a unified treatment.

The starting point of all these approaches is the assumption that (due to the implicit coupling between replicas) the replicated system is composed of *molecules* made of m atoms, each belonging to a different replica. By performing a Legendre transform with respect to the chemical potentials of the particles, as described in Chapter 2, one can express the free energy as a functional of the single molecule density and the interaction potential, see [130] for details. In order to make the computation tractable, one then makes a Gaussian *ansatz* for the probability distribution function of the positions \bar{x} of the replicas within a molecule [115, 130]:

$$\rho(x_1 \cdots x_m) = \rho \int d^3 X \prod_{a=1}^m \frac{1}{(2\pi A)^{3/2}} \exp \left(-\frac{(x_a - X)^2}{2A} \right) \quad (5.9)$$

We can now integrate out all replicas except one. The *effective interaction* between particles in replica 1, v_{eff} , is obtained by averaging the full interaction over the probability distribution of the two

molecules:

$$e^{-\beta v_{\text{eff}}(x_1 - y_1)} \equiv e^{-\beta v(x_1 - y_1)} \left\langle \prod_{a=2}^m e^{-\beta v(x_a - y_a)} \right\rangle_{x_1, y_1} \quad (5.10)$$

$$= \int d^3 x_2 \cdots d^3 x_m d^3 y_2 \cdots d^3 y_m \rho(x_1 \cdots x_m) \rho(y_1 \cdots y_m) \prod_{a=1}^m e^{-\beta v(x_a - y_a)}, \quad (5.11)$$

Due to the Gaussian *ansatz*, and the quadratic form of the harmonic potential Eq.(1.20), the effective interaction has a tractable expression [19], that depends on both parameters A and m . The calculation is schematically represented in Fig. 5.2. Despite the fact that we have Legendre transformed \mathcal{S} , we will keep in the following the notation \mathcal{S} , but make it is formally now a function of ρ , or equivalently of A , since A uniquely parametrizes the density in Eq.(5.9). To come back to the initial free-entropy, one has to do the inverse Legendre transform, and thus find the optimal cage size A^*

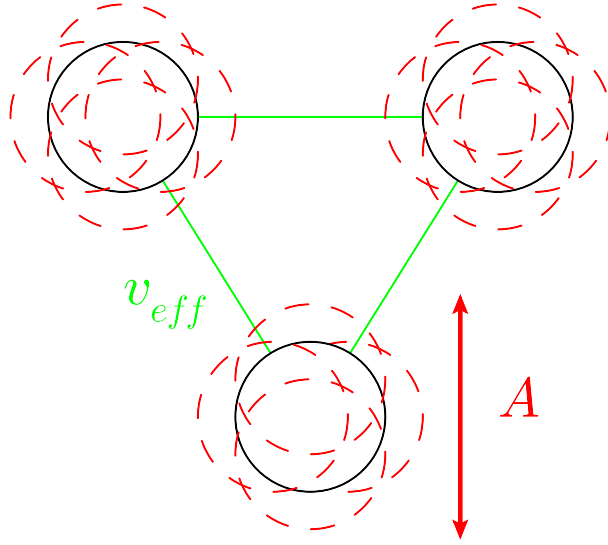


Figure 5.2: A schematic representation of the effective potential approximation. Each particle in the original liquid is replicated m times (dashed spheres). Assuming that the replicated particles form a molecule of average cage size A , in the partition sum, we trace out the degrees of freedom of $(m - 1)$ copies of the liquid to obtain an effective one-component liquid (black spheres) interacting with an effective pair potential v_{eff} (green lines).

The integration of replicas $2 \cdots m$ also induces three-body (and more generally many-body) interactions on replica 1; if we neglect these, and just keep the two-body effective potential, we obtain that the Legendre transform of the free entropy of the replicated liquid with respect to the density is the sum of an harmonic part $\mathcal{S}_h(m, A)$ plus the free energy of a liquid interacting via the effective potential: $\mathcal{S} = \mathcal{S}_h + \mathcal{S}_{\text{liq}}[v_{\text{eff}}]$ [130]. Furthermore, we remark that, when $A = 0$, by definition the probability distribution in Eq.(5.9) becomes a sum of delta functions, and as a consequence, all copies are at the same position. The effective potential in that case is simply m times the original potential. Thus we have that:

$$e^{-\beta v_{\text{eff}}(r)} = e^{-\beta m v(r)} (1 + Q(r)), \quad (5.12)$$

where $Q(r)$, which is directly calculated from the expression of the effective potential, is equal to zero when $A = 0$. Since we expect that, close to the jamming transition, the cage sizes will always be small,

we suppose that $Q(r)$ is a small perturbation, and we make use of equilibrium liquid perturbation theory. We have seen in Eq.(2.83) that the derivative of the Legendre transform of $\ln Z$ is the two-particle distribution function $\rho^{(2)}$:

$$e^{-\beta v_{12}} \frac{\delta \ln Z[\rho]}{\delta e^{-\beta v_{12}}} = \frac{1}{2} \rho_{12}^{(2)} = \frac{1}{2} \rho_1 \rho_2 g_{12}, \quad (5.13)$$

we can thus expand the free-entropy around $e^{-m\beta v}$ at first order to get:

$$\mathcal{S}(m, A; T, \varphi) = S_h(m, A) + \mathcal{S}_{liq}(T/m, \varphi) + \frac{3\varphi}{\pi} \int d^3r g_{liq}(T/m, \varphi; r) Q(r), \quad (5.14)$$

$$S_h(m, A) = \frac{3}{2}(m-1) \ln(2\pi A) + \frac{3}{2}(m-1 + \ln m), \quad (5.15)$$

where $\mathcal{S}_{liq}(T, \varphi) = N^{-1} \log Z_{liq}$ is the free entropy of the liquid, and $g_{liq}(T, \varphi; r)$ its radial distribution function (to be computed at temperature T/m).

Equation (5.14) allows for a full calculation of the replicated free entropy, and allows us to recover both the MP small cage expansion in powers of A at high density, and the PZ expansion in powers of \sqrt{A} at zero temperature, as we will show below. In the following, we do not discuss the details of the calculations, that are extensively described in [19]. Again we emphasize that, due to the Gaussian approximation that we make for the density, and the quadratic form of the potential, the detailed calculations only involve Gaussian integrals. Numerical minimizations must also be performed, for example to compute the optimal number of replicas m^* , or the optimal cage size.

5.1.3 Low temperature liquid theory approximation

Our purpose in interpolating between zero and finite temperature was to be able to probe the vicinity of the jamming point in the (φ, T) phase diagram, thus we are interested mainly in the low temperature behavior of the glass. We can exploit this by making an approximation that will allow us to push the analytical calculation much further. Defining the cavity distribution function y by $g(T, \varphi; r) = e^{-\beta v(r)} y(T, \varphi; r)$ [74], we make the approximation of taking the cavity function of the liquid as a constant and equal to its $T = 0, r = 1$ value, which we call $y_{liq}^{HS}(\varphi)$. As T goes to zero, we see that the exponential factor converges towards a step function around $r = 1$, so that in all integrals that are cut at $r = 1$ by the pair potential, we can safely evaluate y at its $r = 1$ value. Expanding y in powers of T , it is easy to convince oneself that the temperature dependence leads to subleading contributions in the integrals. Thus we suppose:

$$g_{liq}(T/m, \varphi; r) \sim e^{-\beta m v(r)} y_{liq}^{HS}(\varphi), \quad (5.16)$$

which simplifies further the expression of the free-entropy.

The last quantities that we need to compute are the free entropy \mathcal{S}_{liq} and the pair correlation function $g_{liq}(r)$ of the liquid. Given the pair correlation function, which represents the probability of finding a particle at distance r from a particle fixed at the origin, we can express the internal energy U as:

$$U(T, \varphi) = 12\varphi \int_0^\infty dr r^2 g(T, \varphi; r) v(r). \quad (5.17)$$

Plugging the low temperature approximation Eq. (5.16) for the liquid into this, we obtain:

$$U_{liq}(T, \varphi) \underset{T \rightarrow 0}{\sim} 12\varphi y_{liq}^{HS}(\varphi) \int_0^1 dr r^2 (1-r)^2 e^{-\beta(1-r)^2}. \quad (5.18)$$

Making use of the standard identity $U(T) = \frac{\partial(F/T)}{\partial(1/T)}$, we can derive the low temperature approximation for the free entropy of the liquid:

$$\mathcal{S}_{liq}(T, \varphi) \underset{T \rightarrow 0}{\sim} \mathcal{S}_{liq}^{HS}(\varphi) + 6\varphi y_{liq}^{HS}(\varphi) \left[\frac{\sqrt{\pi}}{2} \sqrt{T} (2+T) \operatorname{erf}\left(\frac{1}{\sqrt{T}}\right) + T (e^{-1/T} - 2) \right], \quad (5.19)$$

where $y_{liq}^{HS}(\varphi)$ and $\mathcal{S}_{liq}^{HS}(\varphi)$ are short-hand notations for $y_{liq}(T=0, \varphi; r=1)$ and $\mathcal{S}_{liq}(T=0, \varphi)$.

At this level of approximation, it is clear that the only input that is needed from liquid theory is the equation of state of the hard sphere liquid. From any given equation of state one can easily deduce the hard sphere free entropy \mathcal{S}_{liq}^{HS} and cavity function y_{liq}^{HS} . The most reasonable choice would be to use the phenomenological Carnahan-Starling (CS) equation of state, as in [130], that provides the best fit to the hard sphere pressure.

We instead used the Hyper-Netted Chain approximation described in the end of Chapter 2. Although HNC is known to be less accurate for the hard sphere system, using HNC allows us to also compare our results to the ones obtained from the MP approach valid at large density and finite temperatures. The HNC approximation overestimates y_{liq}^{HS} by 20% in the relevant range of volume fraction $\varphi \sim 0.64$. This has the effect of reducing the glass transition density obtained from the theory, from the value $\varphi_K = 0.62$ obtained from CS [130] to $\varphi_K = 0.58$ obtained with HNC.

Therefore the reader should keep in mind that the glass densities reported in the following are lower than the correct ones. In any case, here we are more interested in the low-temperature scaling in the glass phase than to the actual value of the glass transition density. We also checked that the scaling results are insensitive to the precise choice of the equation of state of the hard sphere liquid.

5.2 Thermodynamics of the glass

5.2.1 Complexity and phase diagram

As discussed above, the glass transition is signaled by the point where the saddle point in Eq. (4.13) reaches the minimum f_{min} at which the complexity $\Sigma(f)$ vanishes. In the replica formalism, the equilibrium complexity $\Sigma(f^*)$ in Eq. (5.2) corresponds to the complexity in Eq. (4.28) evaluated at $m=1$. We call this quantity the “equilibrium” complexity of the liquid $\Sigma_{eq}(T, \varphi)$. The latter is easily computed by expanding the equations around $m=1$

For $\varphi \geq \varphi_K$, the complexity vanishes at a temperature $T_K(\varphi)$, called the Kauzmann temperature, that increases with the density. These results are summarized in the left frame of Fig. 5.3, where we show the complexity as a function of temperature for several volume fractions around φ_K . In the inset we show the zero temperature limit of the complexity Σ_{eq}^{HS} as a function of the density, that vanishes at φ_K .

From the complexity we deduce the phase diagram shown in the right frame of Fig. 5.3. In this figure we report $T_K(\varphi)$, as obtained in the framework of the effective potential approximation, and we compare it with the result obtained from the Mézard-Parisi small cage expansion [18]. In the effective potential case we find that the Kauzmann temperature goes to zero at $\varphi_K \approx 0.5769$, quadratically with the temperature. On the other hand, the result from the small cage expansion is a finite $T_K(\varphi)$ which jumps to zero abruptly at a value of φ which is unrelated to hard sphere results. This is due to fact that the small cage expansion is valid only in the region indicated in Fig. 5.1. On the other hand, our effective potential computation becomes inaccurate when the temperature is too high because of the approximation in Eq. (5.16). Still we obtain a reasonable matching of the two approximation

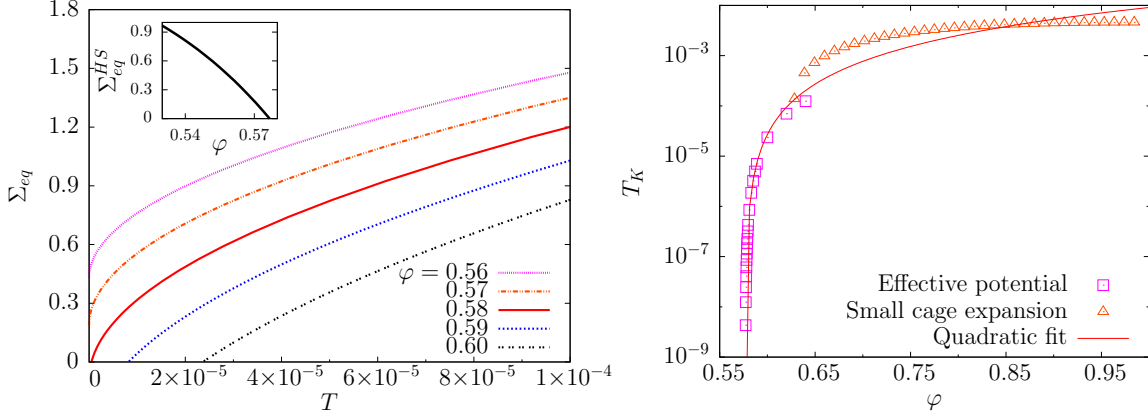


Figure 5.3: Left: Equilibrium complexity against temperature for several volume fractions around ϕ_K , calculated within the effective potential approximation. Inset: complexity of hard spheres, obtained as the $T \rightarrow 0$ limit of the complexity Σ_{eq} , plotted against the volume fraction. Right: Kauzmann temperature against volume fraction, within the the effective potential approach developed in this work (open squares). The quadratic fit (red line) gives an estimated Kauzmann transition for hard spheres at $\phi_K = 0.576898$. The small cage Mézard-Parisi approach breaks down at low temperatures and low densities [115].

schemes for intermediate densities around $\phi = 0.64$. It would be easy, in principle, to reconcile the two approximations at all volume fractions, including the crossover regime, by avoiding the low temperature approximation made in Eq. (5.16), but these computations would require a much heavier numerical treatment.

5.2.2 Relaxation time and glass fragility

The calculation of the liquid complexity, apart from signaling the glass transition, can be related to the relaxation time and fragility of the glass as described in the introduction, through Eq.(1.17) and its mean-field counterpart Eq.(1.19).

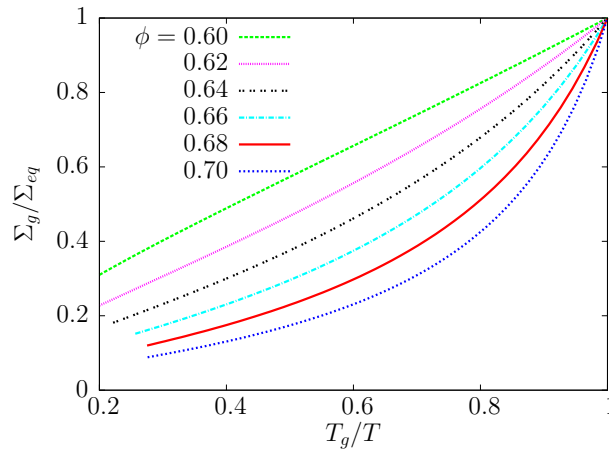


Figure 5.4: A thermodynamic Angell plot of Σ_g/Σ_{eq} , with $\Sigma_g = 1$ as a definition of the glass transition, plotted against T_g/T , for different volume fractions. The thermodynamic fragility is predicted to increase rapidly with volume fraction, in agreement with numerical simulations [20].

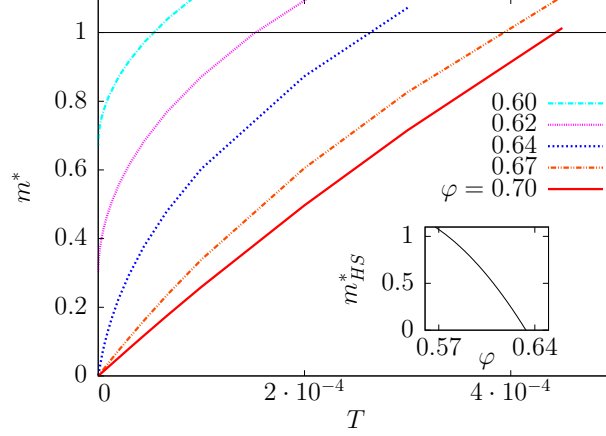


Figure 5.5: Optimal number of replicas m^* as a function of T , for several volume fractions. The inset shows the $T \rightarrow 0$ limit of m^* as a function of the volume fraction.

In Refs. [20, 21], Berthier and Witten showed that, for harmonic spheres, compressing the system leads to a very sensible increase of the fragility. Using our results for the complexity, we are able to qualitatively check whether replica theory can reproduce this feature. Indeed, thanks to Eq. (1.19), the fragility can be extracted equivalently from the relaxation time or from the complexity. Since the fragility is usually evaluated at the conventionally defined laboratory glass transition, we arbitrarily define the glass transition temperature $T_g(\varphi)$ as the temperature at which the equilibrium complexity is equal to one, $\Sigma(T_g(\varphi), \varphi) = 1$, which is a typical value of the configurational entropy at the glass transition in most numerical simulations and experiments (its precise value is immaterial for our purposes). Using these values of T_g and $\Sigma_g = 1$, we can construct an Angell plot similar to Fig. 5.4 of the introduction, but for the complexity. In Fig. 5.4 we show the inverse of the complexity, linked to the logarithm of the relaxation time by Eq. (1.17), plotted against T_g/T , for several densities. The fragility is the slope of the curves in $T_g/T = 1$ [105]. One can clearly see that increasing the density drastically increases the fragility of the glass-former.

5.2.3 Free-energy of the glass

We now turn to the calculation of the free entropy of the glass, \mathcal{S}_{glass} . We have seen that in order to compute $\mathcal{S}_{glass}(T, \varphi)$, one needs to optimize the replicated free entropy $\mathcal{S}(m, A; T, \varphi)/m$ with respect to A first (in order to perform the inverse Legendre transform), then with respect to m , via Eq. (5.8). Calling $A^*(T, \varphi)$ and $m^*(T, \varphi)$ the optimal values of A and m , we obtain:

$$\mathcal{S}_{glass}(T, \varphi) = \frac{\mathcal{S}(m^*(T, \varphi), A^*(T, \varphi); T, \varphi)}{m^*(T, \varphi)}. \quad (5.20)$$

Starting from Eq. (5.20), we can deduce all quantities of interest, for instance the pressure and energy of the glass and its specific heat.

We start from the general thermodynamic relations $U = -d\mathcal{S}/d\beta$ and $p = \beta P/\rho = -\varphi d\mathcal{S}/d\varphi$, where p is the so-called “reduced pressure” or “compressibility factor”. We have that the free-energy of the glass is $\mathcal{S}(m^*, A^*; T, \varphi)/m^*$, where m^* and A^* are determined by optimization of $\mathcal{S}(m, A; T, \varphi)/m$. Therefore, we do not need to take explicit derivatives with respect to m and A , and we can directly compute the derivatives with respect to density and temperature to obtain explicit expressions for the energy and the pressure [19].

An important quantity for the following is the optimal number of replicas m^* . In Fig. 5.5, we show its behavior as a function of the temperature, for different volume fractions. We see that the $T \rightarrow 0$ limit of $m^*(T, \varphi)$ converges when φ is not too large to a finite value, which we call $m_{HS}^*(\varphi)$, and which is shown in the inset. The replica parameter of hard spheres vanishes at a density φ_{GCP} , the glass close packing. This point is the equivalent, in our mean-field picture, of the jamming point of harmonic spheres. The behavior of the cage radius A^* is similar to that of m^* .

Since our goal is to study the vicinity of the jamming point, we have to take into account that the optimal number of replicas, as well as the optimal cage size, vanish at jamming.

From the knowledge of m^* and A^* , we can deduce the energy and specific heat of the glass. We show in Fig. 5.6 the temperature evolution of the specific heat for three densities, one below φ_{GCP} , one very close to it, and one above. Upon crossing the ideal glass transition, the specific heat undergoes a finite jump. We find that the amplitude of this jump increases continuously with φ from φ_K . A qualitatively similar result was obtained in numerical simulations [20], where the jump of specific heat was studied at the numerical glass transition temperature. The behavior of the specific heat correlates well with the evolution of the thermodynamic fragility discussed in Fig. 5.4. Finally, we note that the $T \rightarrow 0$ limit of the specific heat jumps discontinuously from 0 to $3/2$ at φ_{GCP} , which reveals that the ground state properties of the glass phase abruptly change at the jamming transition, as we now study in more detail.

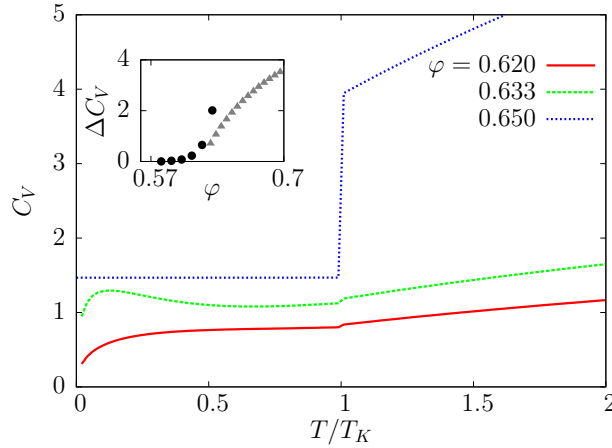


Figure 5.6: Specific heat C_V of the system plotted against T/T_K , for several volume fractions. The curves for $\varphi = 0.620, 0.633$ are obtained with the effective potential method. The curve for $\varphi = 0.650$ is obtained with the Mézard-Parisi small cage expansion [115], since at this density $T_K(\varphi)$ is too high and the effective potential method is not reliable. Inset: Specific heat jump at T_K ; the black dots are obtained with the effective potential approximation, the gray triangles are obtained with the Mézard-Parisi small cage expansion.

5.3 Jamming point of harmonic spheres

We now turn to the study of the region of the phase diagram deep in the glass phase, inside the line $T_K(\varphi)$ and close to the jamming point φ_{GCP} , see Fig. 5.1. In this region, $m^*(T, \varphi)$ is very small, as we discussed in the last section (see Fig. 5.5). In principle, one could just compute $m^*(T, \varphi)$ and then take the limit $T \rightarrow 0$ and $\varphi \rightarrow \varphi_{GCP}$ (“jamming limit”). However, both numerically and analytically,

it is much more convenient to exchange the optimization with respect to m and A with the jamming limit, take the latter first, and then optimize the free energy. This is because, in the jamming limit, many of the integrals that appear in the free energy simplify considerably. However, the scaling of m and A in the jamming limit is different depending on the order of the limits, which emphasizes the asymmetry that exists between both sides of the jamming point. In this section we discuss how to exchange the jamming limit with the optimization procedure.

5.3.1 Zero temperature, below close packing

We consider first the limit $T \rightarrow 0$ for fixed $\varphi < \varphi_{GCP}$. In this case, we are bound to recover the results of [130] for hard spheres. We reproduce here these results, in order to fix the notations and for the sake of completeness.

We expect the optimal number of replicas $m^*(T, \varphi)$ and cage radius $A^*(T, \varphi)$ to tend to finite values $m_{HS}^*(\varphi)$ and $A_{HS}^*(\varphi)$ when $T \rightarrow 0$. Therefore, to recover hard spheres results, one has to take the limit $T \rightarrow 0$ at fixed A and m , and optimize the resulting free entropy over A and m . The corresponding expression for the replicated free entropy coincides with that of [130].

We numerically solved the optimization equations; the result for $m_{HS}^*(\varphi)$ is plotted in the inset of Fig. 5.5. Approaching φ_{GCP} by the left, m_{HS}^* goes to zero linearly:

$$m_{HS}^* \underset{\varphi \rightarrow \varphi_{GCP}}{\propto} (\varphi_{GCP} - \varphi), \quad (5.21)$$

and A_{HS}^* also goes to zero with m as αm . Thus the close packing limit for hard spheres can be computed by taking first the limit $T \rightarrow 0$, and then $m \rightarrow 0$ with $A = \alpha m$. Optimization on A will now become an optimization on α . From the inset of Fig. 5.5 we find

$$\varphi_{GCP} = 0.633353, \quad (5.22)$$

recovering the result of [130].

We can also get the scaling of the reduced pressure for $\varphi \rightarrow \varphi_{GCP}^-$:

$$p_{glass} = \frac{3.03430 \varphi_{GCP}}{\varphi_{GCP} - \varphi}. \quad (5.23)$$

The prefactor is only 1% different from the correct value which is the space dimension $d = 3$, predicted by free volume theory [139] and by the small cage expansion of Ref. [130].

To sum up, we have detected the glass close packing point, at a density consistent with the numerically observed values. Upon approaching this point from lower densities at zero temperature, harmonic spheres behave like hard-spheres, that are in an ideal glassy state, whose reduced pressure is found to diverge at the glass close packing point. By studying this point for higher densities, we will confirm that this point is a critical jamming point, as defined in the numerical simulations [127].

5.3.2 Zero temperature, above close packing

For $\varphi > \varphi_{GCP}$, the harmonic spheres have a finite energy at $T = 0$, due to overlaps. Then, because of the repulsion the spheres are jammed, and A^* vanishes at $T = 0$. It turns out from the numerical calculation of m^* and A^* , both in the small cage expansion [115] and in the potential approximation (see the previous section) that the optimal number of replicas m^* tends to zero when $T \rightarrow 0$. One

finds that $m = T/\tau$ and $A = m\alpha$ with constants α and τ . Therefore for $\varphi > \varphi_{GCP}$ one has to take the $T \rightarrow 0$ limit with $\alpha = A/m$ and $\tau = T/m$ kept constant. Optimization over m and A is replaced by an optimization over α and τ .

The replicated free entropy simplifies considerably in this limit. Many results can then be derived analytically, by noticing that the jamming limit from above corresponds to sending τ to zero. Expanding the equations around $\tau = 0$ allows the derivation of the scaling behavior of the thermodynamic quantities above the jamming point [19]. First we numerically obtain the behavior of the complexity as a function of the energy of the packing, reported in Fig. 5.7.

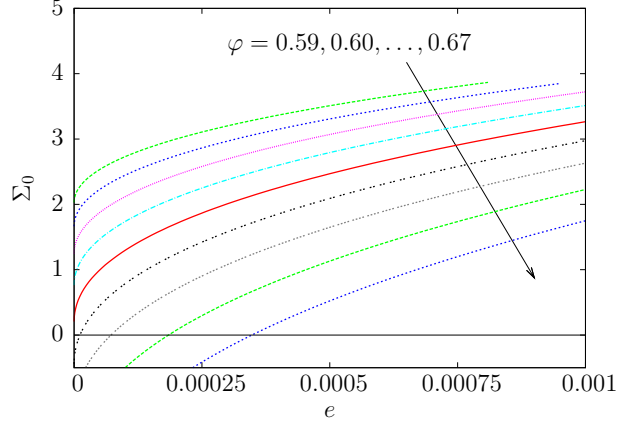


Figure 5.7: Complexity of the energy minima $\Sigma_0(e, \varphi)$ as a function of energy for several densities.

This form of the complexity can be shown to give a quadratic dependance to the ground state energy on $\varphi - \varphi_{GCP}$:

$$e_{GS}(\varphi) \underset{\varphi \rightarrow \varphi_{GCP}}{\propto} (\varphi - \varphi_{GCP})^2. \quad (5.24)$$

The pressure evaluated at φ_{GCP} gives the following scaling:

$$P_{glass}(T=0, \varphi) \underset{\varphi \rightarrow \varphi_{GCP}}{\propto} (\varphi - \varphi_{GCP}). \quad (5.25)$$

Clearly the same scaling could have been obtained from the exact relation $P_{glass}(T=0, \varphi) = \frac{6\varphi^2}{\pi} \frac{de_{GS}}{d\varphi}$.

In this section we have thus derived the scaling laws (5.24) and (5.25) first observed numerically above the jamming transition at zero temperature [127], which indicate that solidity emerges continuously at the jamming density. These results also confirm the postulated correspondence between the jamming transition observed numerically and the glass close packing density defined within our theoretical approach.

5.3.3 Scaling around jamming

We have shown in Secs. 5.3.1 and 5.3.2 that all the thermodynamic quantities are singular at φ_{GCP} and $T=0$; for instance m^* is finite below φ_{GCP} while it vanishes proportionally to T above φ_{GCP} . The reduced pressure is also finite below φ_{GCP} , while it diverges at φ_{GCP} and is formally infinite above φ_{GCP} . Both the energy and the pressure vanish below φ_{GCP} while they are finite above φ_{GCP} .

From this observation, and since all quantities are analytic at finite T , it follows that all these quantities must satisfy scaling relations if T is small enough and φ is close enough to φ_{GCP} [128]. We

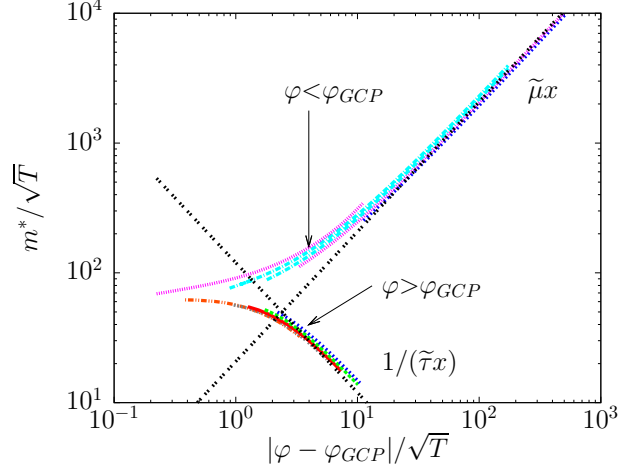


Figure 5.8: Scaling of $m^*(T, \varphi)/\sqrt{T}$ as a function of the rescaled temperature $|\varphi - \varphi_{GCP}|/\sqrt{T}$ for $\varphi = 0.58, 0.59, \dots, 0.70$. The asymptotic forms corresponding to Eq. (5.27) are also reported.

discuss explicitly the case of m^* for which we assume a scaling relation of the form

$$m^*(T, \varphi) = T^\gamma \tilde{m}_\pm \left(\frac{|\varphi - \varphi_{GCP}|}{T^\nu} \right), \quad (5.26)$$

where the two scaling functions correspond to the two sides of the transition. In the hard sphere limit $T \rightarrow 0$ and $\varphi < \varphi_{GCP}$, to recover Eq. (5.21) we need $\tilde{m}_-(x \rightarrow \infty) = \tilde{\mu}x$, where $\tilde{\mu}$ is a constant, and $\gamma = \nu$. For $\varphi > \varphi_{GCP}$ instead, $m^* = T/\tau^*(\varphi)$ and to recover Eq. (5.24) we need $\tilde{m}_+(x \rightarrow \infty) = 1/(\tilde{\tau}x)$, where $\tilde{\tau}$ is a constant, and $\gamma = \nu = 1/2$. Finally, we are led to the scaling

$$\begin{cases} m^*(T, \varphi) = \sqrt{T} \tilde{m}_\pm \left(\frac{|\varphi - \varphi_{GCP}|}{\sqrt{T}} \right), \\ \tilde{m}_-(x \rightarrow \infty) = \tilde{\mu}x, \\ \tilde{m}_+(x \rightarrow \infty) = \frac{1}{\tilde{\tau}x}. \end{cases} \quad (5.27)$$

This scaling is successfully tested in Fig. 5.8.

Qualitatively similar scaling forms (with different exponents) apply to thermodynamic quantities such as the energy, the pressure, or the complexity. Although we do not show the corresponding scaling plots explicitly, the energy and the pressure are plotted and compared with numerical data in the following (Fig. 5.10). Note finally that a scaling plot for the complexity is related, in the spirit of the Adam-Gibbs relation in Eq. (1.17), to the scaling plot of the numerically measured relaxation time reported in Ref. [21].

5.4 The pair correlation function

The pair correlation function is a key quantity that gives a lot of insight into the structure of dense fluids or packings. In this section we derive an expression for the correlation function of the glass and use it to discuss the scaling of the contact peak of $g(r)$ close to the jamming transition.

5.4.1 General expression of the correlation function of the glass

It has been shown in [130, Eqs.(67)-(68)] that one can compute the correlation function of the glass starting from the replicated free energy. This is done by adding a small perturbation $u(r)$ to the

potential of replica 1 and taking the derivative of the free energy with respect to $u(r)$, similarly as in Eq.(5.13), and finally setting u to zero. The glass correlation function is then calculated as:

$$g_{glass}(r) = -\frac{2}{\beta\rho} \left. \frac{\delta\mathcal{S}}{\delta u(r)} \right|_{u=0}. \quad (5.28)$$

We start from Eq. (5.14) and we use approximation (5.16). Since the perturbation acts only on replica 1, we have

$$\mathcal{S}(m, A; T, \varphi) = S_h(m, A) + \mathcal{S}_{liq} \left[\varphi, e^{-\beta m v(r) - \beta u(r)} \right] + \frac{3\varphi}{\pi} y_{liq}^{HS}(\varphi) \int d^3r e^{-\beta m v(r) - \beta u(r)} Q(r), \quad (5.29)$$

and $Q(r)$ depends only on the potentials of replicas 2 to m , so it is independent of u . Taking the derivative with respect to $u(r)$ we have, using again Eq. (5.16):

$$\begin{aligned} g_{glass}(r) &= g_{liq}(T/m, \varphi; r) + y_{liq}^{HS}(\varphi) e^{-\beta m v(r)} Q(r) \\ &= y_{liq}^{HS}(\varphi) e^{-\beta m v(r)} [1 + Q(r)] \\ &= y_{liq}^{HS}(\varphi) e^{-\beta v_{eff}(r)}. \end{aligned} \quad (5.30)$$

Therefore the correlation function of the glass is directly related to the effective potential within the low temperature approximation we used to compute the thermodynamics of the system. Of course, an improved expression for this correlation could be obtained by using the HNC approximation to describe the effective liquid. In that case, $g_{glass}(r)$ would be the HNC correlation of the effective liquid. Still, the much simpler expression (5.30) is enough to capture the scaling of $g_{glass}(r)$ around jamming, at least close to the first peak. In the rest of this section we discuss the scaling form that is obtained starting from Eq. (5.30).

A very interesting quantity related to $g(r)$ is the number of contacts, defined as the number overlaps per particle. Within our low temperature approximation it is given by:

$$\begin{aligned} z(T, \varphi) &= 24\varphi \int_0^1 dr r^2 g_{glass}(r) \\ &= 24\varphi y_{liq}^{HS}(\varphi) \int_0^1 dr r^2 e^{-\beta v_{eff}(r)}. \end{aligned} \quad (5.31)$$

Similarly, the energy of the glass can be computed as:

$$U_{glass}(T, \phi) = 12\phi y_{liq}^{HS}(\phi) \int_0^1 dr r^2 (1-r)^2 e^{-\beta v_{eff}(r)}. \quad (5.32)$$

The starting point of the analysis of the correlation function of the glass are Eq. (5.30) and the expression of the effective potential. In the following we keep the notation $e^{-\beta v_{eff}}$ since this function has a finite limit for $T \rightarrow 0$ even if β is formally infinite.

5.4.2 Scaling of the peak of the pair correlation at finite temperature

Here we discuss the effect of thermal fluctuations on the maximum of $g_{glass}(r)$ near the the $T = 0$ jamming transition at φ_{GCP} . This situation was studied numerically and experimentally in Refs. [165, 80]. We focus on the scaling of this maximum in a region of small T and for $\varphi \sim \varphi_{GCP}$. In Fig. 5.9 we show the behavior of the maximum of $g_{glass}(r)$, which we call g_{max} , as a function of the density, for temperatures ranging from 10^{-5} to 0. This figure demonstrates that we are able to derive analytically all behaviors reported in Refs. [165, 39, 58, 143]. Namely, the density at which the pair correlation

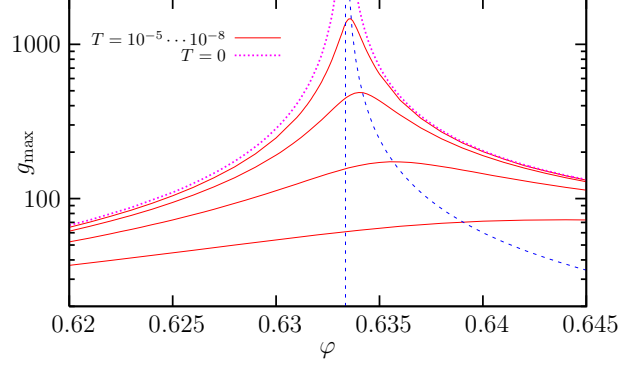


Figure 5.9: Evolution of the maximum of the glass pair correlation function with T and φ . While g_{max} diverges on both sides of the transition at $T = 0$ as $g_{max} \sim |\varphi - \varphi_{GCP}|^{-1}$, this divergence becomes a smooth maximum at finite T near the transition, whose position shifts with temperature. This behavior compares very well with numerical [165, 58, 143] and experimental observations [165, 39].

function reaches its maximum shifts towards higher values when the temperature departs from 0 and increases as \sqrt{T} , while the maximum g_{max} diverges as $|\varphi - \varphi_{GCP}|^{-1}$ on both sides of the transition.

As discussed in the previous section, the zero temperature limit is very different for $\varphi < \varphi_{GCP}$ or $\varphi > \varphi_{GCP}$. Thus we now discuss these two limits separately.

5.4.3 Zero temperature below jamming: hard spheres

As explained above, we send $T \rightarrow 0$ before taking the jamming limit $m \rightarrow 0$ and $A = \alpha m$. By studying the behavior of the effective potential in this limit, we find that it diverges at $r = 1^+$:

$$e^{-\beta v_{\text{eff}}(r)} = \frac{1}{m} \Delta_{\alpha} \left(\frac{r-1}{m\sqrt{4\alpha}} \right), \quad (5.33)$$

where the scaling function Δ is given by:

$$\Delta_{\alpha}(\lambda) = 2 \int_0^{1/\sqrt{4\alpha}} dx x (1 - x\sqrt{4\alpha})^2 e^{-2\lambda x - x^2}. \quad (5.34)$$

For $\varphi \rightarrow \varphi_{GCP}^-$ we found that $m \sim \tilde{\mu}(\varphi_{GCP} - \varphi)$ and the optimal cage size $A^* = \alpha^* m$ with a finite $\alpha^* = \alpha^*(\varphi_{GCP})$, we thus find the following scaling for the pair correlation function:

$$\begin{cases} g_{\text{glass}}(r)(\varphi_{GCP} - \varphi) = f \left[\frac{r-1}{\varphi_{GCP} - \varphi} \right], \\ f(\lambda) = \frac{y_{\text{liq}}^{HS}(\varphi)}{\tilde{\mu}} \Delta_{\alpha^*} \left[\frac{\lambda}{\tilde{\mu}\sqrt{4\alpha^*}} \right], \end{cases} \quad (5.35)$$

The height of the peak scales as:

$$g_{\text{glass}}(r = 1^+, \varphi \rightarrow \varphi_{GCP}) \sim \frac{1.09922}{\varphi_{GCP} - \varphi}, \quad (5.36)$$

and its width as $\varphi_{GCP} - \varphi$.

The number of contacts is the integral of the peak at $r = 1^+$ which is given by

$$\begin{aligned} z &\sim 24\varphi \int_{\text{peak}} dr g_{\text{glass}}(r) \\ &\sim 24\varphi y_{\text{liq}}^{HS}(\varphi) \sqrt{4\alpha^*} \int_0^{\infty} d\lambda \Delta_{\alpha^*}(\lambda) \end{aligned} \quad (5.37)$$

Using the actual values derived in the previous section, we get $z = 6.13720$ for $\varphi = \varphi_{GCP}$, which is slightly above the expected $z = 2d = 6$.

Note that it has been shown in [130] that within a systematic expansion in $\sqrt{\alpha}$, one gets $z = 2d$ at first order. Here instead, in order to match with the soft sphere computation, we are using an approximation scheme which is not a consistent expansion in $\sqrt{\alpha}$. This could explain the fact that $z \neq 2d$. It would be interesting to have a full computation of the next term in the small α expansion to check whether the equality $z = 2d$ survives at this order. Unfortunately this seems to be a quite hard task.

5.4.4 Zero temperature above jamming

For $\varphi > \varphi_{GCP}$, the appropriate limit is to send $T \rightarrow 0$ with $m = T/\tau$ and $A = \alpha m$. We obtain for the effective potential the following leading behavior:

$$e^{-\beta v_{eff}(r)} = \theta(r-1) + \theta(1-r)\theta\left(r - \frac{4\alpha}{\tau+4\alpha}\right) \frac{(1+4\alpha/\tau)[1+(r-1)(1+4\alpha/\tau)]^2}{r^2} e^{-\frac{\tau+4\alpha}{\tau^2}(r-1)^2}. \quad (5.38)$$

Close to φ_{GCP} this function develops a delta peak close to $r = 1$ with height $(\varphi - \varphi_{GCP})^{-1}$ and width $\varphi - \varphi_{GCP}$, in the same way than in the hard-sphere case. The main difference we observe with the hard sphere limit is that, despite the fact that both cases give rise to a delta function at $r = 1$, the mechanism is different since for hard spheres the support is concentrated on $r = 1^+$ while for soft spheres it is concentrated on $r = 1^-$. Another interesting observation is that the theory predicts that $g_{glass}(r)$ should vanish exactly for $r < \frac{4\alpha}{\tau+4\alpha}$; this means that no pair of spheres can have an overlap larger than $\frac{\tau}{\tau+4\alpha}$. Indeed in the limit $\tau \rightarrow 0$ we recover the GCP at which no overlaps are present. Unfortunately, a direct numerical test of this prediction is impossible: this is because when $1-r = \frac{\tau}{\tau+4\alpha}$, the exponential term in Eq. (5.38) is equal to $\exp(-1/(\tau+4\alpha))$. Since both τ and α are already extremely small (of the order of 10^{-3} at best), $g_{glass}(r)$ is extremely small in the region where we predict it to vanish, and numerically the signal to noise ratio becomes too large.

Again in the limit $\varphi \rightarrow \varphi_{GCP}^+$ we obtain the scaling forms

$$\begin{cases} g_{glass}(r)(\varphi - \varphi_{GCP}) = f\left[\frac{1-r}{\varphi - \varphi_{GCP}}\right], \\ f(\lambda) = \frac{y_{liq}^{HS}(\varphi)4\alpha^*}{\tilde{\tau}} \left(1 - \frac{4\alpha^*\lambda}{\tilde{\tau}}\right)^2 e^{-\frac{4\alpha^*\lambda^2}{\tilde{\tau}^2}}, \end{cases} \quad (5.39)$$

The number of contacts is easily obtained from Eq. (5.31) and Eq. (5.38) and we found:

$$z(T=0, \varphi) = z(T=0, \varphi_{GCP}) + C(\varphi - \varphi_{GCP}), \quad (5.40)$$

where $z(T=0, \varphi_{GCP})$ is 6.13720, the same value than in the hard-sphere case. This result is at odds with the numerical finding of a square root behavior [58, 143]. We comment further on this discrepancy, in Sec. 5.6.

Note that this value of $z(T=0, \varphi_{GCP})$ is identical to the one obtained on the hard sphere side (as it can be easily proven analytically), despite the fact that the two definitions of z are not equivalent. In the soft sphere case we defined z as the number of overlaps. On the hard sphere side, this number is strictly zero, therefore we defined z as the integral of the delta peak at $r = 1^+$.

5.5 Scaling around jamming: comparison with numerical data

In this section, we compare the prediction of the theory with numerical data, in particular to test the scaling in temperature and in $\delta\varphi = \varphi - \varphi_{GCP}$ around the glass close packing point.

5.5.1 Details of the numerical procedure

We investigated a system of $N = 8000$ identical harmonic spheres. The system was prepared using the standard procedure of Ref. [126]. We started from a random configuration at high density; we then minimized the energy, and then reduced slowly the density, at each step minimizing the energy again, until a jammed configuration of zero energy and volume fraction φ_j was found. This jammed configuration corresponds, according to the mean-field interpretation of [130], to the $T = 0$, $p \rightarrow \infty$ limit of a given hard sphere glass, or equivalently to the $T \rightarrow 0$, $P \rightarrow 0$ limit of a corresponding soft sphere glass. Starting from that configuration, we prepared configurations at different T and φ by using molecular dynamics simulations as in Ref. [21] to equilibrate the system inside the glass state selected by the initial jammed configuration. Since we always used very small T and $\varphi \sim \varphi_j$, the system is not able to escape from that glass state, so it always remains in the vicinity of the original jammed configuration. This is a crucial requirement to numerically obtain scaling behavior near φ_j as microscopic rearrangements would directly affect the location of φ_j in the simulations [37]. We tested the absence of such an effect in our simulations by repeating the energy minimization starting from some equilibrated configurations at different T and φ , and checking that we always found the same value of φ_j (within numerical errors). For the particular series of run described below, we estimated $\varphi_j = 0.643152 \pm 0.000020$ by fitting the zero temperature energy using $e(\varphi) \propto (\varphi - \varphi_j)^2$.

5.5.2 Difficulties in the comparison with the theory

When comparing the theory with the numerical data, we face two difficulties. First of all, the value of φ_j depends on the numerical protocol and on its particular realization we used, and therefore cannot be directly compared with φ_{GCP} . Note that φ_{GCP} should represent an upper bound for φ_j , whatever the protocol, but the value $\varphi_{GCP} = 0.633353$ we report seems to contradict this statement. The reason is simply that our theoretical computations are based on the HNC equation of state for liquid hard spheres, which (as discussed above), underestimates the value of φ_{GCP} : a better result is obtained using the Carnahan-Starling equation of state, which gives $\varphi_{GCP} = 0.683$, consistently with the value of φ_j found above [130]. To avoid confusion, here we stick to the use of the HNC equation of state; the theoretical calculations can be easily repeated for any other equation of state, and the scaling around φ_{GCP} is unaffected by this choice. Once again we stress that the absolute values of density reported here should always be taken with this caveat in mind. Since we are interested here mainly in the relative distance to jamming, which is $\varphi - \varphi_j$ for the numerical data, and $\varphi - \varphi_{GCP}$ for the theory, the absolute values of density are not crucial for our purposes.

The second difficulty is the following. For hard spheres, the theory predicts that the reduced pressure diverges as $p_{glass}^{HS} \sim 3\varphi_{GCP}/(\varphi_{GCP} - \varphi)$, while $y_{glass}^{HS}(\varphi) \sim 1.1/(\varphi_{GCP} - \varphi)$ for $\varphi \rightarrow \varphi_{GCP}^-$. As one can easily check, these scalings imply that the theory violates the exact thermodynamic relation $p_{glass}^{HS} = 1 + 4\varphi y_{glass}^{HS}(\varphi)$, as already noticed in [130]. In particular, the divergence of p_{glass}^{HS} is correct, while the coefficient of the divergence of $y_{glass}^{HS}(\varphi)$ is overestimated by a factor of ~ 1.46562 . We will comment on the origin of this problem in Sec. 5.6. This error affects the prefactors in the scalings of $g_{glass}(r)$ and of z around φ_{GCP} . To correct for this error, we rescaled the $\delta\varphi$ of the numerical data in such a way that the coefficient of the divergence of y_{glass}^{HS} is the same as the theoretical one.

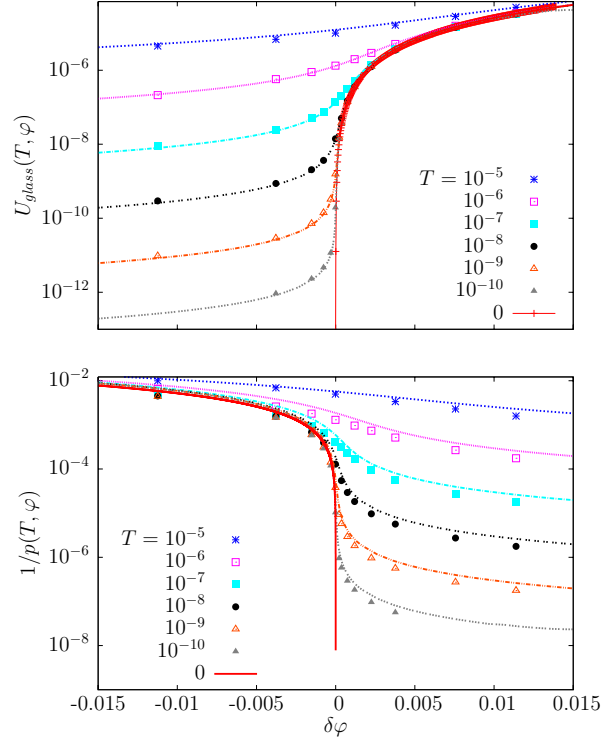


Figure 5.10: Energy $U_{glass}(T, \varphi)$ (top panel) and inverse reduced pressure $1/p_{glass}(T, \varphi)$ (bottom panel) as functions of distance from jamming $\delta\varphi$, for several temperatures. We define $\delta\varphi = \varphi - \varphi_{GCP}$ for the theory, and $\delta\varphi = 1.46562(\varphi - \varphi_j)$ for the numerical data.

To summarize, when comparing numerical data with the theory, we consider $\delta\varphi = \varphi - \varphi_{GCP}$ for the theory, and $\delta\varphi = 1.46562(\varphi - \varphi_j)$ for the numerical data such that the values of $\eta_{glass}^{HS}(\delta\varphi)$ for theory and simulations are exactly the same close to $\delta\varphi = 0$. Note that this adjustment is based solely on the analysis of the hard sphere side of the jamming transition ($\delta\varphi < 0$), but we find that it allows to describe the full scaling also for positive $\delta\varphi$.

If the reader is uncomfortable with the above reasonings, another way of thinking is that we need to adjust two free parameters (the position of the transition and the amplitude of the rescaling of $\delta\varphi$) to obtain the best comparison of theory and numerical simulations. While the location is φ_j was always adjusted in previous work [58, 143, 126, 155], we need to adjust also one prefactor as we seek to compare theoretical predictions to simulations in absolute values, and not only at the level of leading diverging contributions.

5.5.3 Energy, pressure, average coordination

We start our discussion by the simplest observables. In Fig. 5.10 we plot the average energy $U_{glass}(T, \varphi)$ and the inverse reduced pressure $1/p_{glass}(T, \varphi)$ as functions of $\delta\varphi$ for several temperatures. The agreement between theory and numerical data, with the rescaling of $\delta\varphi$ discussed above, is nearly perfect. The scaling around jamming is clearly visible in the figures. For instance, $U_{glass}(T, \varphi)$ tends to a finite value for $\delta\varphi > 0$, while for $\delta\varphi < 0$ it goes to zero as a power law, since in this case the system becomes a hard sphere glass. Similarly, the reduced pressure is finite for $\delta\varphi < 0$, while it diverges proportionally to β for $\delta\varphi > 0$, since in this case the pressure is finite at zero temperature. At finite

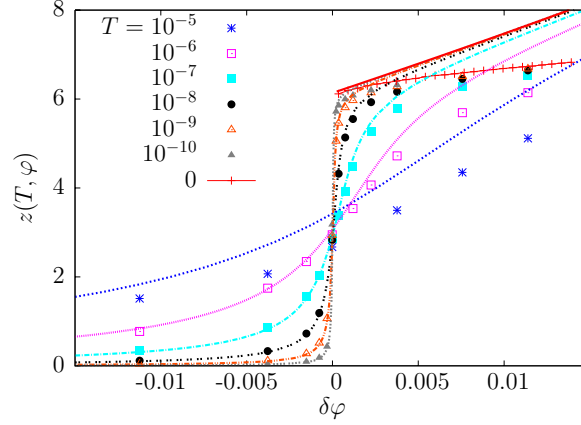


Figure 5.11: Average number of contacts z as a function of distance from jamming $\delta\varphi$, for several temperatures. We define $\delta\varphi = \varphi - \varphi_{GCP}$ for the theory, and $\delta\varphi = 1.46562(\varphi - \varphi_j)$ for the numerical data.

temperature, the curves interpolate between the two regimes. Scaling functions similarly to the ones shown in Fig. 5.8 for m^* can easily be constructed.

In Fig. 5.11 we report the average coordination number $z(T, \varphi)$, as a function of $\delta\varphi$ for several temperatures. At $T = 0$, the average coordination jumps from 0 to 6 (for numerical data) or to 6.13720 (for the theory). For $\delta\varphi > 0$, the average coordination grows linearly in $\delta\varphi$ for the theory, while it grows as $\delta\varphi^{1/2}$ for the numerical data. Therefore, the theory fails to capture the correct evolution of this structural property at $\delta\varphi > 0$ and $T = 0$.

A more detailed description of what happens is obtained by looking to the data at finite T . When temperatures become too large, e.g. at $T = 10^{-5}$, the theory eventually fails because of the low- T approximation we made on the liquid theory in Eq. (5.16). For any fixed temperature $T \leq 10^{-6}$, we observe that the theory describes perfectly the numerical data for $\delta\varphi < 0$ and also for positive $\delta\varphi$ up to some crossover value $\delta\varphi_h(T)$. Around $\delta\varphi_h(T)$ the theory starts deviating from the numerical data. The data in Fig. 5.11 suggest that $\delta\varphi_h(T)$ is an increasing function of T , i.e. that for higher temperatures the theory performs better, if the temperature is low enough that approximation (5.16) makes sense. Indeed, we expect that for $\delta\varphi_h(T) \rightarrow 0$ for $T \rightarrow 0$, since at $T = 0$ the theory fails to capture the behavior of the contact number at $\delta\varphi > 0$. We will come back to this point below.

5.5.4 Correlation function

We now report data for the scaling of the contact peak of $g_{glass}(r)$ near jamming. We first consider a fixed $\delta\varphi < 0$, and change the temperature. In Fig. 5.12 we report data for $\delta\varphi = -0.00078$ for several temperatures. In this regime the theory works very well down to $T = 0$; this is expected since we know that the theory works at $T = 0$ for hard spheres [130].

Next, we consider a fixed $\delta\varphi > 0$ and plot $g_{glass}(r)$ for several temperatures. This is done in Fig. 5.13 for four different values of $\delta\varphi$. Here, we observe that, like for the average coordination (Fig. 5.11), the theory works very well at moderately large T . However, on lowering T , at some point we observe that the numerical $g_{glass}(r)$ saturates to a limiting curve which has a maximum at $r < 1$. By contrast, the theoretical curves slowly evolve towards the $T = 0$ theoretical limit, which is a half-Gaussian centered in $r = 1$, with its $r > 1$ part removed.

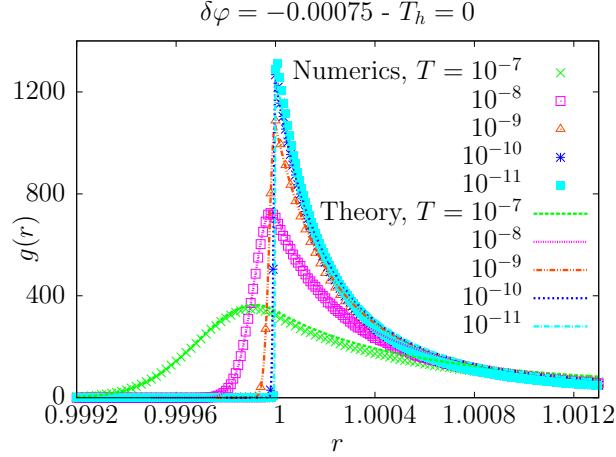


Figure 5.12: Pair correlation $g_{glass}(r)$ just below jamming predicted by theory (full lines) and measured in numerical simulations (symbols). Here $\delta\varphi = -0.00075$.

Therefore, below a certain temperature $T_h(\delta\varphi)$ (the inverse of the function $\delta\varphi_h(T)$ mentioned above), a deviation between theory and numerical data is observed close to the maximum of $g_{glass}(r)$. Clearly, the deviation between data and theory is a smooth crossover, so determining $T_h(\delta\varphi)$ is not easy. Here we choose the following procedure. The numerical data accumulate on a master curve as $T \rightarrow 0$. Therefore we define $T_h(\delta\varphi)$ as the value of temperature at which the theoretical curve best fits the $T \rightarrow 0$ numerical curve. As an example, in the upper left panel of Fig. 5.13, we see that the theoretical curve for $T = 10^{-10}$ fits very well the numerical curves for both $T = 10^{-10}, 10^{-11}$, while the $T = 10^{-11}$ theoretical curve is quite different. We fix $T_h = 10^{-10}$ for this value of $\delta\varphi$. Clearly the ambiguity on the precise numerical value of T_h is rather large. Despite this, we are able to qualitatively confirm that $T_h(\delta\varphi)$ is an increasing function of $\delta\varphi$, as already suggested in the previous section. The function $T_h(\delta\varphi)$ determined from the pair correlation functions is reported in Fig. 5.14. It emerges continuously from zero above φ_{GCP} . A comparison with the temperature scale given by the glass temperature shows that it is orders of magnitude smaller than T_K . Thus it is only in the small regime of $T < T_h$ and $\varphi > \varphi_{GCP}$ that our the effective potential approach misses some important physics, as we discuss below in Sec. 5.5.5.

Finally, in Fig. 5.15 we show that $g_{glass}(r)$, at $T = 0$, follows the scaling relations predicted by the theory, Eqs. (5.35) and (5.39), for $|\delta\varphi| \rightarrow 0$, with different scaling functions on the two sides of the transition. While the scaling is perfect for $\delta\varphi < 0$ [130], for $\delta\varphi > 0$ there is a small deviation around the maximum as already discussed, which is however very small in the scaling regime for $\delta\varphi \rightarrow 0$.

5.5.5 Discussion

The main discrepancy between the theory and numerical data is in the region $\delta\varphi > 0$ and very small temperature $T < T_h(\delta\varphi)$. Here, the average coordination scaling $z \propto \delta\varphi^{1/2}$ at $T = 0$ is not obtained. Furthermore, the shape of the peak of $g_{glass}(r)$ is only partially captured by the theory. We tentatively attribute these discrepancies to the particular nature of the vibrational modes at $T = 0$ and $\delta\varphi > 0$. It has been shown that in this regime the low-frequency spectrum is dominated by spatially correlated vibrational modes. These modes cannot be described by our approach, in which vibrations are assumed to be Gaussian and only two-body correlations are taken into account. Therefore it is to be expected that the particular features of the jamming transition that are related to these correlated

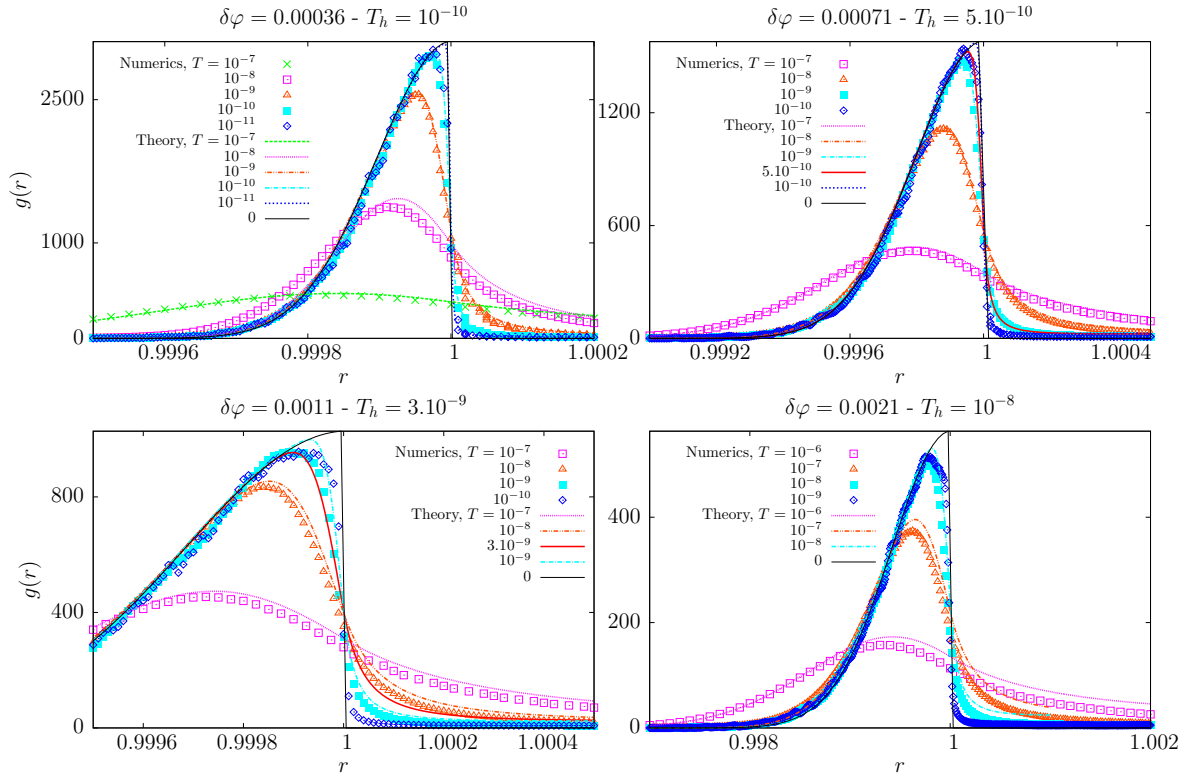


Figure 5.13: Pair correlations $g_{glass}(r)$ above jamming predicted by theory (full lines) and measured in numerical simulations (symbols). The agreement is very good for $T > T_h(\delta\varphi)$, the values of $T_h(\delta\varphi)$ are reported above the figures. Below $T_h(\varphi)$, the numerical curves do not evolve anymore, while the theoretical curves continue to evolve towards the $T = 0$ theoretical limit.

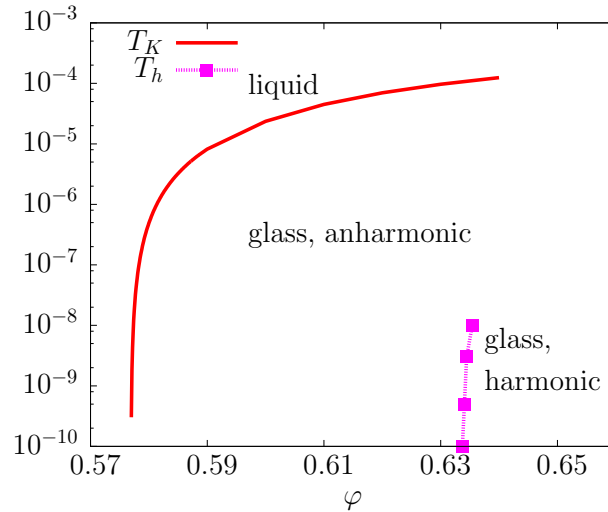


Figure 5.14: The crossover temperature $T_h(\varphi)$, as determined from Fig. 5.13, and compared with the Kauzmann temperature from Fig. 5.3.

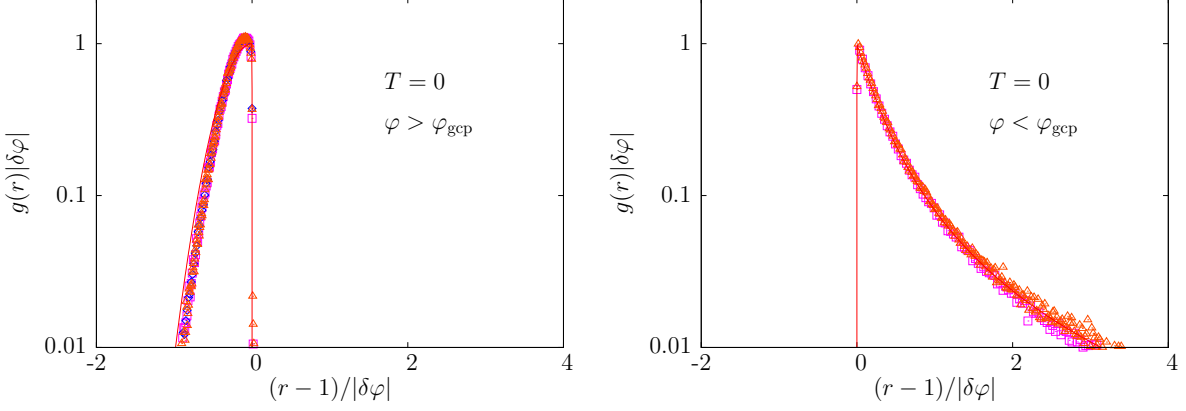


Figure 5.15: Scaling functions at $T = 0$ above (left) and below (right) the jamming transition showing the convergence of the first peak near $r = 1$ to a delta function with asymmetric scaling functions on both sides of the transition. To ease visualization, we show the evolution of $g(r)/g_{\text{max}}$, where g_{max} can be read from Fig. 5.9.

soft modes are not well reproduced by our theory.

On the hard sphere side, the soft modes induce a square-root divergence of the pair correlation function $g_{\text{glass}}(r) \propto 1/\sqrt{r-1}$. Yet, for $\delta\varphi \rightarrow 0^-$, this square root singularity is well separated from the contact peak [130]; therefore the shape of the scaling function for the contact peak is not affected by the soft modes and it is indeed correctly reproduced by the theory (see [130] and Fig. 5.15).

On the other side of the transition and for small $\delta\varphi > 0$ both the contact peak and the square root singularity are shifted by $\delta\varphi$. In particular the square root contribution should become $g_{\text{glass}}(r) \sim 1/\sqrt{r-1+a\delta\varphi}$. Inserting this form of $g_{\text{glass}}(r)$ into Eq. (5.31) yields the result that $z = z_0 + c\delta\varphi^{1/2}$, where z_0 is the contribution of the contact peak. While z_0 is clearly unaffected by the shift, the scaling of z with $\delta\varphi$ directly stems from the square root singularity of the pair correlation function. Therefore, the scaling of z is dominated by the soft modes contribution, which might explain why it is not well captured by our theory.

On the other hand, inserting the same expression in the general formula for the internal energy, Eq. (5.17), one finds that $e_{GS} \sim \tilde{e}\delta\varphi^2 + d\delta\varphi^{5/2}$, the first term being the contribution of the contact peak, the second being the one of the square root singularity. Therefore, for the energy the contribution of the anomalous modes is subdominant, and for this reason we observe that the theory reproduces well the numerical data in this case. The anomalous correction $\delta\varphi^{5/2}$ is of course not reproduced by the theory, that gives an expansion of e_{GS} in integer powers of $\delta\varphi$, but these are subdominant terms.

We also suspect that the shape of $g_{\text{glass}}(r)$ near the peak is also influenced by a mixing of the contact peak with the square root singularity. While both contributions are well separated for $\varphi < \varphi_j$, this is not necessarily the case above jamming, which likely explains the small deviations observed in Figs. 5.13 and 5.15, but we could not find an empirical or scaling argument to disentangle both contributions.

Finally, it is interesting to remark that these deviations between theory and simulations are washed out by a finite temperature $T > T_h(\delta\varphi)$. We suspect that $T_h(\delta\varphi)$ represents a temperature scale at which anharmonicity becomes relevant [163], and where the zero-temperature vibrational modes become irrelevant. Above this crossover temperature, vibrations are probably much less correlated and our approximations become correct. Interestingly, since $T_h(\delta\varphi) \rightarrow 0$ for $\delta\varphi \rightarrow 0^+$, we conclude

that the correlations at $\delta\varphi = 0$ are extremely fragile, such that an arbitrary small temperature is able to destroy them and restore the agreement between theory and numerical data.

5.6 Conclusions

In this final section we summarize our results and we discuss some perspectives for future work.

5.6.1 Summary of results

Understanding the physical properties of dense packings of soft repulsive particles is a fully nonequilibrium problem, because the jamming transition occurs in the absence of thermal fluctuations deep inside a glassy phase where phase space is dominated by the existence of a large number of metastable states.

Nevertheless, we showed that it can successfully be addressed using equilibrium statistical mechanics tools. We have developed a mean-field replica theory of the jamming transition of soft repulsive spheres which satisfactorily derives, from first principles, the existence and location of a jamming transition. This transition, that happens only at $T = 0$, is exactly the same as the SAT/UNSAT transition of random constraint satisfaction problems [119, 112, 96]: it is the point where the Parisi parameter m^* that characterizes the 1RSB glass phase goes to zero, the reduced pressure of the hard sphere glass diverges, or, equivalently, its pressure and energy become finite. Within our approach, the jamming transition takes place deep into the glassy phase, and is thus a phenomenon which is physically distinct from the glass transition itself [103]. Finally, we have shown that the average coordination jumps from zero to ~ 6 at the transition, and we derived scaling functions that describe well the contact peak of the pair correlation function.

Again, the absolute values of density reported in this study are affected by the fact that we used the HNC equation of state for the liquid [130], and thus quantitative agreement with simulations cannot be expected. Still, we found that the scaling around jamming is almost insensitive to the particular equation of state that is chosen for the liquid. We also investigated the region of small T around the jamming transition. We showed that the theory reproduces quite well the scaling numerical data with T and $\delta\varphi$, the distance from the jamming transition. On the hard spheres side of the transition ($\delta\varphi < 0$) the theory works well down to $T = 0$. On the soft sphere side ($\delta\varphi > 0$) we have identified a temperature $T_h(\delta\varphi)$ below which, according to our interpretation, correlated vibrations that are neglected in our theory become relevant for some observables, and produce a series of interesting scalings that are not captured by our theory [162, 155, 98]. The most striking of these is the scaling of the number of contacts which our theory fails to reproduce.

5.6.2 Technical aspects

It is a major open problem to try and include in the theory a correct description of the divergent correlations in the vibrational modes that are relevant for $\delta\varphi > 0$ and $T < T_h(\delta\varphi)$. Additionally, there are several more technical aspects on which the theory could be improved, even in the region where it works quite well.

Our theory falls within the general framework of the replica method, using the molecular liquid formulation of [114, 115]. However, to be able to describe the jamming transition, we had to develop a new approximation scheme, that is based on the effective potentials formulation of [130], and allows

one to view the molecular liquid as a simple liquid with effective potentials involving an arbitrary number of particles. Our approximation scheme is based on the following steps:

1. As in [130], we neglect the three (and more)-body interactions, and retain the two-body effective potential only.
2. In addition, we observe that the effective potential is given by the original potential (rescaled by a factor m) plus a small perturbation, therefore we use liquid perturbation theory to write the free energy of the replicated liquid as in Eq. (5.14).
3. Finally, we performed the low temperature approximation Eq. (5.16), in order to simplify the numerical calculations.

The last two approximations have been done mainly for practical reasons. However, we found that they are related to the first one. Indeed, if we get rid of approximation 3, we introduce an explicit dependence of y_{liq} on temperature, hence on τ in the limit $T \rightarrow 0$ and $\delta\varphi > 0$. It is easy to realize that this dependence affects the scaling close to jamming. An additional $\sqrt{\tau}$ term appears in the small τ expansion, which implies that $\tau \propto \delta\varphi^2$ and $e \propto \delta\varphi^3$. An inspection of the small τ expansion reveals that if y_{liq} does not depend on τ , then a delicate cancellation happens to eliminate the $\tau^{1/2}$ term and produce the correct scalings. The crucial observation is that the anomalous term contains the derivative of y_{liq} with respect to temperature, which is related to a three-body correlation function. Therefore we speculate that in a full treatment this term is cancelled by a term coming from the three body interaction potential. Therefore, getting rid of the third step of approximation might require taking into account three-body correlations as well.

This is of course an extremely interesting direction for future research, mainly because we suspect that getting rid of approximation 2 should allow us to eliminate the violation of the exact thermodynamic relation $p_{glass}^{HS} = 1 + 4\varphi y_{glass}^{HS}(\varphi)$ that occurs in the theory and forces us to rescale $\delta\varphi$ in order to compare with numerical data. It is also possible that taking into account interactions involving several particles one could capture at least partially the long range correlations at jamming.

5.6.3 Some general directions for future work

Our approach is general enough to be systematically improved and generalized to various models (e.g. Hertzian potentials, or truncated Lennard-Jones potential). Moreover, recent work reported on a method to compute the shear modulus within the replica approach [164, 154]. This could allow us to add the external drive to the theory, and obtain a complete theoretical picture of the jamming transition in the three dimensional temperature, density, stress jamming phase diagram originally proposed by Liu and Nagel [97].

Finally, we believe that in the long term these studies could open a way towards a quantitative renormalization group treatment of structural glasses, following recent studies that formulated the renormalization group for lattice models [32, 30]. If successful, this program could lead to a correct treatment of long-range correlations in the glass phase, and in particular at the jamming point, and could also allow us to address the behavior of pair correlations over a broader range of distances, since pair correlation functions also exhibit singular behavior beyond the contact peak [58, 143], while the structure factor [59] and isothermal compressibility [17] also display intriguing anomalies at large scale which remain to be predicted theoretically.

Chapter 6

Conclusion and perspectives

In this thesis, we have focused on the theoretical study of the transitions towards an amorphous solid state: the glass transition and the jamming transition. Our general approach has been to focus on finite-dimensional realistic models of structural glasses, and to concentrate on the derivation, from the sole knowledge of the pair potential and the evolution equation of the system, of the transition from supercooled liquid to glass, or from non-jammed to jammed.

For practical reasons, when an explicit numerical calculation was needed, we specialized to the system of harmonic spheres, mainly because of its special importance in the field of the jamming transition. The harmonic spheres have bounded interaction strength and range, two properties that we exploited respectively in Chapter 3 and 5.

6.1 Dynamics near the glass transition

We first studied the dynamics of a system of harmonic spheres and developed a simple perturbative approach, that predicts the existence of a glass transition in a compact way, giving some hope to the extension of such theory to higher-orders. By using the strength of the interaction between particles of the system as an expansion parameter, we were able to recover, as the lowest order correction to the ideal gas dynamics, a closed equation on the non-ergodicity factor of the system that is very close to the one obtained within mode-coupling theory. However, the situation is still unsatisfactory, due to a $U(1)$ symmetry that has been broken by hand in our formulation. However, the situation could be improved, and several proposals have been put forward in other areas of physics [92, 93]. The mathematical problem has now been formulated in a coherent way, and falls in the general class of the 2PI approximations of the free-energy of interacting bosons, which directly connects to hard condensed matter physics.

In retrospect, the use of the strength of the interaction as an expansion parameter sheds light on a set of numerical works by Ikeda and Miyazaki [78, 76, 77], who observed that mode-coupling predictions became good for the high density Gaussian-core model. This model indeed falls in the generic class of bounded repulsive potentials, which behave like ideal gases in the high density limit, i. e. the strength of the interaction can be taken as a small parameter in this case. Thus the statics become mean-field [99] at high density, and the dynamics start obeying closely the mode-coupling phenomenology.

Apart from that case, several theoretical approaches still need to be reconciled. Szamel formulated a diagrammatic formulation of the mode-coupling theory for Brownian dynamics [150], which could

provide another correct starting point for improvement of the theory. Independently, the approach of Kawasaki and Kim [87], which is based on the more traditional Martin-Siggia-Rose formalism, uses a loop expansion to derive the same result as mode-coupling theory. One advantage of Szamel's formulation over the latter is that it contains explicitly the high-order correlation functions of the equilibrium liquid, whereas these correlations must be uncovered by non-perturbative arguments in the case of standard field-theory. The task is straightforward for the two-point correlation function, but we expect it to be much harder in the case of higher-order correlation functions.

We are left with three distinct approaches, the three of them being satisfying in one respect: our approach provides an expansion parameter, the approach of Szamel takes properly into account the static properties of the system, and the one of Kawasaki and Kim respects properly all symmetries of the evolution equation. A dynamical approach that could unify these three approaches would be a major breakthrough in the field.

Once a satisfying first-principle derivation of the existence of a glass transition will be derived, it will be easy to deduce the corresponding expressions for the four-point functions that are currently used in numerical works or in experiments, and they will naturally become long range due to the sudden appearance of a non-zero value of the non-ergodicity parameter [151, 16, 15].

However, it has been argued early that the apparition of a non-zero ergodicity parameter is merely an artifact of numerical simulations and experiments, that are not able to wait for a sufficient time the equilibration of the system. In that case, a cross-over to dynamics that are controlled by the static landscape is expected to take place, which, in the replica interpretation at least, would eventually also lead to ergodicity breaking, but with a very different underlying mechanism.

Another possibility would be that a transition of dynamical nature indeed takes place, but is described by a more complicated (dynamical) order parameter. This possibility is supported by recent numerical simulations [111, 133] that uncovered a hidden dynamical transition associated with the glass transition. However, the matter of connecting this discovery with observed behaviors of the two- or four- point correlation functions, or to thermodynamic quantities is still elusive. Moreover the theoretical study of such transitions on realistic models is expected to be quite involved.

6.2 Bridging the gap between statics and dynamics

Independently of dynamical calculations, we also considered the random-first-order transition theory, that focuses on the metastable states of the static free-energy landscape. This set of theoretical predictions are based on the assumption that the long-time dynamics of the system are dominated by the deep minima of the free-energy landscape. By resorting to the replica method, and liquid state theory, one is able to predict the appearance of a non-zero non-ergodicity parameter. The predictions coming from replica theory and mode-coupling theory for this quantity were already noticed to share a similar form [152, 130]. Szamel used this similarity to show that, in terms of replica theory, the mode-coupling result is obtained with a reasonable assumption of vanishing current between different metastable states, and further use of factorization approximations much like in the original mode-coupling derivation. We adopted another approach and asked, within the static replica theory, for a precise comparison between the dynamical and the static self-consistent equations for the non-ergodicity parameter. The dynamical equation limits itself to a two-mode approximation, so we performed the equivalent approximation in the static context. An immediate observation was that a term containing the three-body static correlation function is obtained in both approaches, but the dominant one, that contains two-body correlation, is absent from replica theory, and seems to emerge

from purely dynamical calculations.

This calculation allowed to correctly identify the class of diagrams that are relevant in the static computation, which can allow for a unified framework for replica theory computations. For example, one could make contact with the Mézard-Parisi [115] and Parisi-Zamponi [130] approximation schemes, or more generally with the effective potential approximation derived in Chapter 5, by making a Gaussian ansatz on the form of the off-diagonal correlation function, and perform cage expansions afterwards.

Once an approximation that is able to detect the glass transition (such as replicated HNC) has been found, the calculation that we performed also serves as a basis for setting up a Landau-like expansion around this approximation, by using the fact that the bifurcation mechanism with which the non-ergodicity appears gives rise to soft modes in the system.

In a broader perspective, the interplay between the metastable states (i.e. minima of the static free-energy), that are at the basis of the reasonings in replica theory, and dynamical quantities should be investigated. This is by definition impossible in the static context, and has to be investigated in a dynamical calculation. More precisely, one has to consider the low lying excited states of the evolution operator of the system, and try to put them in correspondence with the minima of the static free-energy, in the spirit of [24]. An analytical approach that would be able to address this question for realistic models of glasses is unfortunately for the moment out of reach. However, such a finding would be mandatory if it were found that no dynamical order parameter describes the glass transition properly, as suggested above.

Despite this intrinsic limitation of replica theory, it is an important task to push its predictions as far as possible in order to set the stage in case for a theory that would be able to incorporate both static and dynamical aspects of the glass transition.

6.3 Towards a full theory of the jamming transition

Finally, we have developed, based on replica theory, a microscopic theory for the jamming transition of harmonic spheres, able to quantitatively recover many observed scalings near the jamming transition. Of the three main questions discussed in this thesis, this is where the current theoretical tools give the most satisfying results. Indeed, the very high density at which the jamming transition takes place justifies most of the approximations performed by replica theory: the out-of-equilibrium procedures used to construct those states place the system directly in an ergodicity broken picture, where the system is trapped around one given local minima of the free-energy. The very high density justifies an expansion in the sizes of the cages seen by the particles, which also serves as an order parameter for the transition.

This successes allowed to clearly separate the glass transition, for which replica theory provides at worst an upper bound in terms of density, and the jamming transition, which occurs for densities even larger than this upper bound.

Despite these successes, we have seen that our theory is not able to capture the long-range correlations that appear precisely at the jamming transition. However, it is only natural to expect this since we limited ourselves to two-body correlations. A non-linear mechanism that would allow for the appearance of system-wide correlations could be provided by the inclusion of three-body interactions, which is easily done in principle, although the numerical cost of such extension of the theory could be important.

The importance of rattlers in the computation is also left aside by our approximations, and can

also have an important impact on the critical scalings at jamming. This aspect could be incorporated in the theory by allowing for non-Gaussian forms of the cage. This would require an optimization of the free-energy over a one-dimensional function instead of a single parameter, and would be also a hard numerical task.

Publications

- P1** H. Jacquin and L. Berthier, Soft Matter **6**, 2970 (2010)
Anomalous structural evolution of soft particles: Equilibrium liquid state theory
<http://dx.doi.org/10.1039/B926412D>
- P2** L. Berthier, E. Flenner, H. Jacquin, and G. Szamel, Phys. Rev. E **81**, 031505 (2010)
Scaling of the glassy dynamics of soft repulsive particles: a mode-coupling approach
<http://dx.doi.org/10.1103/PhysRevE.81.031505>
- P3** L. Berthier, H. Jacquin, and F. Zamponi, J. Stat. Mech. P01004 (2011)
Can the jamming transition be described using equilibrium statistical mechanics ?
<http://dx.doi.org/10.1088/1742-5468/2011/01/P01004>
- P4** H. Jacquin, L. Berthier, and F. Zamponi, Phys. Rev. Lett. **106**, 135702 (2011)
Microscopic Mean-Field theory of the jamming transition
<http://dx.doi.org/10.1103/PhysRevLett.106.135702>
- P5** H. Jacquin and F. van Wijland, Phys. Rev. Lett. **106**, 210602 (2011)
Field theoretic formulation of a mode-coupling equation for colloids
<http://dx.doi.org/10.1103/PhysRevLett.106.210602>
- P6** L. Berthier, H. Jacquin, and F. Zamponi, Phys. Rev. E **84**, 051103 (2011)
Microscopic theory of the jamming transition of harmonic spheres
<http://dx.doi.org/10.1103/PhysRevE.84.051103>

Bibliography

- [1] G. Adam and J. H. Gibbs. On the temperature dependence of cooperative relaxation properties in glass-forming liquids. *J. Chem. Phys.*, 43(1):139–146, 1965. doi:[10.1063/1.1696442](https://doi.org/10.1063/1.1696442).
- [2] A. Andreanov, G. Biroli, J.-P. Bouchaud, and A. Lefèvre. Field theories and exact stochastic equations for interacting particle systems. *Phys. Rev. E*, 74:030101, 2006. doi:[10.1103/PhysRevE.74.030101](https://doi.org/10.1103/PhysRevE.74.030101).
- [3] A. Andreanov, G. Biroli, and A. Lefèvre. Dynamical field theory for glass-forming liquids, self-consistent resummations and time-reversal symmetry. *J. Stat. Mech.*, page P07008, 2006. doi:[10.1088/1742-5468/2006/07/P07008](https://doi.org/10.1088/1742-5468/2006/07/P07008).
- [4] A. Andreanov, J.-P. Bouchaud, and G. Biroli. Mode coupling as a landau theory of the glass transition. *Europhys. Lett.*, 88:16001, 2009. doi:[10.1209/0295-5075/88/16001](https://doi.org/10.1209/0295-5075/88/16001).
- [5] C. A. Angell. Structural instability and relaxation in liquid and glassy phases near the fragile liquid limit. *J. Non-Cryst. Solids*, 102:205–221, 1988. doi:[10.1016/0022-3093\(88\)90133-0](https://doi.org/10.1016/0022-3093(88)90133-0).
- [6] C. A. Angell. Formation of glasses from liquids and biopolymers. *Science*, 267(5206):1924–1935, 1995. doi:[10.1126/science.267.5206.1924](https://doi.org/10.1126/science.267.5206.1924).
- [7] N. W. Ashcroft and N. D. Mermin. *Solid State Physics*. Holt Saunders, New York, 1976.
- [8] A. Ayadim, P. Germain, and S. Amokrane. Mode-coupling theory for the glass transition: Test of the convolution approximation for short-range interactions. *Phys. Rev. E*, 84(6):061502, 2011. doi:[10.1103/PhysRevE.84.061502](https://doi.org/10.1103/PhysRevE.84.061502).
- [9] J.-L. Barrat, W. Götze, and A. Latz. The liquid-glass transition of the hard-sphere system. *J. Phys.: Condens. Matter*, 1:7163–7170, 1989. doi:[doi:10.1088/0953-8984/1/39/027](https://doi.org/10.1088/0953-8984/1/39/027).
- [10] R. J. Baxter. Direct correlation functions and their derivatives with respect to particle density. *J. Chem. Phys.*, 41:553, 1964. doi:[10.1063/1.1725907](https://doi.org/10.1063/1.1725907).
- [11] U. Bengtzelius, W. Götze, and A. Sjolander. Dynamics of supercooled liquids and the glass transition. *J. Phys. C*, 17(33):5915–5934, 1984. doi:[doi:10.1088/0022-3719/17/33/005](https://doi.org/10.1088/0022-3719/17/33/005).
- [12] C. H. Bennett. Serially deposited amorphous aggregates of hard spheres. *J. Appl. Phys.*, 43:2727, 1972. doi:[10.1063/1.1661585](https://doi.org/10.1063/1.1661585).
- [13] B. J. Berne and R. Pecora. *Dynamic Light Scattering*. Wiley, New York, 1976.
- [14] L. Berthier and G. Biroli. Theoretical perspective on the glass transition and amorphous materials. *Rev. Mod. Phys.*, 83(2):587, 2011. doi:[10.1103/RevModPhys.83.587](https://doi.org/10.1103/RevModPhys.83.587).

- [15] L. Berthier, G. Biroli, J.-P. Bouchaud, W. Kob, K. Miyazaki, and D. R. Reichman. Spontaneous and induced dynamic correlations in glass formers. II. Model calculations and comparison to numerical simulations. *J. Chem. Phys.*, 126:184504, 2007. [doi:10.1063/1.2721555](https://doi.org/10.1063/1.2721555).
- [16] L. Berthier, G. Biroli, J.-P. Bouchaud, W. Kob, K. Miyazaki, and D. R. Reichman. Spontaneous and induced dynamic fluctuations in glass formers. I. General results and dependence on ensemble and dynamics. *J. Chem. Phys.*, 126:184503, 2007. [doi:10.1063/1.2721554](https://doi.org/10.1063/1.2721554).
- [17] L. Berthier, P. Chaudhuri, C. Coulais, O. Dauchot, and P. Sollich. Suppressed compressibility at large scale in jammed packings of size-disperse spheres. *Phys. Rev. Lett.*, 106:120601, 2011. [doi:10.1103/PhysRevLett.106.120601](https://doi.org/10.1103/PhysRevLett.106.120601).
- [18] L. Berthier, H. Jacquin, and F. Zamponi. Can the jamming transition be described using equilibrium statistical mechanics ? *J. Stat. Mech.*, page P01004, 2011. [doi:10.1088/1742-5468/2011/01/P01004](https://doi.org/10.1088/1742-5468/2011/01/P01004).
- [19] L. Berthier, H. Jacquin, and F. Zamponi. Microscopic theory of the jamming transition of harmonic spheres. *Phys. Rev. E*, 84(5):051103, 2011. [doi:10.1103/PhysRevE.84.051103](https://doi.org/10.1103/PhysRevE.84.051103).
- [20] L. Berthier and T. A. Witten. Compressing nearly hard sphere fluids increases glass fragility. *Europhys. Lett.*, 86(1):10001, 2009. [doi:10.1209/0295-5075/86/10001](https://doi.org/10.1209/0295-5075/86/10001).
- [21] L. Berthier and T. A. Witten. Glass transition of dense fluids of hard and compressible spheres. *Phys. Rev. E*, 80(2):021502, 2009. [doi:10.1103/PhysRevE.80.021502](https://doi.org/10.1103/PhysRevE.80.021502).
- [22] K. Binder and W. Kob. *Glassy materials and disordered solids: An introduction to their statistical mechanics*. World Scientific, 2005.
- [23] G. Biroli and J.-P. Bouchaud. *Structural Glasses and Supercooled Liquids: Theory, Experiment, and Applications*, chapter The Random First-Order Transition Theory of Glasses: a critical assessment. John Wiley & Sons, Hoboken, New Jersey, 2009.
- [24] G. Biroli and R. Monasson. Relationship between long timescales and the static free-energy in the hopfield model. *J. Phys. A*, 31:L391–L396, 1998. [doi:10.1088/0305-4470/31/21/001](https://doi.org/10.1088/0305-4470/31/21/001).
- [25] P. Blasiak, A. Horzela, K. A. Penson, A. I. Solomon, and G. H. E. Duchamp. Combinatorics and boson normal ordering: A gentle introduction. *Am. J. Phys.*, 75(7):639–646, 2007. [doi:10.1119/1.2723799](https://doi.org/10.1119/1.2723799).
- [26] J.-P. Bouchaud. The mode-coupling theory of supercooled liquids: Does it wear any clothes? <http://www.condmatjournalclub.org/?p=1022>, 2010.
- [27] J.-P. Bouchaud and G. Biroli. On the Adam-Gibbs-Kirkpatrick-Thirumalai-Wolynes scenario for the viscosity increase in glasses. *J. Chem. Phys.*, 121:7347, 2004. [doi:DOI:10.1063/1.1796231](https://doi.org/10.1063/1.1796231).
- [28] G. Brambilla, D. El Masri, M. Pierno, L. Berthier, L. Cipelletti, G. Petekidis, and A. B. Schofield. Probing the equilibrium dynamics of colloidal hard spheres above the mode-coupling glass transition. *Phys. Rev. Lett.*, 102(8):085703, 2009. [doi:10.1103/PhysRevLett.102.085703](https://doi.org/10.1103/PhysRevLett.102.085703).
- [29] E. A. Calzetta and B.-L. B. Hu. *Non-Equilibrium quantum field theory*. Cambridge University Press, 2008.

- [30] C. Cammarota, G. Biroli, M. Tarzia, and G. Tarjus. Renormalization group analysis of the random First-Order transition. *Phys. Rev. Lett.*, 106(11):115705, 2011. [doi:10.1103/PhysRevLett.106.115705](https://doi.org/10.1103/PhysRevLett.106.115705).
- [31] M. Cardenas, S. Franz, and G. Parisi. Constrained Boltzmann-Gibbs measures and effective potential for glasses in hypernetted chain approximation and numerical simulations. *J. Chem. Phys.*, 110(3):1726–1734, 1999. [doi:10.1063/1.478028](https://doi.org/10.1063/1.478028).
- [32] M. Castellana, A. Decelle, S. Franz, M. Mézard, and G. Parisi. Hierarchical random energy model of a spin glass. *Phys. Rev. Lett.*, 104(12):127206, 2010. [doi:10.1103/PhysRevLett.104.127206](https://doi.org/10.1103/PhysRevLett.104.127206).
- [33] T. Castellani and A. Cavagna. Spin glass theory for pedestrians. *J. Stat. Mech.*, page P05012, 2005. [doi:10.1088/1742-5468/2005/05/P05012](https://doi.org/10.1088/1742-5468/2005/05/P05012).
- [34] M. E. Cates and Sriram Ramaswamy. Do Current-Density nonlinearities cut off the glass transition? *Phys. Rev. Lett.*, 96(13):135701, 2006. [doi:10.1103/PhysRevLett.96.135701](https://doi.org/10.1103/PhysRevLett.96.135701).
- [35] A. Cavagna. Supercooled liquids for pedestrians. *Phys. Rep.*, 476(4-6):51–124, 2009. [doi:10.1016/j.physrep.2009.03.003](https://doi.org/10.1016/j.physrep.2009.03.003).
- [36] P. Charbonneau, A. Ikeda, G. Parisi, and F. Zamponi. Glass transition and random close packing above three dimensions. *Phys. Rev. Lett.*, 107(18):185702, 2011. [doi:10.1103/PhysRevLett.107.185702](https://doi.org/10.1103/PhysRevLett.107.185702).
- [37] P. Chaudhuri, L. Berthier, and S. Sastry. Jamming transitions in amorphous packings of frictionless spheres occur over a continuous range of volume fractions. *Phys. Rev. Lett.*, 104(16):165701, 2010. [doi:10.1103/PhysRevLett.104.165701](https://doi.org/10.1103/PhysRevLett.104.165701).
- [38] P. Chaudhuri, S. Karmakar, C. Dasgupta, H. R. Krishnamurthy, and A. K. Sood. Equilibrium glassy phase in a polydisperse hard-sphere system. *Phys. Rev. Lett.*, 95(24):248301, 2005. [doi:10.1103/PhysRevLett.95.248301](https://doi.org/10.1103/PhysRevLett.95.248301).
- [39] X. Cheng. Experimental study of the jamming transition at zero temperature. *Phys. Rev. E*, 81:031301, 2010. [doi:10.1103/PhysRevE.81.031301](https://doi.org/10.1103/PhysRevE.81.031301).
- [40] M. Cini. *Topics and Methods in Condensed Matter Theory*. Springer, 2007.
- [41] M. Clusel, E. I. Corwin, A. O. N. Siemens, and J. Brujic. A 'granocentric' model for random packing of jammed emulsions. *Nature*, 460:611–615, 2009. [doi:10.1038/nature08158](https://doi.org/10.1038/nature08158).
- [42] J. D. Cole. On a quasi-linear parabolic equation occurring in aerodynamics. *Quart. Appl. Math.*, 1951.
- [43] R. Colin, A. M. Alsayed, J.-C. Castaing, R. Goyal, L. Hough, and B. Abou. Spatially heterogeneous dynamics in a thermosensitive soft suspension before and after the glass transition. *Soft Matter*, 7:4504–4514, 2011. [doi:10.1039/c0sm01184c](https://doi.org/10.1039/c0sm01184c).
- [44] J. H. Conway and N. J. A. Sloane. *Sphere Packings, Lattices and Groups*. Spriger-Verlag, New York, 1993.
- [45] J. M. Cornwall, R. Jackiw, and E. Tomboulis. Effective action for composite operators. *Phys. Rev. D*, 10(8):2428–2445, 1974. [doi:10.1103/PhysRevD.10.2428](https://doi.org/10.1103/PhysRevD.10.2428).

- [46] L. F. Cugliandolo and J. Kurchan. Analytical solution of the off-equilibrium dynamics of a long-range spin-glass model. *Phys. Rev. Lett.*, 71(1):173–176, 1993. doi:[10.1103/PhysRevLett.71.173](https://doi.org/10.1103/PhysRevLett.71.173).
- [47] S. P. Das and G. F. Mazenko. Fluctuating nonlinear hydrodynamics and the liquid-glass transition. *Phys. Rev. A*, 34(3):2265–2282, 1986. doi:[10.1103/PhysRevA.34.2265](https://doi.org/10.1103/PhysRevA.34.2265).
- [48] C. Dasgupta and O. T. Valls. Free energy landscape of a dense hard-sphere system. *Phys. Rev. E*, 59(3):3123–3134, 1999. doi:[10.1103/PhysRevE.59.3123](https://doi.org/10.1103/PhysRevE.59.3123).
- [49] C. De Dominicis. Variational formulations of equilibrium statistical mechanics. *J. Math. Phys.*, 3(5):983–1002, 1962. doi:[10.1063/1.1724313](https://doi.org/10.1063/1.1724313).
- [50] C. De Dominicis. Techniques de renormalisation de la théorie des champs et dynamique des phénomènes critique. *J. Phys. Colloques*, 37:C1–247–C1–253, 1976. doi:[10.1051/jphyscol:1976138](https://doi.org/10.1051/jphyscol:1976138).
- [51] C. De Dominicis and P. C. Martin. Stationary entropy principle and renormalization in normal and superfluid system. i. algebraic formulation. *J. Math. Phys.*, 5(1):14–30, 1964. doi:[10.1063/1.1704062](https://doi.org/10.1063/1.1704062).
- [52] C. De Dominicis and P. C. Martin. Stationary entropy principle and renormalization in normal and superfluid systems. ii. diagrammatic formulation. *J. Math. Phys.*, 5(1):31–59, 1964. doi:[10.1063/1.1704064](https://doi.org/10.1063/1.1704064).
- [53] D. Dean. Langevin equation for the density of a system of interacting langevin processes. *J. Phys. A*, 29:613–617, 1996. doi:[10.1088/0305-4470/29/24/001](https://doi.org/10.1088/0305-4470/29/24/001).
- [54] A. R. Denton and N. W. Ashcroft. High-order direct correlation functions of uniform classical liquids. *Phys. Rev. A*, 39(1):426–429, 1989. doi:[10.1103/PhysRevA.39.426](https://doi.org/10.1103/PhysRevA.39.426).
- [55] A. R. Denton and N. W. Ashcroft. Density-functional approach to the structure of classical uniform fluids. *Phys. Rev. A*, 44(2):1219–1227, 1991. doi:[10.1103/PhysRevA.44.1219](https://doi.org/10.1103/PhysRevA.44.1219).
- [56] B. Derrida. Random-energy model: Limit of a family of disordered models. *Phys. Rev. Lett.*, 45(2):79–82, 1980. doi:[10.1103/PhysRevLett.45.79](https://doi.org/10.1103/PhysRevLett.45.79).
- [57] M. Doi. Second quantization representation for classical many- particle system. *J. Phys. A*, 9(9):1465, 1976. doi:[10.1088/0305-4470/9/9/008](https://doi.org/10.1088/0305-4470/9/9/008).
- [58] A. Donev, S. Torquato, and F. H. Stillinger. Pair correlation function characteristics of nearly jammed disordered and ordered hard-sphere packings. *Phys. Rev. E*, 71(1):011105, 2005. doi:[10.1103/PhysRevE.71.011105](https://doi.org/10.1103/PhysRevE.71.011105).
- [59] A. Donev, S. Torquato, and F. H. Stillinger. Unexpected density fluctuations in jammed disordered sphere packings. *Phys. Rev. Lett.*, 95:090604, 2005. doi:[10.1103/PhysRevLett.95.090604](https://doi.org/10.1103/PhysRevLett.95.090604).
- [60] D. J. Durian. Foam mechanics at the bubble scale. *Phys. Rev. Lett.*, 75:4780, 1995. doi:[10.1103/PhysRevLett.75.4780](https://doi.org/10.1103/PhysRevLett.75.4780).
- [61] M. Dzero, J. Schmalian, and P. G. Wolynes. Replica theory for fluctuations of the activation barriers in glassy systems. *Phys. Rev. B*, 80:024204, 2009. doi:[10.1103/PhysRevB.80.024204](https://doi.org/10.1103/PhysRevB.80.024204).

- [62] D. El Masri, G. Brambilla, M. Pierno, G. Petekidis, A. B. Schofield, L. Berthier, and L. Cipelletti. Dynamic light scattering measurements in the activated regime of dense colloidal hard spheres. *J. Stat. Mech.*, page P07015, 2009. doi:[10.1088/1742-5468/2009/07/P07015](https://doi.org/10.1088/1742-5468/2009/07/P07015).
- [63] A. Fernandez-Nieves, H. Wyss, J. Mattsson, and D. A. Weitz, editors. *Microgel suspensions*. Wiley-VCH, 2011.
- [64] G. H. Fredrickson and H. C. Andersen. Kinetic ising model of the glass transition. *Phys. Rev. Lett.*, 53(13):1244–1247, 1984. doi:[10.1103/PhysRevLett.53.1244](https://doi.org/10.1103/PhysRevLett.53.1244).
- [65] G. H. Fredrickson and H. C. Andersen. Facilitated kinetic ising models and the glass transition. *J. Chem. Phys.*, 83(11):5822–5831, 1985. doi:[10.1063/1.449662](https://doi.org/10.1063/1.449662).
- [66] J. H. Gibbs and E. A. Di Marzio. Nature of the glass transition and the glassy state. *J. Chem. Phys.*, 28(3):373–383, 1958. doi:[10.1063/1.1744141](https://doi.org/10.1063/1.1744141).
- [67] D. L. Goodstein. *States of matter*. Prentice-Hall, Inc., Englewood Cliffs, New Jersey, 1975.
- [68] W. Götze. Properties of the glass instability treated within a mode coupling theory. *Z. Phys. B*, 60(2-4):195–203, 1985. doi:[10.1007/BF01304439](https://doi.org/10.1007/BF01304439).
- [69] W. Götze. Recent tests of the mode-coupling theory for glassy dynamics. *J. Phys.: Condens. Matter*, 11(10A):1–45, 1999. doi:[10.1088/0953-8984/11/10A/002](https://doi.org/10.1088/0953-8984/11/10A/002).
- [70] W. Götze and L. Sjögren. α -relaxation near the liquid-glass transition. *J. Phys. C*, 20:879–894, 1987. doi:[doi:10.1088/0022-3719/20/7/005](https://doi.org/10.1088/0022-3719/20/7/005).
- [71] W. Götze and L. Sjögren. The glass transition singularity. *Z. Phys. B*, 65(4):415–427, 1987. doi:[10.1007/BF01303763](https://doi.org/10.1007/BF01303763).
- [72] J. L. Green, K. Ito, K. Xu, and C. A. Angell. Fragility in liquids and polymers: new, simple quantifications and interpretations. *J. Phys. Chem. B*, 103(20):3991–3996, 1999. doi:[10.1021/jp983927i](https://doi.org/10.1021/jp983927i).
- [73] D. J. Gross and M. Mézard. The simplest spin glass. *Nucl. Phys. B*, 240:431, 1984. doi:[10.1016/0550-3213\(84\)90237-2](https://doi.org/10.1016/0550-3213(84)90237-2).
- [74] J. P. Hansen and I. R. McDonald. *Theory of simple liquids*. Academic Press, London, 1986.
- [75] E. Hopf. The partial differential equation $u_t + uu_x = xu_{xx}$. *Comm. Pure Appl. Math.*, 3:201–230, 1950. doi:[10.1002/cpa.3160030302](https://doi.org/10.1002/cpa.3160030302).
- [76] A. Ikeda and K. Miyazaki. Glass transition of the monodisperse gaussian core model. *Phys. Rev. Lett.*, 106(1):015701, 2011. doi:[10.1103/PhysRevLett.106.015701](https://doi.org/10.1103/PhysRevLett.106.015701).
- [77] A. Ikeda and K. Miyazaki. Slow dynamics of the high density gaussian core model. *J. Chem. Phys.*, 135:054901, 2011. doi:[10.1063/1.3615949](https://doi.org/10.1063/1.3615949).
- [78] A. Ikeda and K. Miyazaki. Thermodynamic and structural properties of the high density gaussian core model. *J. Chem. Phys.*, 135:024901, 2011. doi:[10.1063/1.3609277](https://doi.org/10.1063/1.3609277).
- [79] R. Jackiw. Functional evaluation of the effective potential. *Phys. Rev. D*, 9(6):1686–1701, 1974. doi:[10.1103/PhysRevD.9.1686](https://doi.org/10.1103/PhysRevD.9.1686).

- [80] H. Jacquin and L. Berthier. Anomalous structural evolution of soft particles: Equilibrium liquid state theory. *Soft Matter*, 6:2970, 2010. doi:[10.1039/b926412d](https://doi.org/10.1039/b926412d).
- [81] H. M. Jaeger, S. R. Nagel, and R. P. Behringer. Granular solids, liquids, and gases. *Rev. Mod. Phys.*, 68:1259, 1996. doi:[10.1103/RevModPhys.68.1259](https://doi.org/10.1103/RevModPhys.68.1259).
- [82] H. K. Janssen. Field-theoretic method applied to critical dynamics. In Charles P. Enz, editor, *Dynamical Critical Phenomena and Related Topics*, volume 104, pages 25–47. Springer Berlin Heidelberg, Berlin, Heidelberg, 1979. doi:[10.1007/3-540-09523-3_2](https://doi.org/10.1007/3-540-09523-3_2).
- [83] H. K. Janssen. *Topics in Modern Statistical Physics*, chapter On the renormalized field-theory of nonlinear critical relaxation. World Scientific, Singapore, 1992.
- [84] W. Kauzmann. The nature of the glassy state and the behavior of liquids at low temperatures. *Chem. Rev.*, 43(2):219–256, 1948. doi:[10.1021/cr60135a002](https://doi.org/10.1021/cr60135a002).
- [85] K. Kawasaki. Stochastic model of slow dynamics in supercooled liquids and dense colloidal suspensions. *Physica A*, 208(1):35–64, 1994. doi:[10.1016/0378-4371\(94\)90532-0](https://doi.org/10.1016/0378-4371(94)90532-0).
- [86] B. Kim and K. Kawasaki. The mode coupling theory in the fdr-preserving field theory of interacting brownian particles. *J. Phys. A*, 40:F33–F42, 2007. doi:[10.1088/1751-8113/40/1/F04](https://doi.org/10.1088/1751-8113/40/1/F04).
- [87] B. Kim and K. Kawasaki. A fluctuation-dissipation relationship-preserving field theory for interacting brownian particles: one-loop theory and mode coupling theory. *J. Stat. Mech.*, page P02004, 2008. doi:[10.1088/1742-5468/2008/02/P02004](https://doi.org/10.1088/1742-5468/2008/02/P02004).
- [88] K. Kim and T. Munakata. Glass transition of hard sphere systems: Molecular dynamics and density functional theory. *Phys. Rev. E*, 68(2):021502, 2003. doi:[10.1103/PhysRevE.68.021502](https://doi.org/10.1103/PhysRevE.68.021502).
- [89] T. R. Kirkpatrick, D. Thirumalai, and P. G. Wolynes. Scaling concepts for the dynamics of viscous liquids near an ideal glassy state. *Phys. Rev. A*, 40(2):1045–1054, 1989. doi:[10.1103/PhysRevA.40.1045](https://doi.org/10.1103/PhysRevA.40.1045).
- [90] T. R. Kirkpatrick and P. G. Wolynes. Connections between some kinetic and equilibrium theories of the glass transition. *Phys. Rev. A*, 35(7):3072–3080, 1987. doi:[10.1103/PhysRevA.35.3072](https://doi.org/10.1103/PhysRevA.35.3072).
- [91] T. R. Kirkpatrick and P. G. Wolynes. Stable and metastable states in mean-field potts and structural glasses. *Phys. Rev. B*, 36(16):8552–8564, 1987. doi:[10.1103/PhysRevB.36.8552](https://doi.org/10.1103/PhysRevB.36.8552).
- [92] T. Kita. Conserving gapless theory for weakly interacting bose gases. *J. Phys. Soc. Jpn*, 75(4):044603, 2006. doi:[10.1143/JPSJ.75.044603](https://doi.org/10.1143/JPSJ.75.044603).
- [93] T. Kita. Self-consistent perturbation expansion for bose-einstein condensates satisfying goldstone’s theorem and conservation laws. *Phys. Rev. B*, 80:214502, 2009. doi:[10.1103/PhysRevB.80.214502](https://doi.org/10.1103/PhysRevB.80.214502).
- [94] W. Kob and H. C. Andersen. Testing mode-coupling theory for a supercooled binary Lennard-Jones mixture. II. intermediate scattering function and dynamic susceptibility. *Phys. Rev. E*, 52(4):4134, 1995. doi:[10.1103/PhysRevE.52.4134](https://doi.org/10.1103/PhysRevE.52.4134).
- [95] F. Krzakala and J. Kurchan. Landscape analysis of constraint satisfaction problems. *Phys. Rev. E*, 76(2):021122, 2007. doi:[10.1103/PhysRevE.76.021122](https://doi.org/10.1103/PhysRevE.76.021122).

- [96] F. Krzakala and L. Zdeborová. Potts glass on random graphs. *Europhys. Lett.*, 81(5):57005, 2008. doi:[10.1209/0295-5075/81/57005](https://doi.org/10.1209/0295-5075/81/57005).
- [97] A. J. Liu and S. R. Nagel. Jamming isn't just cool anymore. *Nature*, 396:21, 1998. doi:[10.1038/23819](https://doi.org/10.1038/23819).
- [98] A. J. Liu, S. R. Nagel, W. van Saarloos, and M. Wyart. *Dynamical Heterogeneities in Glasses, Colloids, and Granular Media ed (Oxford: Oxford University Press) at press*. Oxford University Press, 2010.
- [99] A. A. Louis, P. G. Bolhuis, and J. P. Hansen. Mean-field fluid behavior of the gaussian core model. *Phys. Rev. E*, 62:7961–7972, 2000.
- [100] B. D. Lubachevsky and F. H. Stillinger. Geometric properties of random disk packings. *J. Stat. Phys.*, 60:561–583, 1990. doi:[10.1007/BF01025983](https://doi.org/10.1007/BF01025983).
- [101] V. Lubchenko and P. G. Wolynes. Theory of structural glasses and supercooled liquids. *Annu. Rev. Phys. Chem.*, 58(1):235–266, 2007. doi:[10.1146/annurev.physchem.58.032806.104653](https://doi.org/10.1146/annurev.physchem.58.032806.104653).
- [102] J. M. Luttinger and J. C. Ward. Ground-state energy of a many-fermion system ii. *Phys. Rev.*, 118(5):1417–1427, 1960. doi:[10.1103/PhysRev.118.1417](https://doi.org/10.1103/PhysRev.118.1417).
- [103] R. Mari, F. Krzakala, and J. Kurchan. Jamming versus glass transitions. *Phys. Rev. Lett.*, 103(2):025701, 2009. doi:[10.1103/PhysRevLett.103.025701](https://doi.org/10.1103/PhysRevLett.103.025701).
- [104] P. C. Martin, E. D. Siggia, and H. A. Rose. Statistical dynamics of classical systems. *Phys. Rev. A*, 8(1):423–437, 1973. doi:[10.1103/PhysRevA.8.423](https://doi.org/10.1103/PhysRevA.8.423).
- [105] L.-M. Martinez and C. A. Angell. A thermodynamic connection to the fragility of glass-forming liquids. *Nature*, 410:663–667, 2001. doi:[10.1038/35070517](https://doi.org/10.1038/35070517).
- [106] J. C. Maxwell. On the calculation of the equilibrium and stiffness of frames. *Phil. Mag. Series 4*, 27(182):294–299, 1864. doi:[10.1080/14786446408643668](https://doi.org/10.1080/14786446408643668).
- [107] J. E. Mayer and E. W. Montroll. Molecular distribution. *J. Chem. Phys.*, 9(1):2–16, 1941. doi:[10.1063/1.1750822](https://doi.org/10.1063/1.1750822).
- [108] J.E. Mayer and M. G. Mayer. *Statistical Mechanics*. Wiley, New York, 1940.
- [109] P. Mayer, K. Miyazaki, and D. R. Reichman. Cooperativity beyond caging: Generalized Mode-Coupling theory. *Phys. Rev. Lett.*, 97(9):095702, 2006. doi:[10.1103/PhysRevLett.97.095702](https://doi.org/10.1103/PhysRevLett.97.095702).
- [110] E. Meeron. Nodal expansions. III. exact integral equations for particle correlation functions. *J. Math. Phys.*, 1(3):192–201, 1960. doi:[10.1063/1.1703652](https://doi.org/10.1063/1.1703652).
- [111] M. Merolle, J. P. Garrahan, and D. Chandler. Space-time thermodynamics of the glass transition. *Proc. Nat. Acad. Sci.*, 102(31):10837–10840, 2005.
- [112] M. Mézard and A. Montanari. *Information, Physics, and Computation*. Oxford University Press, 2009.
- [113] M. Mézard and G. Parisi. A tentative replica study of the glass transition. *J. Phys. A*, 29(20):6515–6524, 1996. doi:[10.1088/0305-4470/29/20/009](https://doi.org/10.1088/0305-4470/29/20/009).

-
- [114] M. Mézard and G. Parisi. A first-principle computation of the thermodynamics of glasses. *J. Chem. Phys.*, 111(3):1076–1095, 1999. doi:[10.1063/1.479193](https://doi.org/10.1063/1.479193).
- [115] M. Mézard and G. Parisi. Thermodynamics of glasses: A first principles computation. *Phys. Rev. Lett.*, 82(4):747–750, 1999. doi:[10.1103/PhysRevLett.82.747](https://doi.org/10.1103/PhysRevLett.82.747).
- [116] M. Mézard, G. Parisi, and M. A. Virasoro. *Spin glass theory and beyond*. World Scientific, Singapore, 1987.
- [117] K. Miyazaki and D. R. Reichman. Mode-coupling theory and the fluctuation–dissipation theorem for nonlinear langevin equations with multiplicative noise. *J. Phys. A*, 38:L343–L355, 2005. doi:[10.1088/0305-4470/38/20/L03](https://doi.org/10.1088/0305-4470/38/20/L03).
- [118] R. Monasson. Structural glass transition and the entropy of the metastable states. *Phys. Rev. Lett.*, 75(15):2847–2850, 1995. doi:[10.1103/PhysRevLett.75.2847](https://doi.org/10.1103/PhysRevLett.75.2847).
- [119] R. Monasson. Introduction to phase transitions in random optimization problems. In J.P. Bouchaud, M. Mézard, and J. Dalibard, editors, *Complex Systems*, Les Houches, France, 2007. Elsevier.
- [120] H. Mori. Transport, collective motion, and brownian motion. *Progr. Theor. Phys.*, 33(3):423–455, 1965. doi:[10.1143/PTP.33.423](https://doi.org/10.1143/PTP.33.423).
- [121] T. Morita. Theory of classical fluids: Hyper-netted chain approximation, ii. *Progr. Theor. Phys.*, 21(3):361–382, 1959. doi:[10.1143/PTP.21.361](https://doi.org/10.1143/PTP.21.361).
- [122] T. Morita and K. Hiroike. Integral equation for pair distribution function. *Progr. Theor. Phys.*, 23:385–387, 1959. doi:[10.1143/PTP.23.385](https://doi.org/10.1143/PTP.23.385).
- [123] T. Morita and K. Hiroike. A new approach to the theory of classical fluids. III. *Progr. Theor. Phys.*, 25:537–578, 1961. doi:[10.1143/PTP.25.537](https://doi.org/10.1143/PTP.25.537).
- [124] J. W. Negele and H. Orland. *Quantum many-particle systems*. Westview Press, 1998.
- [125] T. H. Nishino and H. Hayakawa. Fluctuation-dissipation-relation-preserving field theory of the glass transition in terms of fluctuating hydrodynamics. *Phys. Rev. E*, 78:061502, 2008. doi:[10.1103/PhysRevE.78.061502](https://doi.org/10.1103/PhysRevE.78.061502).
- [126] C. S. O’Hern, S. A. Langer, A. J. Liu, and S. R. Nagel. Random packings of frictionless particles. *Phys. Rev. Lett.*, 88(7):075507, 2002. doi:[10.1103/PhysRevLett.88.075507](https://doi.org/10.1103/PhysRevLett.88.075507).
- [127] C. S. O’Hern, L. E. Silbert, A. J. Liu, and S. R. Nagel. Jamming at zero temperature and zero applied stress: The epitome of disorder. *Phys. Rev. E*, 68(1):011306, 2003. doi:[10.1103/PhysRevE.68.011306](https://doi.org/10.1103/PhysRevE.68.011306).
- [128] P. Olsson and S. Teitel. Critical Scaling of Shear Viscosity at the Jamming Transition. *Phys. Rev. Lett.*, 99(17):178001, 2007. doi:[10.1103/PhysRevLett.99.178001](https://doi.org/10.1103/PhysRevLett.99.178001).
- [129] L. S. Ornstein and F. Zernike. Accidental deviations of density and opalescence at the critical point of a single substance. *KNAW, Proceedings*, 17(II):793–806, 1914. Available from: <http://www.dwc.knaw.nl/biografie/pmknaw/?pagetype=publDetail&pId=PU00012727>.

- [130] G. Parisi and F. Zamponi. Mean-field theory of hard sphere glasses and jamming. *Rev. Mod. Phys.*, 82(1):789–845, 2010. doi:[10.1103/RevModPhys.82.789](https://doi.org/10.1103/RevModPhys.82.789).
- [131] L. Peliti. Path integral approach to birth-death processes on a lattice. *J. Physique*, 46:1469–1483, 1985. doi:[10.1051/jphys:019850046090146900](https://doi.org/10.1051/jphys:019850046090146900).
- [132] J. K. Percus. Approximation methods in classical statistical mechanics. *Phys. Rev. Lett.*, 8(11):462–463, 1962. doi:[10.1103/PhysRevLett.8.462](https://doi.org/10.1103/PhysRevLett.8.462).
- [133] E. Pitard, V. Lecomte, and F. van Wijland. Dynamic transition in an atomic glass former: A molecular-dynamics evidence. *Europhys. Lett.*, 96:56002, 2011.
- [134] T. V. Ramakrishnan and M. Yussouf. First-principles order-parameter theory of freezing. *Phys. Rev. B*, 19(5):2775–2794, 1979. doi:[10.1103/PhysRevB.19.2775](https://doi.org/10.1103/PhysRevB.19.2775).
- [135] F. Ritort and P. Sollich. Glassy dynamics of kinetically constrained models. *Adv. Phys.*, 52(4):219–342, 2003. doi:[10.1080/0001873031000093582](https://doi.org/10.1080/0001873031000093582).
- [136] C. A. Rogers. *Packing and Covering*. Cambridge University Press, Cambridge, 1964.
- [137] G. S. Rushbrooke and H. I. Scoins. On the theory of fluids. *Proc. R. Soc. Lond. A*, 216:203–218, 1953. doi:[10.1098/rspa.1953.0017](https://doi.org/10.1098/rspa.1953.0017).
- [138] E. E. Salpeter. On mayer’s theory of cluster expansions. *Ann. Phys.*, 5(3):183–223, 1958. doi:[10.1016/0003-4916\(58\)90058-7](https://doi.org/10.1016/0003-4916(58)90058-7).
- [139] Z. W. Salsburg and W. W. Wood. Equation of state of classical hard spheres at high density. *J. Chem. Phys.*, 37:798, 1962. doi:[10.1063/1.1733163](https://doi.org/10.1063/1.1733163).
- [140] B. R. Saunders and B. Vincent. Microgel particules as model colloids : theory, properties and applications. *Advances in Colloid and Interface Science*, 80:1–25, 1999.
- [141] F. Sciortino and W. Kob. Debye-Waller factor of liquid silica: Theory and simulation. *Phys. Rev. Lett.*, 86(4):648–651, 2001. doi:[10.1103/PhysRevLett.86.648](https://doi.org/10.1103/PhysRevLett.86.648).
- [142] H. Senff and W. Richtering. Influence of cross-link density on rheological properties of temperature-sensitive microgel suspensions. *Colloid & Polym. Sci.*, 278(9):830–840, 2000. doi:[10.1007/s003960000329](https://doi.org/10.1007/s003960000329).
- [143] L. E. Silbert, A. J. Liu, and S. R. Nagel. Structural signatures of the unjamming transition at zero temperature. *Phys. Rev. E*, 73(4):041304, 2006. doi:[10.1103/PhysRevE.73.041304](https://doi.org/10.1103/PhysRevE.73.041304).
- [144] Y. Singh. Density-functional theory of freezing and properties of the ordered phase. *Phys. Rep.*, 207(6):351–444, 1991. doi:[10.1016/0370-1573\(91\)90097-6](https://doi.org/10.1016/0370-1573(91)90097-6).
- [145] Y. Singh, J. P. Stoessel, and P. G. Wolynes. Hard-sphere glass and the density-functional theory of aperiodic crystals. *Phys. Rev. Lett.*, 54(10):1059–1062, 1985. doi:[10.1103/PhysRevLett.54.1059](https://doi.org/10.1103/PhysRevLett.54.1059).
- [146] L. Sjögren. Kinetic theory of current fluctuations in simple classical liquids. *Phys. Rev. A*, 22(6):2866–2882, 1980. doi:[10.1103/PhysRevA.22.2866](https://doi.org/10.1103/PhysRevA.22.2866).
- [147] C. Song, P. Wang, and H. A. Makse. A phase diagram for jammed matter. *Nature*, 453(7195):629, 2008. doi:[10.1038/nature06981](https://doi.org/10.1038/nature06981).

- [148] F. H. Stillinger, E. A. Di Marzio, and R. L. Kornegay. Systematic approach to explanation of the rigid disk phase transition. *J. Chem. Phys.*, 40(6):1564–1576, 1964. doi:[10.1063/1.1725362](https://doi.org/10.1063/1.1725362).
- [149] G. Szamel. Is a “homogeneous” description of dynamic heterogeneities possible? *J. Chem. Phys.*, 121(8):3355–3358, 2004. doi:[10.1063/1.1783873](https://doi.org/10.1063/1.1783873).
- [150] G. Szamel. Dynamics of interacting brownian particles: A diagrammatic formulation. *J. Chem. Phys.*, 127(8):084515, 2007. doi:[10.1063/1.2759487](https://doi.org/10.1063/1.2759487).
- [151] G. Szamel. Divergent four-point dynamic density correlation function of a glassy suspension. *Phys. Rev. Lett.*, 101:205701, 2008. doi:[10.1103/PhysRevLett.101.205701](https://doi.org/10.1103/PhysRevLett.101.205701).
- [152] G. Szamel. Dynamic glass transition: Bridging the gap between mode-coupling theory and the replica approach. *Europhys. Lett.*, 91(5):56004, 2010. doi:[10.1209/0295-5075/91/56004](https://doi.org/10.1209/0295-5075/91/56004).
- [153] G. Szamel and E. Flenner. Independence of the relaxation of a supercooled fluid from its microscopic dynamics: Need for yet another extension of the mode-coupling theory. *Europhys. Lett.*, 67(5):779–785, 2004. doi:[10.1209/epl/i2004-10117-6](https://doi.org/10.1209/epl/i2004-10117-6).
- [154] G. Szamel and E. Flenner. Emergence of Long-Range correlations and rigidity at the dynamic glass transition. *Phys. Rev. Lett.*, 107(10):105505, 2011. doi:[10.1103/PhysRevLett.107.105505](https://doi.org/10.1103/PhysRevLett.107.105505).
- [155] M. van Hecke. Jamming of soft particles: Geometry, mechanics, scaling and isostaticity. *J. Phys.: Condens. Matter*, 22(3):033101, 2010. doi:[10.1088/0953-8984/22/3/033101](https://doi.org/10.1088/0953-8984/22/3/033101).
- [156] N. G. van Kampen. *Stochastic processes in physics and chemistry*. Elsevier Science & Technology Books, 2007.
- [157] J. M. J. van Leeuwen, J. Groeneveld, and J. de Boer. New method for the calculation of the pair correlation function. i. *Physica*, 25:792–808, 1959. doi:[10.1016/0031-8914\(59\)90004-7](https://doi.org/10.1016/0031-8914(59)90004-7).
- [158] W. van Meegen, T. C. Mortensen, S. R. Williams, and J. Müller. Measurement of the self-intermediate scattering function of suspensions of hard spherical particles near the glass transition. *Phys. Rev. E*, 58(5):6073–6085, 1998. doi:[10.1103/PhysRevE.58.6073](https://doi.org/10.1103/PhysRevE.58.6073).
- [159] S. Whitelam, L. Berthier, and J. P. Garrahan. Dynamic criticality in Glass-Forming liquids. *Phys. Rev. Lett.*, 92(18):185705, 2004. doi:[10.1103/PhysRevLett.92.185705](https://doi.org/10.1103/PhysRevLett.92.185705).
- [160] S. Whitelam, L. Berthier, and J. P. Garrahan. Renormalization group study of a kinetically constrained model for strong glasses. *Phys. Rev. E*, 71(2):026128, 2005. doi:[10.1103/PhysRevE.71.026128](https://doi.org/10.1103/PhysRevE.71.026128).
- [161] G. C. Wick. The evaluation of the collision matrix. *Phys. Rev.*, 80(2):268–272, 1950. doi:[10.1103/PhysRev.80.268](https://doi.org/10.1103/PhysRev.80.268).
- [162] M. Wyart, L. E. Silbert, S. R. Nagel, and T. A. Witten. Effects of compression on the vibrational modes of marginally jammed solids. *Phys. Rev. E*, 72(5):051306, 2005. doi:[10.1103/PhysRevE.72.051306](https://doi.org/10.1103/PhysRevE.72.051306).
- [163] N. Xu, V. Vitelli, A. J. Liu, and S. R. Nagel. Anharmonic and quasi-localized vibrations in jammed solids – modes for mechanical failure. *Europhys. Lett.*, 90:56001, 2010. doi:[10.1209/0295-5075/90/56001](https://doi.org/10.1209/0295-5075/90/56001).

- [164] H. Yoshino and M. Mézard. Emergence of rigidity at the structural glass transition: a first principle computation. *Phys. Rev. Lett.*, 105:015504, 2010. [doi:10.1103/PhysRevLett.105.015504](https://doi.org/10.1103/PhysRevLett.105.015504).
- [165] Z. Zhang, N. Xu, D. T. N. Chen, P. Yunker, A. M. Alsayed, K. B. Aptowicz, P. Habdas, A. J. Liu, S. R. Nagel, and A. G. Yodh. Thermal vestige of the zero-temperature jamming transition. *Nature*, 459(7244):230, 2009. [doi:10.1038/nature07998](https://doi.org/10.1038/nature07998).
- [166] J. Zinn-Justin. *Quantum Field Theory and Critical Phenomena*. Clarendon Press, Oxford, 1989.
- [167] R. Zwanzig. *Non-equilibrium statistical mechanics*. Oxford University Press, 2001.